

## INFORMATION TO USERS

While the most advanced technology has been used to photograph and reproduce this manuscript, the quality of the reproduction is heavily dependent upon the quality of the material submitted. For example:

- Manuscript pages may have indistinct print. In such cases, the best available copy has been filmed.
- Manuscripts may not always be complete. In such cases, a note will indicate that it is not possible to obtain missing pages.
- Copyrighted material may have been removed from the manuscript. In such cases, a note will indicate the deletion.

Oversize materials (e.g., maps, drawings, and charts) are photographed by sectioning the original, beginning at the upper left-hand corner and continuing from left to right in equal sections with small overlaps. Each oversize page is also filmed as one exposure and is available, for an additional charge, as a standard 35mm slide or as a 17"x 23" black and white photographic print.

Most photographs reproduce acceptably on positive microfilm or microfiche but lack the clarity on xerographic copies made from the microfilm. For an additional charge, 35mm slides of 6"x 9" black and white photographic prints are available for any photographs or illustrations that cannot be reproduced satisfactorily by xerography.



8707847

John, Sarah

SOLUTION TO QUANTUM LIOUVILLE EQUATION IN PHASE SPACE--VIA A  
STOCHASTIC PROCESS

*The College of William and Mary in Virginia*

PH.D. 1986

University  
Microfilms  
International 300 N. Zeeb Road, Ann Arbor, MI 48106



**PLEASE NOTE:**

In all cases this material has been filmed in the best possible way from the available copy. Problems encountered with this document have been identified here with a check mark ✓.

1. Glossy photographs or pages \_\_\_\_\_
2. Colored illustrations, paper or print \_\_\_\_\_
3. Photographs with dark background \_\_\_\_\_
4. Illustrations are poor copy \_\_\_\_\_
5. Pages with black marks, not original copy \_\_\_\_\_
6. Print shows through as there is text on both sides of page \_\_\_\_\_
7. Indistinct, broken or small print on several pages ✓
8. Print exceeds margin requirements \_\_\_\_\_
9. Tightly bound copy with print lost in spine \_\_\_\_\_
10. Computer printout pages with indistinct print \_\_\_\_\_
11. Page(s) \_\_\_\_\_ lacking when material received, and not available from school or author.
12. Page(s) \_\_\_\_\_ seem to be missing in numbering only as text follows.
13. Two pages numbered \_\_\_\_\_. Text follows.
14. Curling and wrinkled pages \_\_\_\_\_
15. Dissertation contains pages with print at a slant, filmed as received \_\_\_\_\_
16. Other \_\_\_\_\_  
\_\_\_\_\_  
\_\_\_\_\_

University  
Microfilms  
International



SOLUTION TO QUANTUM LIOUVILLE EQUATION IN PHASE SPACE  
-VIA A STOCHASTIC PROCESS

---

A Dissertation  
Presented to  
The Faculty of the Department of Physics  
The College of William and Mary in Virginia

In Partial Fulfillment  
Of the Requirements for the Degree of  
Doctor of Philosophy


---

by  
Sarah John  
1986

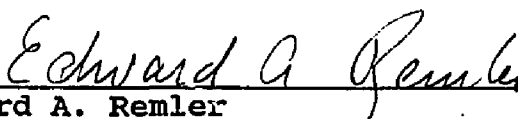
APPROVAL SHEET

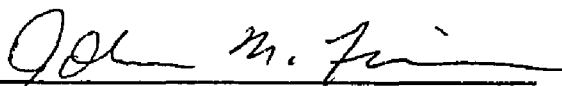
This dissertation is submitted in partial fulfillment of  
the requirements for the degree of


Doctor of Philosophy

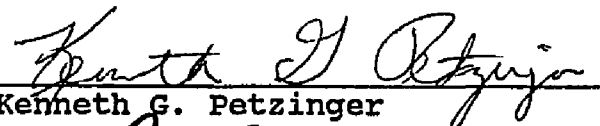
  
\_\_\_\_\_  
Sarah John

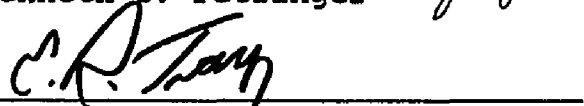
Approved, December 1986

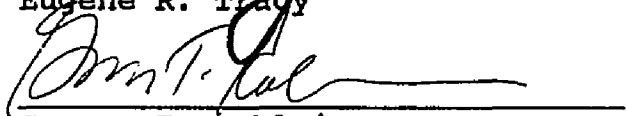
  
\_\_\_\_\_  
Edward A. Remler

  
\_\_\_\_\_  
John M. Finn

  
\_\_\_\_\_  
Henry Krakauer

  
\_\_\_\_\_  
Kenneth G. Petzinger

  
\_\_\_\_\_  
Eugene R. Tracy

  
\_\_\_\_\_  
George T. Rublein  
Mathematics Department

## TABLE OF CONTENTS

	Page
Acknowledgements.....	vi
List of Tables.....	vii
List of Figures.....	viii
Abstract.....	x
<u>Chapter</u>	
1.Introduction.....	2
1.1 The Wigner Function .....	4
1.2 Time evolution of the Wigner Function.....	8
1.3 Numerical Solutions.....	9
2.Time development of the Wigner function	
-An exactly solvable case.....	12
2.1 The initial state Wigner function.....	12
2.2 The exact formulation-expansion in orthonormal states.....	13
2.3 The classical development .....	16
2.4 Results contrasting the classical and exact solution .....	16
Figure Captions, figures 1-7.....	20
2.6 Moments of the distribution.....	28
Figure Captions, figures 8-10.....	31

3.The Quantum Liouville Equation	
-A Numerical Approximation.....	35
3.1 An approximate expansion for time development ..	35
3.2 A numerical method .....	36
4.Quantum development in the quasi-classical limit.	
A test of the stochastic method.....	43
4.1 Quantum development of a delta function.....	43
4.2 Quantum development of a Gaussian distribution..	45
4.3 A numerical test comparing the exact vs. the	
stochastic development.....	46
Figure captions, figures 11-14.....	52
Figure captions, figures 15-22.....	57
5.Time development of the Wigner function	
-via the stochastic process.....	66
5.1 The Algorithm.....	67
5.2 Computer Runs.....	75
Figure Captions,figures 23-36.....	80
5.3 Moments of the distribution.....	95
Figure Captions, figures 37-38.....	96
5.4 Statistics.....	99
5.5 Conclusions.....	101

6. Summary	
6.1 Summary.....	102
6.2 Future Applications.....	103

Appendix

1. An introduction to quantum Liouville equation.....	105
2.....	107
3.....	114
4.....	116
5.....	122
A. Stochastic quantum development -using a discrete differentiation process.....	127
figure Captions, figures 39-40.....	129
B. Quantum development using a Lorentzian distribution.....	132
figure captions, figures 41-42.....	134
figure caption , figure 43.....	139
Flow Charts.....	144
Bibliography.....	147
Vita.....	149

## ACKNOWLEDGEMENTS

I wish to express my appreciation for the invaluable guidance of Professor E.A.Remler throughout the course of this work .

Also great thanks go to the computer centre for its facilities, and to Pete Hoyle for consultations during the development of the software.

I am also grateful to the department for providing me with a teaching assistantship.

LIST OF TABLES

Table	page
1. The different cases studied .....	19
2. Value of parameters in the approximate scheme...	79
3. Statistics of averages.....	100

List of figures

figures	page
1. The initial Wigner distribution function .....	21
2. The initial contours .....	22
<u>Comparison of classical contours with exact</u>	
3. $\beta=1, k_2 = 1, T = 12\pi$ .....	23
4. $\beta=1, k_2 = .5, T = 12\pi$ .....	24
5. $\beta=.5, k_2 = .5, T = 12\pi$ .....	25
6. $\beta=.25, k_2 = .5, T = 12\pi$ .....	26
7. 3-D view exact $\beta=.25, k_2 = .5, T = 6\pi$ .....	27
<u>Classical and exact averages vs.time</u>	
8. top: $\beta = 1, k_2 = 1$ bottom: $\beta = .5, k_2 = .5$ .....	32
<u>Averages, correlation, width vs. time</u>	
9. $\beta = 1, k_2 = .5$ .....	33
10. $\beta = .5, k_2 = .5$ .....	34
<u>Quantum Development of a gaussian distribution</u>	
11. $I(p,a)$ vs. $p$ for a gaussian distribution.....	53
12. $J(p,a)$ vs. $p$ for a gaussian distribution.....	54
13. $J(p,a)$ vs. $p$ for $a = .001$ .....	55
14. $J'(p,a)$ vs. $p$ for $a = .001$ .....	56
<u>Curves comparing the exact with the stochastic quantum development</u>	
15. Variation with number.....	58

16. Variation with number of smoothing functions.....	59
17. Statistical variation.....	60
18. Variation with 'a'.....	61
19. Variation with $\alpha$ -s.....	62
<u>Variation with bin-size N = 1000</u>	
20. $\alpha$ -s = .2.....	63
21. $\alpha$ -s = .3.....	64
22. $\alpha$ -s = .4.....	65
<u>Comparison of classical, exact and approximate contours</u>	
23-25. $\beta = 1, k_2 = 1, T = \pi/3, 2\pi/3, \pi$ .....	81
26-28. $\beta = 1, k_2 = .5, T = 2\pi/3, 4\pi/3, 2\pi$ .....	84
29-32. $\beta = .5, k_2 = .5, T = \pi, 2\pi, 3\pi, 4\pi$ .....	87
33-35. $\beta = .25, k_2 = .5, T = \pi, 2\pi, 3\pi$ .....	91
36. 3-D view of exact and approx, $\beta = .25, k_2 = .5, T = 3\pi$ ....	94
37. Averages vs. number of points.....	97
<u>Comparison of classical, exact and approximate averages</u>	
38. $\beta = .5, k_2 = .5$ .....	98
39-40. Comparison of exact with stochastic curves- discrete differentiation.....	130
41. exact quantum development for lorentzian.....	135
42. Comparison of exact with stochastic curve for lorentzian.....	136
43. Paths of constant phase.....	140

## ABSTRACT

A numerical technique for the solution of the Quantum Liouville equation is discussed which is expected to be useful for mixed states describing highly excited many body systems.

The equation is represented in phase-space, where the density operator becomes the Wigner function. The Liouville operator which determines its time evolution, separates into a classical and quantum term. When the Wigner function varies slowly in momentum, the quasi-classical approximation is valid in which one keeps only the first order quantum term in the Liouville equation.

The Wigner function is represented by a sample set of gaussian smeared points. In an iterative time development scheme, the points are propagated first along a classical phase-space trajectory, which is then followed by a quantum development. The latter is represented by a stochastic process incorporated into the numerical procedure as a generalized Markovian process.

This method is numerically tested for an anharmonic quartic potential. The contours of the Wigner function at different time intervals are compared with the purely classical and exact results. It is seen that it provides a definite improvement over the purely classical approximation. Various averages are also compared and sources of error discussed.

In addition it was discovered that intermediate mixed states show a 'quantum focussing' effect, wherein the function peaks to values greater than the original maximum. This quantum-mechanical effect did not appear in the pure case, and disappears because of Liouville's theorem for highly mixed states which are essentially classical. There are other numerical schemes, which treat the points as moving in an effective potential, wherein the points retain their identity. These again by Liouville's theorem cannot show this focussing effect.

SOLUTION TO QUANTUM LIOUVILLE EQUATION IN PHASE SPACE

-VIA A STOCHASTIC PROCESS

## Chapter 1

### Introduction

It is of fundamental interest to study the time development of complex quantum mechanical systems. A convenient formulation for this purpose may be made in phase space by the Wigner-Weyl representation,<sup>1-7</sup> where the quantum mechanical state and operators are represented as joint functions of co-ordinate and momentum variables. Not only does this formalism yield expressions which may be directly compared with classical mechanics, but these are also most suited to deal with quantum mechanical states which are highly mixed. In this thesis it is our purpose to develop an approximate numerical technique in the Wigner(Weyl) formalism, applicable to the study of the time evolution of mixed states.

Mixed states occur typically in many body systems where the energy eigenstates are closely spaced, and one can only deal with averages over a distribution of pure states known only via a probability distribution (see appendix 1 for an explanation of pure and mixed states). The Wigner representation of these mixed states in phase

space are slowly varying functions of the coordinates . For functions with slow variation in momentum coordinates, it will be shown that the equation of motion, when expanded in increasing powers of momentum derivatives, converges towards the classical limit. Systems where the momentum variation of the function is so slow, that the first order quantum correction is sufficient for the description of its time evolution, will be termed quasi-classical systems. We will be solving the quantum Liouville equation, which determines the time evolution of the density operator of a quantum mechanical system ,in the quasi-classical approximation, in phase space, by a stochastic procedure.

The method discussed here can find direct applications to nuclear heavy ion collision problems, such as in the Time Dependent Hartree Fock (TDHF) methods. 1-D calculations for collision between infinite slabs of nuclear matter by TDHF have been attempted, using time dependent single particle wave functions <sup>8</sup>. An extension to three dimensional calculations of these methods involve expensive computing facilities. Another approach to TDHF, using a pseudoparticle simulation of the Wigner function was basically limited to a classical approximation.<sup>9</sup>

Analytic schemes for the solution of quantum Liouville equation have also been attempted in recent years. Such methods include an approximate scheme by

solving for a set of coupled self-consistent equations for the density matrix using the Wigner function<sup>11</sup>. Another scheme is to represent the remainder term as an exact expression, in the series expansion of the quantum Liouville equation<sup>12</sup>. The general utility of such methods is yet to be worked out.

Here we attempt a direct numerical solution to the time dependence of the Wigner function, by incorporating the quantum effects via a generalized Markov process. The advantage of this formulation will be an easy extension to higher dimensions, and the study of various other problems, such as collision problems, highly excited many body systems, few body problems etc.

### 1.1 The Wigner Function

One of the natural backgrounds in which a comparison between classical and quantum mechanics may be made is the phase space - a  $2n$  dimensional space with the dynamical variable and its conjugate momenta as generalized co-ordinates. It is possible to reformulate quantum mechanics in phase space in a manner suggested by Wigner(Weyl). In this formalism linear operators are represented as joint functions of  $(x,p)$  by the Wigner(Weyl) transform defined for an operator  $A$  as

$$A_{\omega}(x,p) = \int dy e^{ipy} \langle x-iy|A|x+iy\rangle$$

The Wigner function is a representation of the

quantum mechanical state as a function in phase space.<sup>14-20</sup> If  $\rho$  is the density operator representing the state, the Wigner function is defined by (we set  $\hbar=1$ )

$$f_{\omega}(x,p) = \int dy e^{ipy} \langle x-\frac{1}{2}y | \rho | x+\frac{1}{2}y \rangle$$

or alternatively

$$f_{\omega}(x,p) = \int dy e^{-ixy} \langle p-\frac{1}{2}y | \rho | p+\frac{1}{2}y \rangle$$

For a pure state  $\rho = |\Psi\rangle\langle\Psi|$  which gives

$$f_{\omega}(x,p) = \int dy e^{ipy} \Psi^*(x+\frac{1}{2}y) \Psi(x-\frac{1}{2}y)$$

The Wigner function can be considered as a quantum-mechanical probability distribution with the following properties.

1. It is a hermitian, bilinear form of the wave function  $\Psi$ .
2. The following properties parallel the classical distribution function

$$\frac{1}{2\pi} \int dp f_{\omega}(x,p) = \langle x | \rho | x \rangle$$

$$\frac{1}{2\pi} \int dx f_{\omega}(x,p) = \langle p | \rho | p \rangle$$

i.e. if integrated over  $p$  it gives the correct probabilities for the different values of  $x$ , and similarly for  $x \leftrightarrow p$  with

$$\frac{1}{2\pi} \int dx dp f_{\omega}(x,p) = 1$$

3. For an operator A whose Wigner transform is  $A_\omega$ , the expectation value is given by

$$\langle A \rangle = \frac{1}{2\pi} \int dx dp A_\omega(x,p) f_\omega(x,p) \quad (1.1)$$

Hence in the Quantum mechanical picture we have a quantum mechanical distribution function evolving in time, and expectation values of observables are given as averages of Wigner transforms of operators, over this distribution.

4. The Wigner function is real. i.e.  $f^* = f$ . This follows from property 1.

However, the Wigner function is not a true 'probability' distribution function because the function itself can attain negative values. In contrast the classical distribution functions are always positive.

The Wigner function has found a wide range of applications in fields which include fundamental aspects of quantum mechanics, statistical mechanics, collision theory etc.

#### Some typical Wigner functions

All the cases presented here represent pure states. In some instances, the states are eigenstates of some typical Hamiltonian.

1. Delta function in free space  $\psi(x) = \delta(x - x_i)$

$$\begin{aligned} f_\omega(x,p) &= \int dy e^{ipy} \delta(x+ky-x_i) \delta(x-ky-x_i) \\ &= e^{ip2(x-x_i)} \delta(2(x-x_i)) \\ &= \frac{1}{2} \delta(x-x_i) \end{aligned}$$

that is  $f_\omega$  is non-zero on a straight line parallel to p axis at  $x = x_i$ .

2. A free minimum wave packet

The time dependence of the free-packet can be separated in momentum space as:

$$C(p,t) = C(p) e^{-ip^2 t/2m}$$

where  $C(p)$  is a minimum packet peaked at  $p_0, x_0$  with width  $\sqrt{\sigma}$

$$C(p) = \frac{1}{(2\pi\sigma)^{1/2}} e^{[-(p-p_0)^2/4\sigma - ip \cdot x_0]}$$

and the corresponding Wigner function is

$$f_\omega(x,p,t) = \frac{1}{2} e^{-(p-p_0)^2/2\sigma} e^{-2\sigma(x-x_0-v_p t)^2}$$

3. Harmonic Oscillator : Energy eigenstates

The normalised oscillator wave functions are

$$\psi_n(x) = (m\omega)^{1/4} (2^n n! / \pi)^{-1/2} H_n(m\omega x/\hbar) e^{-m\omega x^2/2}$$

where  $H_n$  is the Hermite polynomial of order  $n$  and the corresponding Wigner function is

$$f_\omega(x,p) = \frac{1}{\omega} (-1)^n e^{-2H(x,p)/\omega} L_n^{(0)}[4H(x,p)/\omega]$$

where  $H$  is the Hamiltonian and  $L_n$  is a Laguerre

polynomial.

$$L_n^{(0)}(x) = n! \sum_{m=0}^n \binom{n}{m} \frac{(-x)^m}{m!}$$

These functions have negative regions, showing that the Wigner function is not positive definite throughout phase space.

### 1.2 Time Evolution of the Wigner Function.

The time evolution is given by the Wigner transform of the quantum Liouville equation for the density operator.

$$i \partial \rho / \partial t = [H, \rho]$$

Taking the Wigner transform of both sides, and using the formula for the Wigner transform of a product of two functions:

$$(AB)_\omega = A_\omega(x, p) e^{\Lambda/2i} B_\omega(x, p)$$

where  $\Lambda$  is the Poisson Bracket operator defined by

$$\Lambda = \hat{\nabla}_p \cdot \hat{\nabla}_x - \hat{\nabla}_x \cdot \hat{\nabla}_p$$

where the arrows denote the direction in which the  $\nabla$  operator is to be applied. This gives

$$\partial f_\omega(t) / \partial t = -2 H \sin(\Lambda/2) f_\omega(t) \quad (1.2)$$

A formal solution to the equation is

$$f_\omega(t) = e^{[-2tH \sin(\Lambda/2)]} f_\omega(0) \quad (1.3)$$

Now expanding the sin term in equation 1.2 we get

$$\begin{aligned} \partial f_\omega(t) / \partial t &= -H \Lambda f_\omega + (1/24) H \Lambda^3 f_\omega + \dots \\ &= (L_C + L_Q) f_\omega \end{aligned} \quad (1.4)$$

where  $L_C$  is the Classical Liouville operator and  $L_Q$  the quantum Liouville operator given by

$$\begin{aligned} L_C &= -H \Lambda \\ &= \frac{\partial H}{\partial x} \frac{\partial}{\partial p} - \frac{\partial H}{\partial p} \frac{\partial}{\partial x} \\ L_Q &= (1/24) H \Lambda^3 - (1/1920) H \Lambda^5 + \dots \end{aligned}$$

Assuming an Hamiltonian of the form

$$\begin{aligned} H &= p^2/2m + V(x) \\ L_Q &= -\frac{1}{24} \frac{\partial^3 H}{\partial x^3} \frac{\partial^3}{\partial p^3} + \frac{1}{1920} \frac{\partial^5 H}{\partial x^5} \frac{\partial^5}{\partial p^5} + \dots \end{aligned}$$

(for a more general Hamiltonian, operator derivatives w.r.t.  $x$  also appear.)

In the quasi-classical limit, for slowly varying functions of the momenta we keep only the first term in  $L_Q$  and neglect higher order derivatives. Hence the quasi-classical limit is defined by

$$L_Q = (1/24) H \Lambda^3$$

In the classical limit eqn 1.4 reduces to the classical Liouville equation.

$$\begin{aligned} \partial f_\omega / \partial t &= -H \Lambda f_\omega \\ &= -\{H, f_\omega\} \end{aligned}$$

The R.H.S. is the Poisson Bracket. This is the classical correspondence that one naturally desires.

### 1.3 Numerical Solutions

In some typical numerical calculations in current

literature, the Wigner function is represented by a sampled set of points in phase space and these points are propagated classically under an effective potential defined by <sup>10</sup>

$$\frac{\partial V_{\text{eff}}}{\partial x} \frac{\partial f}{\partial p} = \frac{\partial V}{\partial x} \frac{\partial f}{\partial p} - \frac{1}{24} \frac{\partial^3 V}{\partial x^3} \frac{\partial^3 f}{\partial p^3} + \dots$$

In such calculations, a representative point in phase space retains its identity as a delta function in time. These classically deterministic motions for the points have given good results in the study for stationary bound states. However, this method is extremely limited in its applicability.

Whereas in classical mechanics one can talk of the trajectory of a point, in the quantum mechanical Liouville equation it will be seen that the effect of the first order quantum operator is to transform the point into an oscillatory function of the Airy form along the momentum coordinate. The concept of a trajectory is lost by such transformations.

We incorporate this functional change of a point into a numerical procedure which solves for the Quantum Liouville equation in the quasi-classical limit.

As a model a simple one dimensional system is considered in a quartic anharmonic Hamiltonian. In this case there are no terms higher than the first order in the quantum operator. Infact we are solving for the exact quantum Liouville equation in this potential.

Therefore this model will be most suited to test for the efficacy of the numerical approximations introduced here to incorporate the first order quantum term to the classical approximation. It must be emphasized that the effects of suppressing higher order terms in a quasi-classical approximation is not discussed in this thesis, but one may reasonably assume that for slowly varying functions in momentum space, the order of magnitude of the higher order terms are much smaller than the quasi-classical term.

The numerical solutions so obtained are compared with an exact formulation for the same system using an expansion in terms of a basis set of normalized harmonic oscillator wave functions.

In Chapter 2 we contrast the exact formulation with the purely classical evolution of an arbitrary initial state Wigner distribution representing a mixed state.

In Chapter 3 we formulate a numerical method for the solution of the Quantum Liouville equation in phase space by a stochastic procedure.

In Chapter 4 we test for the methods developed in 3 for the pure quantum development of a gaussian function.

In Chapter 5 we present an algorithm to implement the method for the time development of the Wigner function and compare the results with that in Chapter 2.

## chapter 2

### Time Development of the Wigner function-An exactly solvable Case.

#### Introduction

In this chapter the classical motion is contrasted with the exact quantum mechanical motion for a class of initial Wigner distributions representing mixed states. For the classical case, the path of the distribution is followed in time using the classical Liouville equation. An exact quantum mechanical solution is obtained by expanding in a basis set of orthonormal wave functions.

#### 2.1 The Initial state Wigner function

Let  $f_{\omega}(x,p,0)$  represent a class of initial Wigner distributions for mixed states. Let us consider its time development in an anharmonic potential. Such a detailed study has previously been done for the pure case.<sup>22</sup> We extend the work to mixed states.

A convenient initial form chosen for  $f_{\omega}(0)$  is a gaussian function centered at  $(x_0,p_0)$

$$f_{\omega}(x, p, 0) = 2 \exp(-\beta(x-x_0)^2/k^2 - \beta k^2 (p-p_0)^2)$$

where  $\beta$  defines the extent of mixing and  $k$  determines the asymmetry of the distribution. For  $\beta=1$  the corresponding  $\rho_0 = |\psi\rangle\langle\psi|$  is a pure state with  $\psi(x) = \exp(-(x-x_0)^2 - i x p_0)$ , a minimum wave packet.  $\beta < 1$  implies a mixed state and the Wigner function correspondingly becomes broader and hence a more slowly varying function of the coordinates.

A normalization factor of  $\beta/2\pi$  is chosen so that  $f_{\omega}(x_0, p_0, 0)$  always has a maximum value of 2.

$$\frac{\beta}{2\pi} \int f_{\omega} dx dp = 1 \quad (2.1)$$

## 2.2 The exact formulation - expansion in orthonormal states.

We study the time development of the wigner function in a potential given by

$$V(x) = \frac{1}{2} k_1 x^2 + \frac{1}{4} k_2 x^4 \quad (2.2)$$

The time dependence is given by

$$f_{\omega}(t) = \int dy e^{i p y} \langle x - \frac{1}{2} y | \rho(t) | x + \frac{1}{2} y \rangle \quad (2.3)$$

A solution for this can be obtained by expanding in a basis set of normalised harmonic oscillator wave functions represented variously as  $|m\rangle, |n\rangle, |q\rangle, |s\rangle$  and a basis set of the eigenstates of the total hamiltonian represented as  $|u\rangle, |v\rangle$ .

$$\begin{aligned}
f_{\omega}(t) &= \sum_{m,n} \int dy e^{iPy} \langle x-\frac{1}{2}y|m\rangle \langle m|\rho(t)|n\rangle \langle n|x+\frac{1}{2}y\rangle \\
&= \sum \langle\langle xp|mn\rangle\rangle \langle\langle mn|\rho\rangle\rangle
\end{aligned} \tag{2.4}$$

where

$$\langle\langle xp|mn\rangle\rangle = \int dy e^{iPy} \langle x-\frac{1}{2}y|m\rangle \langle n|x+\frac{1}{2}y\rangle$$

and

$$\langle\langle mn|\rho\rangle\rangle = \langle m|\rho(t)|n\rangle$$

It can be shown<sup>22</sup> (see also Appendix 2.1)

$$\begin{aligned}
\langle\langle xp|mn\rangle\rangle &= 2 \sqrt{\pi} N_m N_n \exp(-x^2-p^2) 2^{m+n} \\
&\sum_k^{\min(m,n)} \frac{m!n!(-2)^{-k} (x+ip)^{m-k} (x-ip)^{n-k}}{k!(m-k)!(n-k)!}
\end{aligned}$$

where  $N_n = (2^n n! \sqrt{\pi})^{-\frac{1}{2}}$

Now

$$\begin{aligned}
\langle\langle mn|\rho\rangle\rangle &= \langle m|\rho(t)|n\rangle \\
&= \sum_{u,v} \langle m|u\rangle \langle u|e^{-iHt}\rho(0)e^{iHt}|v\rangle \langle v|n\rangle \\
&= \sum_{u,v,q,s} e^{-i(\omega_u-\omega_v)t} \langle m|u\rangle \langle u|q\rangle \langle q|\rho(0)|s\rangle \langle s|v\rangle \langle v|n\rangle
\end{aligned}$$

where  $\omega_u$  and  $\omega_v$  are the eigenfrequencies and  $\langle m|u\rangle$  etc. are the overlap integrals of the eigenstates of  $H$  with the harmonic oscillator wave function. These may be written as

$$\langle u|m\rangle = \int \langle u|x\rangle \langle x|m\rangle dx$$

where  $\langle x|m\rangle$  is the representative for harmonic oscillator wave function and  $\langle x|u\rangle$  represents the eigenfunction of the Hamiltonian given by

$$H u = E u$$

where 
$$H = -\frac{\hbar^2}{2m} \frac{d^2}{dx^2} + V(x)$$

A fourth-order Runge Kutta method is used to solve this equation numerically to obtain the eigenfunction  $\langle x|u\rangle$ .

#### Evaluation of $\langle q|\rho(0)|s\rangle$

These are the matrix elements of the mixed state density with the harmonic oscillator wave functions.

Expressing  $\langle q|\rho_0|s\rangle$  as

$$\langle q|\rho_0|s\rangle =$$

$$\int dx' dy' \langle q|x' - iy'\rangle \langle x' - iy'|\rho_0|x' + iy'\rangle \langle x' + iy'|s\rangle$$

where  $\langle q|x' - iy'\rangle$  etc. is the harmonic oscillator wave functions and

$$\langle x - iy|\rho_0|x + iy\rangle = \frac{1}{2\pi} \int e^{-ipy} f_\omega(x, p, 0) dp$$

See Appendix 23 for an explicit evaluation of  $\langle q|\rho_0|s\rangle$ .

Finally equation 2.4 may be rewritten as

$$f_\omega(x, p, t) = \sum_m \sum_n^m (2 - \delta_{mn}) \operatorname{Re}(\langle\langle xp|mn\rangle\rangle \langle\langle mn|\rho(t)\rangle\rangle)$$

(2.5)

The above form may now be computed. The algorithm followed is basically as given in [22]. A maximum of 20

basis states were used. Wider distributions should naturally require more basis states. In each case runs were made with a smaller number of states to test for convergence. A typical snapshot took about 10 minutes of IBM computing time.

### 2.3 The Classical Development

To draw the classical contours Liouville's Theorem may be used, which states that the volume occupied by a system in phase space remains a constant. This implies that the density in the neighbourhood of any system point will be a constant. Therefore it is sufficient to choose a set of points initially lying on the same equi-density curve, propagate them in time using Hamilton's equation,

$$\dot{x} = \partial H / \partial p \quad \dot{p} = - \partial H / \partial x$$

and the final density curve is obtained by simply joining the final set of points.

### 2.4 Results contrasting the classical and exact solution

Table 1 gives the different cases studied.

The exact contours are contrasted with the classical approximation for  $\text{time} = 12\pi$ . See figures 1-7  
We note the following features:

### Classical

The classical motion develops whorls and tendrils and spreads itself into all available phase space consistent with energy. As seen from the contours there is a fine scale structure associated with it. That is, within the whorls and tendrils densities range from the maxima to zero.

### Quantum: Pure Case

For the pure case, the distribution keeping its form as a unit blob oscillates back and forth, very much like a semi-rigid body. The motion is that of a minimum wave-packet obeying the uncertainty relations. It is seen that the maximum does not increase beyond the initial value. In fact, a spreading or decrease in intensity from its maxima has been reported in [22] for states starting at high momenta. ( $p_0 = 3$ ).

The Wigner function also develops large negative regions .

### Mixed State

The mixed state motion is more complex. In addition there appears high intensity regions where the Wigner function exceeds the value of the initial maximum of 2. This 'quantum focussing' is more intense for higher mixed states. (Compare figures 5 and 6) This was a totally unexpected phenomenon, because, as was seen, the

pure state showed a dissipation effect, if any, and again, for very small  $\beta$  (representing highly mixed states), the system becomes classical and Liouville's theorem again guarantees that focussing effects will disappear. Therefore this focussing is an intermediate mixed state effect. The peaks remain even for very large times, with a small modulation in its maximum value.

Table 1.

The various cases studied

Case	State	Mix( $\beta$ )	Anharmon( $k_2$ )
1.	pure	1	1
2.	pure	1	.5
3.	mixed	.5	.5
4.	mixed	.5	.25

figures 1-7

fig 1. A typical Initial Wigner distribution at  $t = 0$

fig 2. Initial contours at values of 0.5, 1, 1.5

(counting from outermost towards the centre)

for  $\beta = 1, 1.5, .5, .25$  Note increase in width for smaller values of  $\beta$ . (The scale has been changed for  $\beta = .25$ )

fig 3 - 6. Each of these figures represent snapshots at time =  $12\pi$ . The top set shows the contours for the classical(left) and exact(right) respectively. Dotted curves begin to appear at a value of 2.5. The lower set is the 3-D view of the exact solution, one at a tilt of  $70^\circ$  and the other looking down the p axis.

fig 7. A picture at time =  $6\pi$  for  $\beta = .25$ ,  $k_2 = .5$

Note the narrow peak in the middle.

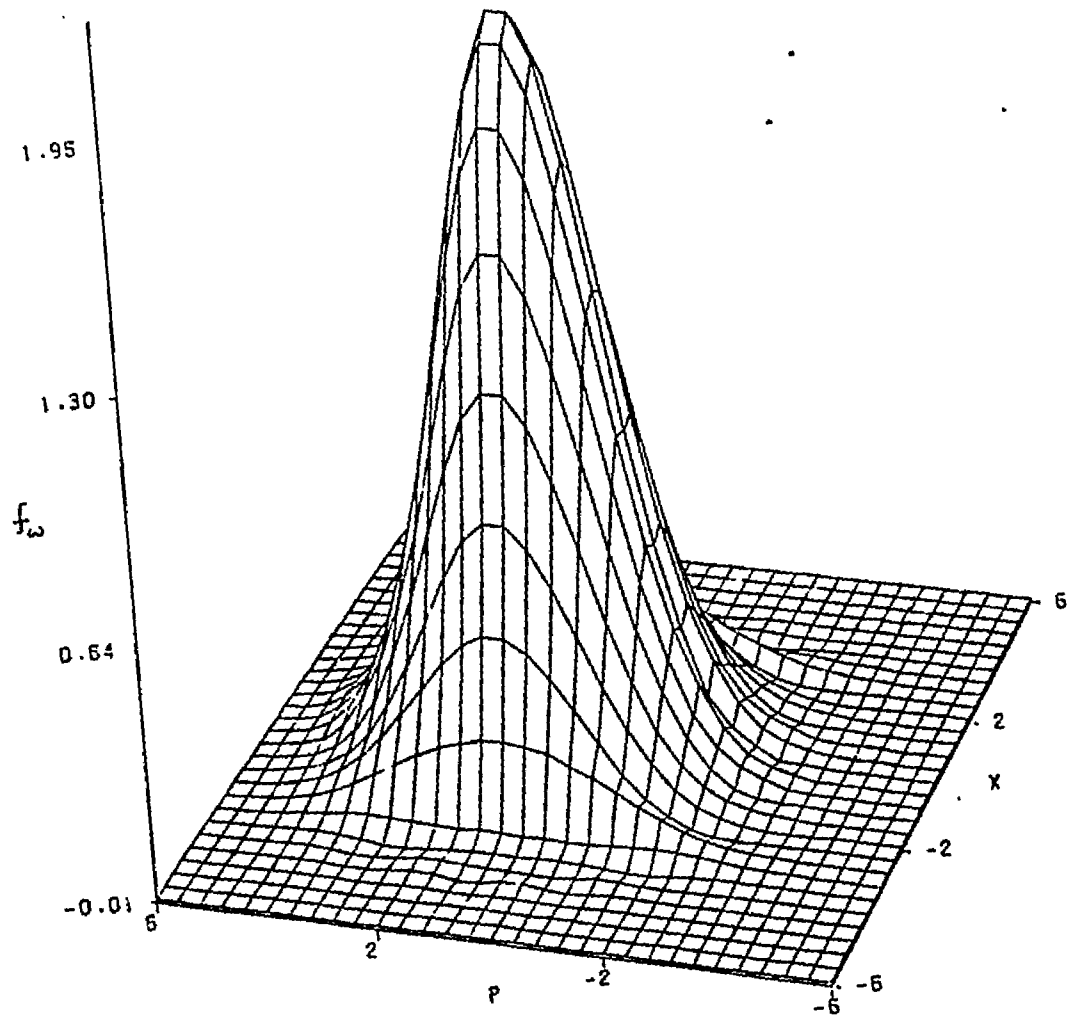


Figure 1. A typical initial Wigner distribution function.  
 $\beta = .25 \quad T = 0$

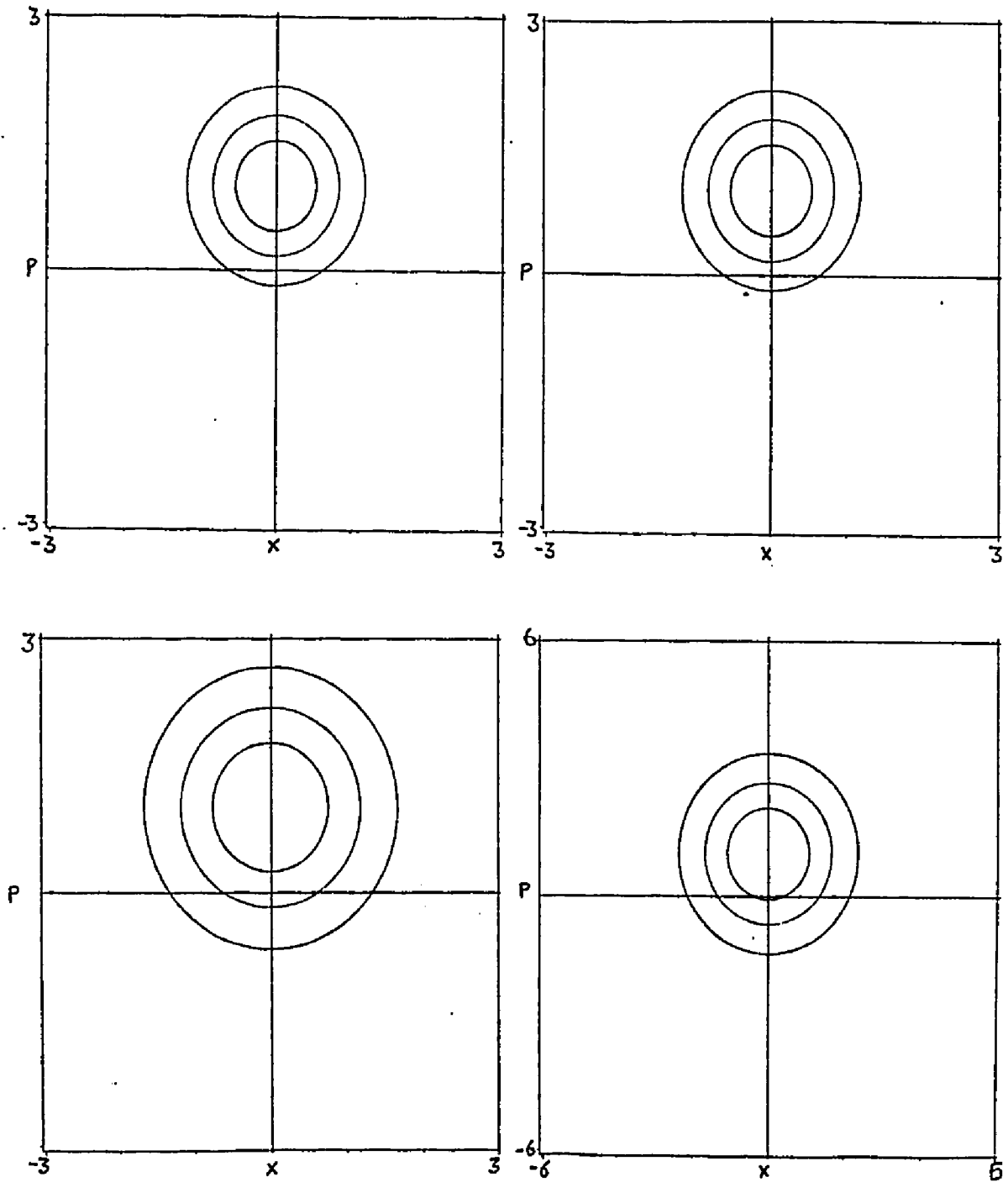


Figure 2. The initial contours at values of .5, 1, 1.5  
for  $\beta = 1, 1, .5, .25$

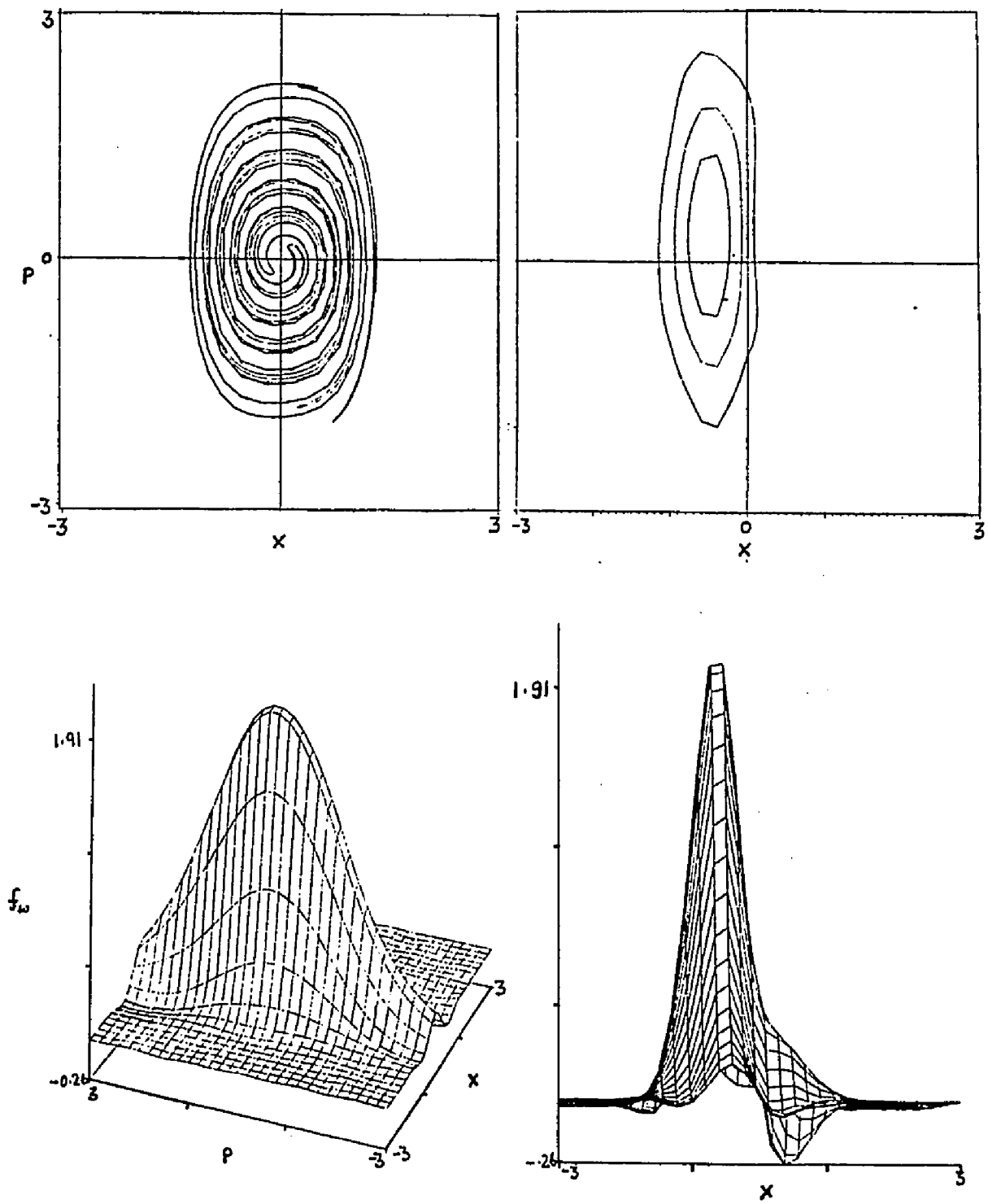


Figure 3.  $\beta = 1$   $k_2 = 1$   $T = 12\pi$

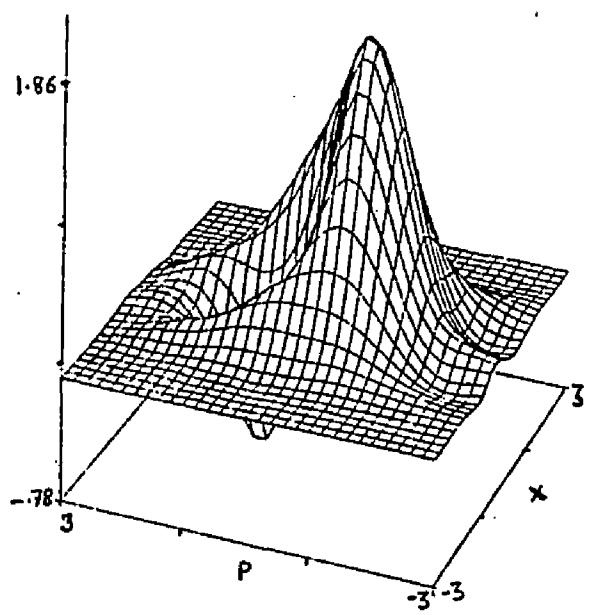
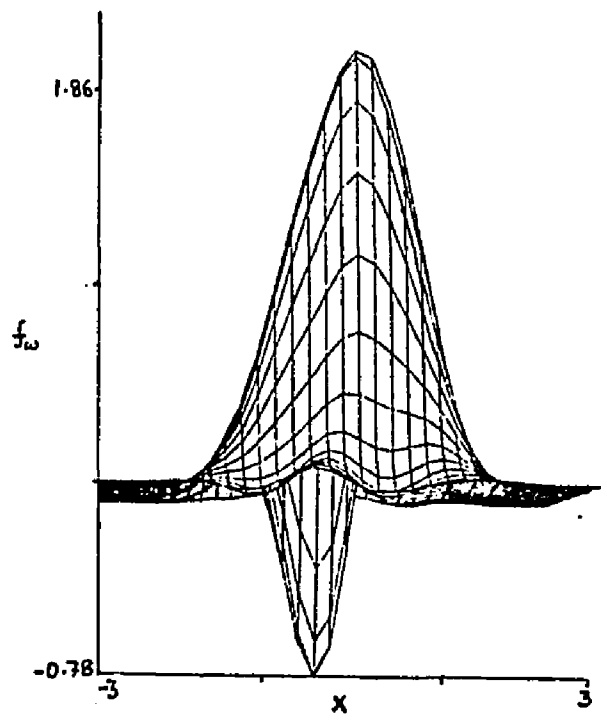
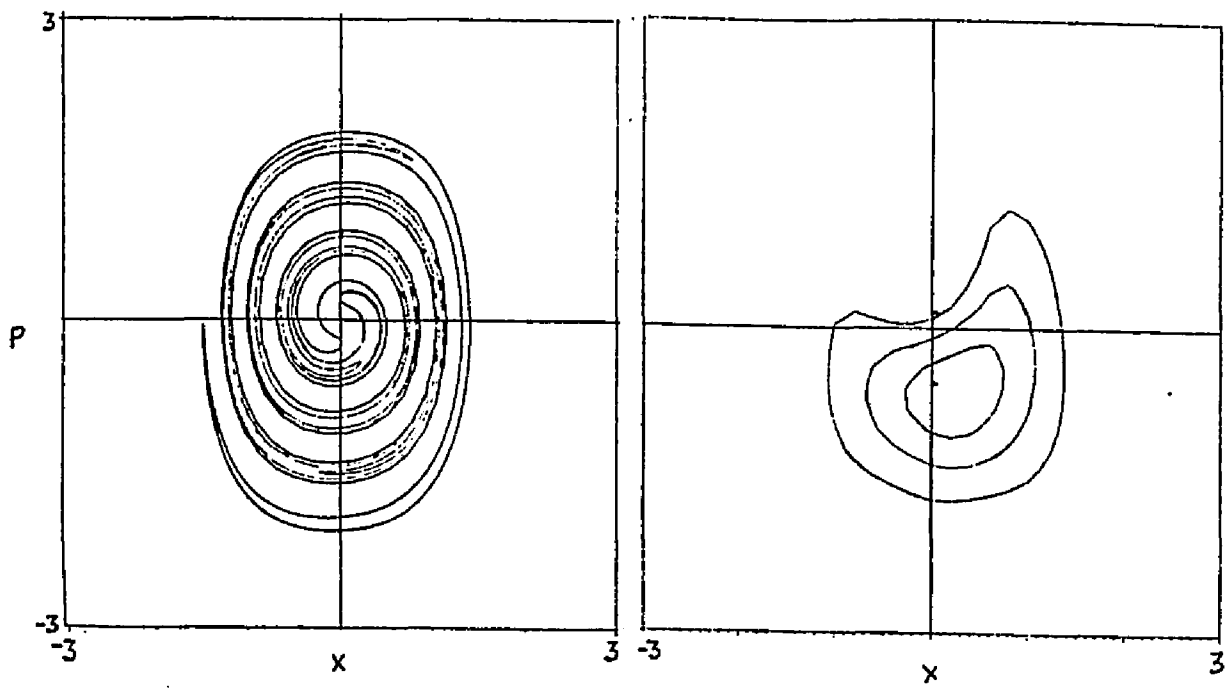


Figure 4.  $\beta = 1$   $k_2 = .5$   $T = 12\pi$

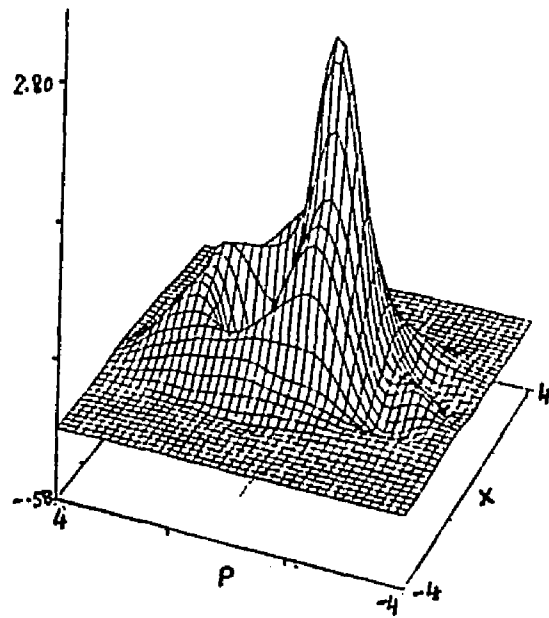
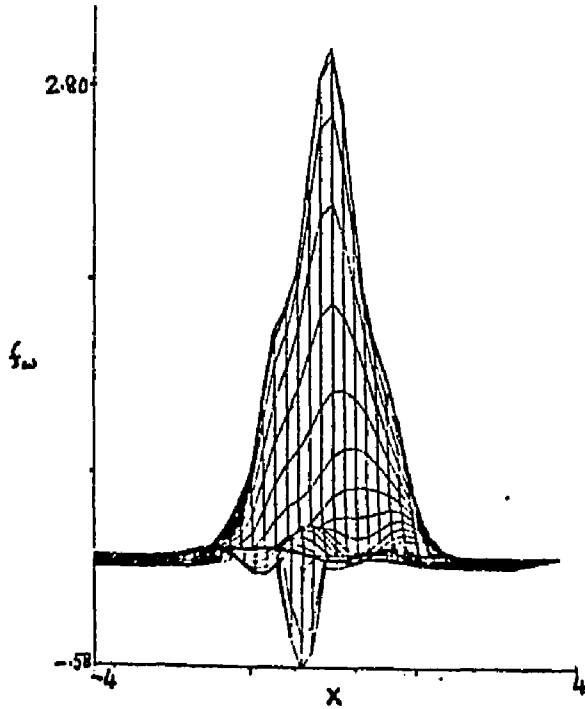
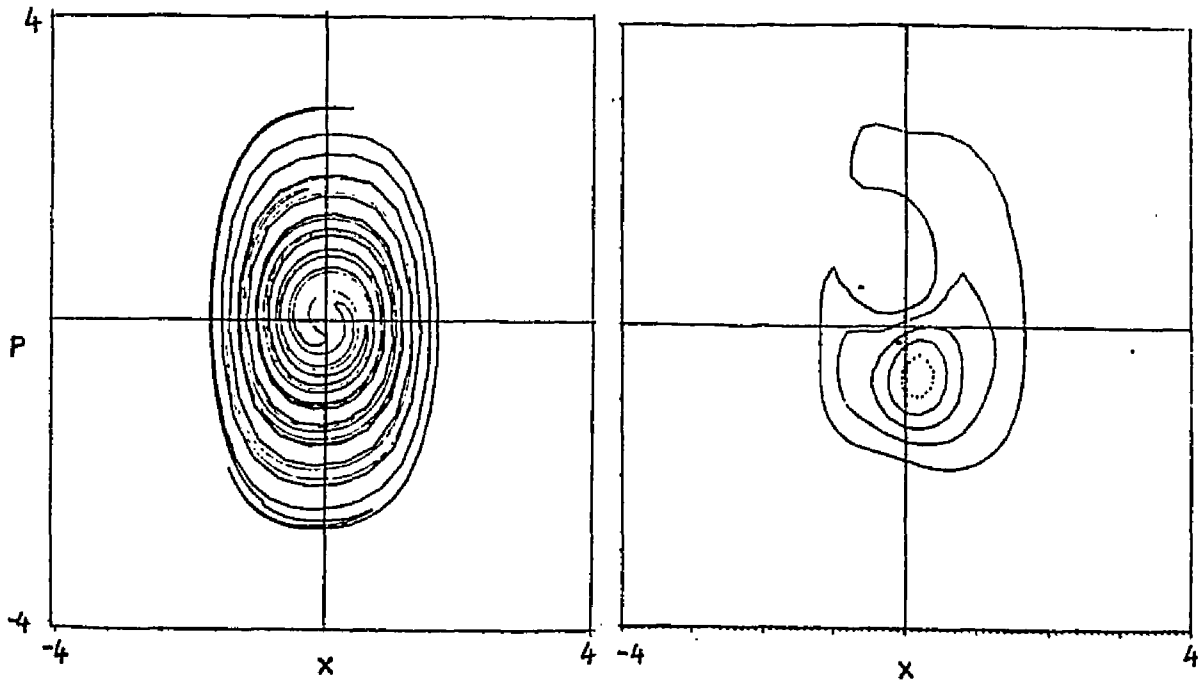


Figure 5.  $\beta = .5$   $k_2 = .5$   $T = 12\pi$

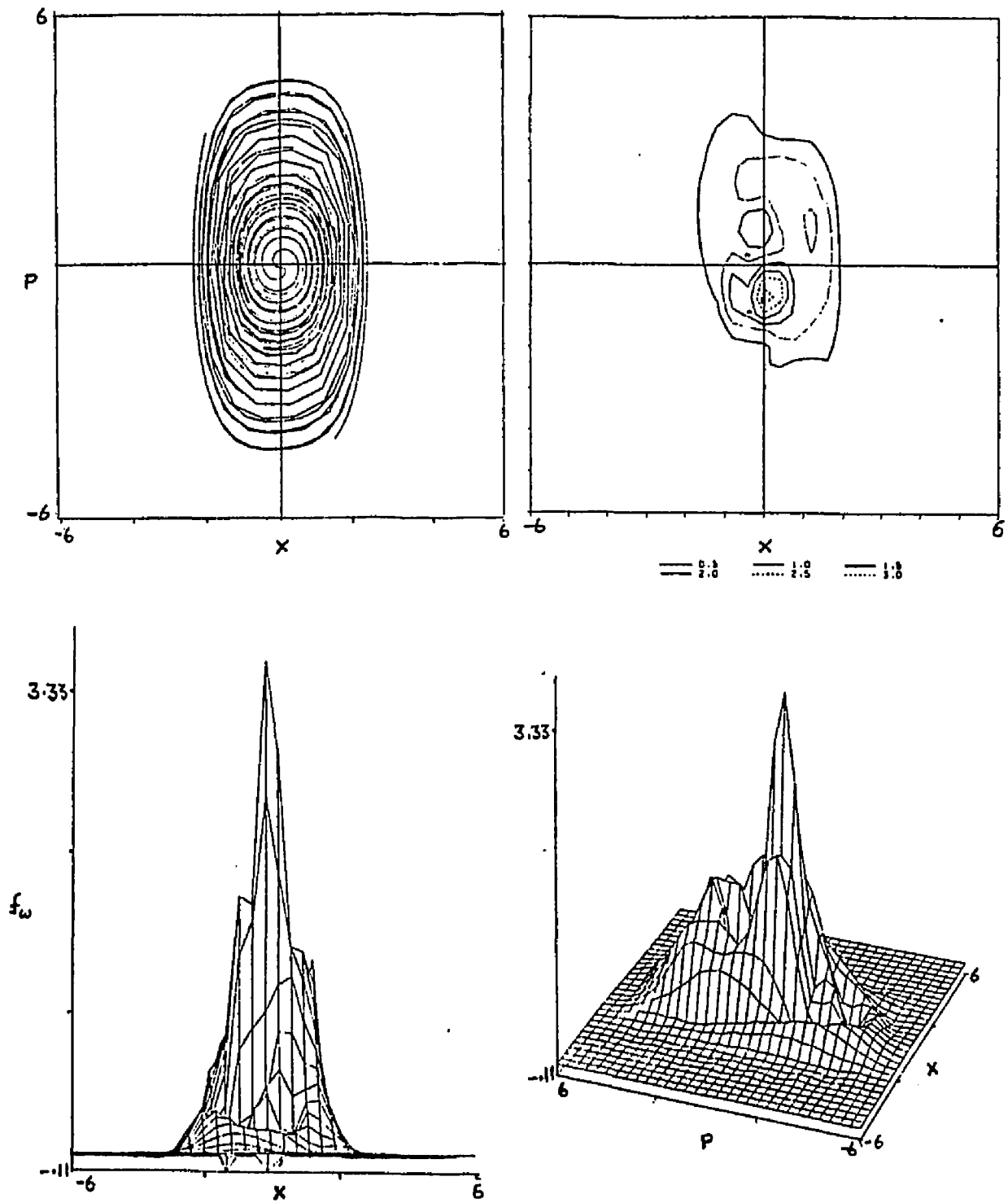


figure 6.  $\beta = .25$   $k_2 = .5$   $T = 12\pi$

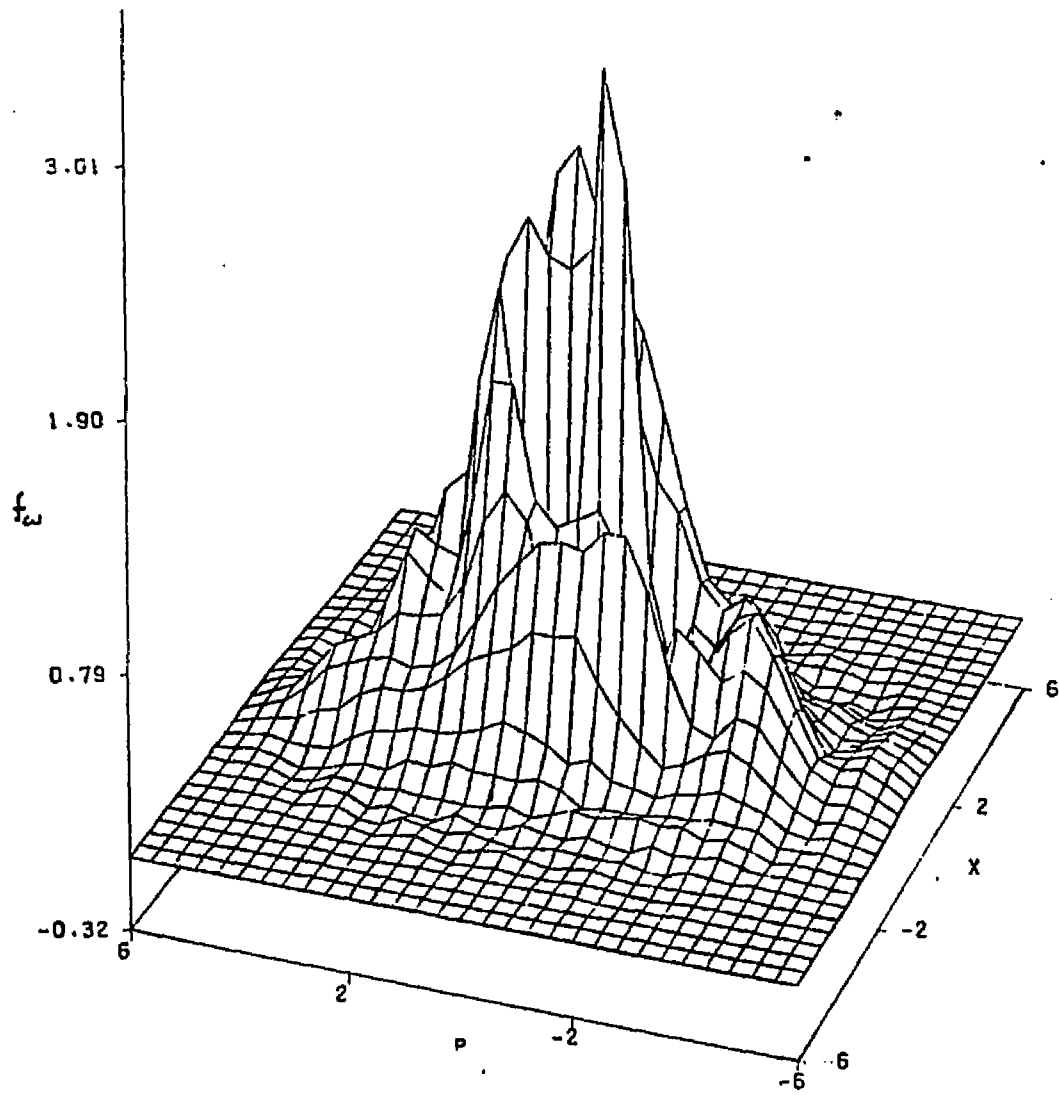


figure 7.  $\beta = .25$   $k_2 = .5$   $T = 6\pi$

## 2.5 Moments of the distribution

In this section the moments for the classical and the exact distributions are computed. These show interesting features.

### Classical Moments

Whereas the Liouville's theorem proved useful for drawing constant density contours, it is not suitable to extract information about the moments of the distribution.

For this purpose we initially populate phase-space with a set of sampled points

$$f_{\omega}(x,p,0) = (2\pi/N\beta) \sum \sigma_i \delta(x-x_i) \delta(p-p_i)$$

(the normalization is chosen such that it satisfies equation 2.3 and  $\sigma_i$  represents the sign of the function at the point  $x_i, p_i$ ) and propagate these points by the Hamilton's equations. In this case the points themselves do not carry information about the function but rather it is the density of points which defines the local function.

Averages are calculated as follows:

$$\langle x \rangle = 1/N \sum x_i \sigma_i$$

$$\langle p \rangle = 1/N \sum p_i \sigma_i$$

$$\langle x^2 \rangle = 1/N \sum x_i^2$$

$$\langle p^2 \rangle = 1/N \sum p_i^2$$

$$\langle xp \rangle = 1/N \sum x_i * p_i$$

with the width defined as

$$\alpha_x = \sqrt{(\langle x^2 \rangle - \langle x \rangle^2)}$$

and the correlation function as

$$\text{corr} = (\langle xp \rangle - \langle x \rangle \langle p \rangle) / (\alpha_x \alpha_p)$$

It is seen fig(8-10) that the total amplitude of the motion decays very rapidly, as the distribution of points acting independently spreads out uniformly in phase space consistent with energy. The widths also attain a constant value very rapidly. The motion becomes totally uncorrelated in the x and p variables.

#### Moments of the Quantum mechanical distribution

Expressions for the various moments may be derived. The expectation value of any observable is

$$\langle r \rangle = \frac{\beta}{2\pi} \int f_\omega(x, p) r dx dp$$

Substitute from equation 2.5

$$= \text{Re} \sum_m \sum_n^m (2 - \delta_{mn}) \langle \langle mn | \rho \rangle \rangle \frac{\beta}{2\pi} \int \langle \langle xp | mn \rangle \rangle r dx dp$$

$$= \text{Re} \sum \sum (2 - \delta_{mn}) \langle \langle mn | \rho \rangle \rangle \langle r \rangle_{mn}$$

where

$$\langle r \rangle_{mn} = \frac{\beta}{2\pi} \int \langle \langle xp | mn \rangle \rangle r dx dp$$

See appendix 2.5 for the explicit forms for  $\langle x \rangle_{mn}$ ,

$\langle p \rangle_{mn}$ ,  $\langle x^2 \rangle_{mn}$ ,  $\langle p^2 \rangle_{mn}$ ,  $\langle xp \rangle_{mn}$

### Pure Case

The frequency of the averages and the widths are basically that of a harmonic oscillator  $\approx 2\pi$ . In addition there appears a slow amplitude modulation. This implies that only a finite number of harmonic oscillator functions contribute significantly in the expansion and the modulations occur when these functions move in and out of phase recurrently.

It is of interest to note that a time dependent study of a probability distribution (not Wigner distribution) for a coherent state in an exactly solvable Hamiltonian shows these recurrences.<sup>13</sup>

### Mixed State

For highly mixed states the recurrence time is larger, as more representative states contribute significantly. Though the averages show a more pronounced modulation, the variances are more arbitrary in nature. This is because of the more complex structure into which the distribution evolves.

figures 8 - 10

fig 8. These show the variation of  $\langle x \rangle$  and  $\langle p \rangle$  with time for the classical and the exact case. The classical is denoted by the dotted line and the exact by the solid line.

fig 9-10. The top left represents  $\langle p \rangle$  plotted against  $\langle x \rangle$ . Top right represents the correlation function with time defined as  $\text{corr} = (\langle xp \rangle - \langle x \rangle \langle p \rangle) / \alpha_x \alpha_p$ . The bottom set represents the widths for  $x$  and  $p$  defined as  $\alpha_x = \sqrt{(\langle x^2 \rangle - \langle x \rangle^2)}$ . The dotted curves represents classical development.

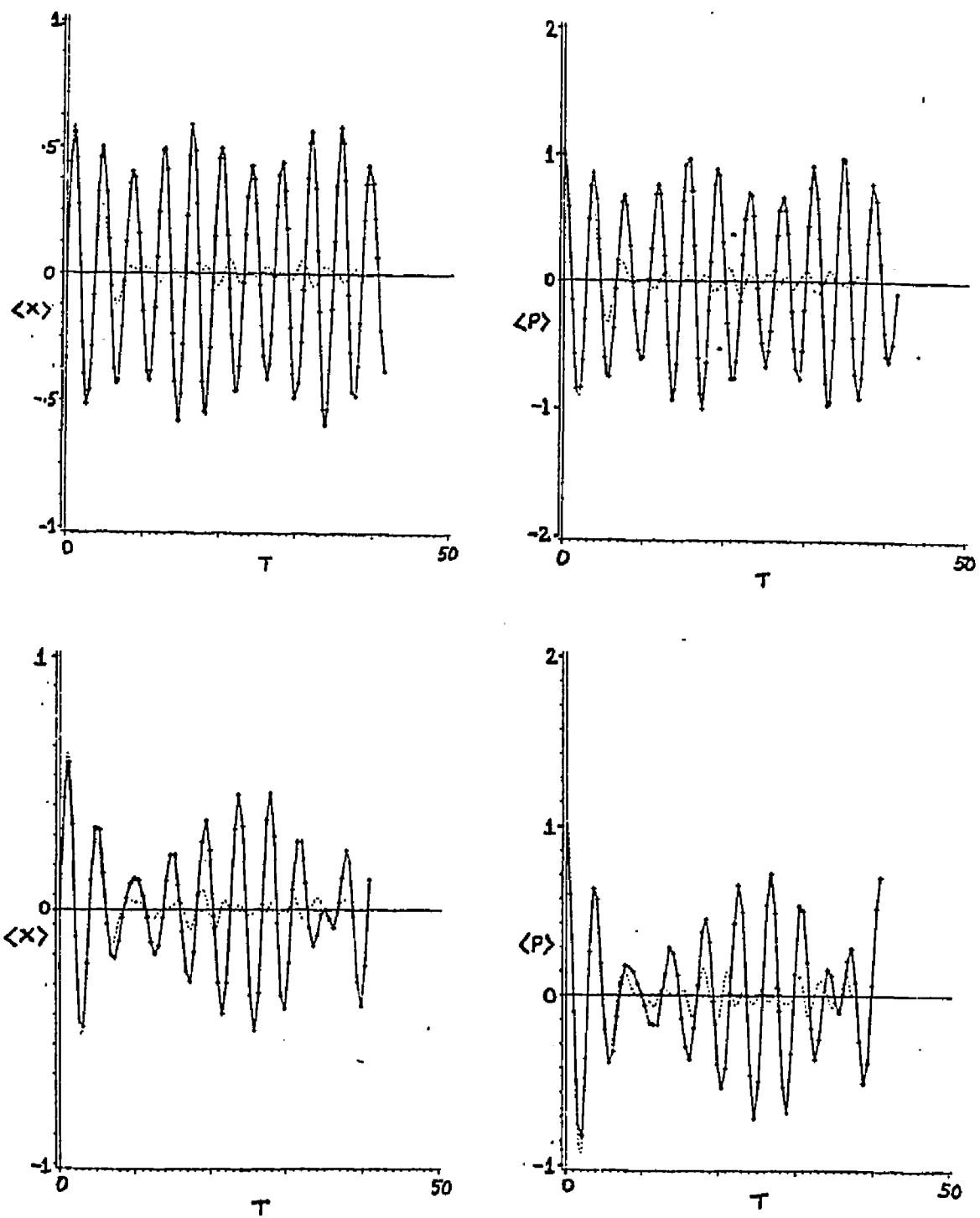


figure 8. top :  $\beta = 1$   $k_2 = 1$

bottom:  $\beta = .5$   $k_2 = .5$

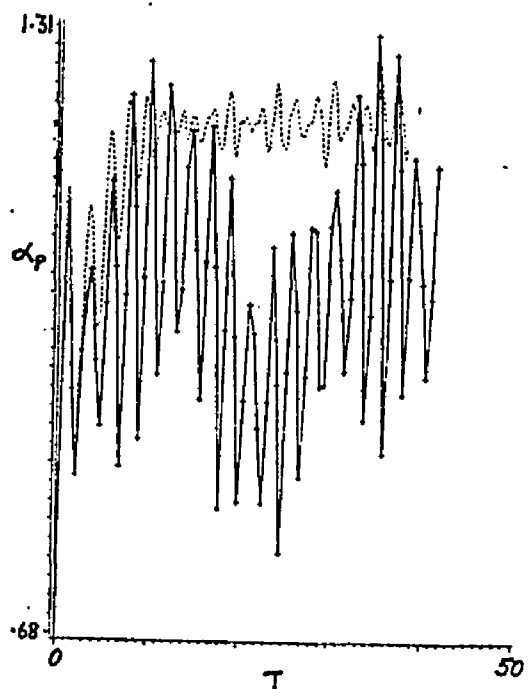
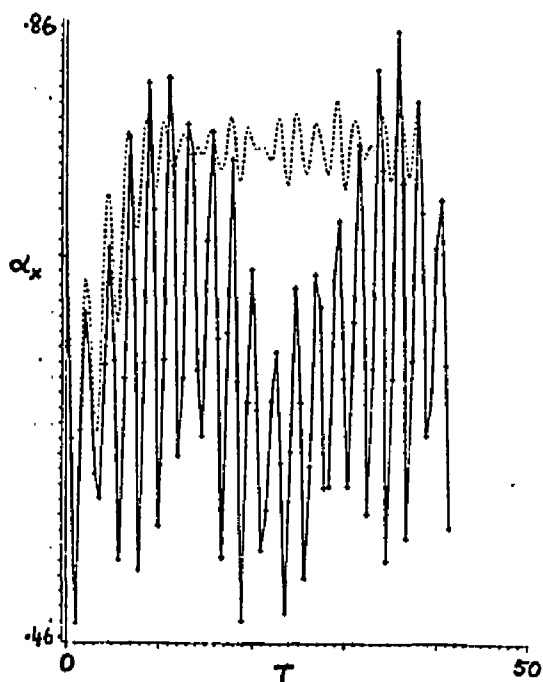
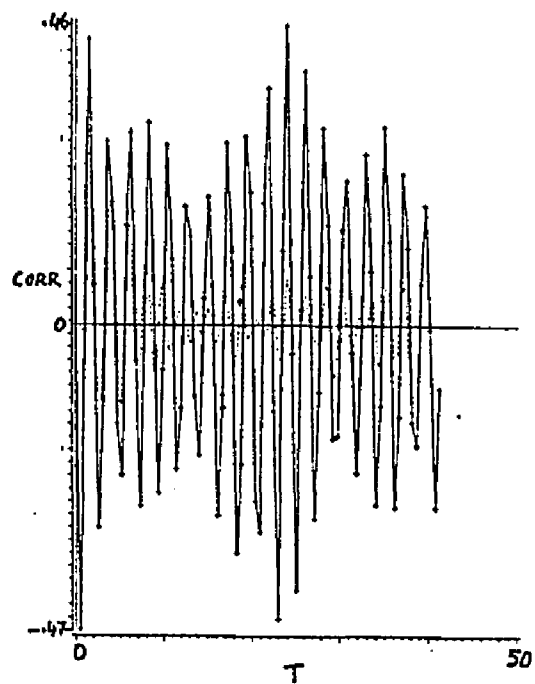
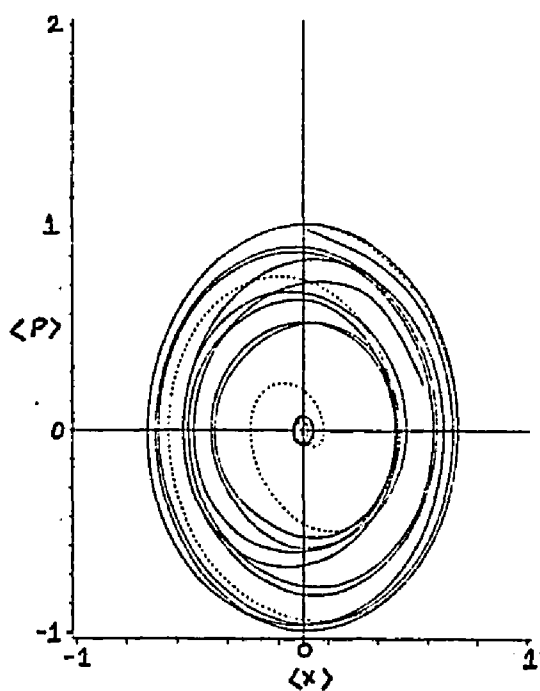


figure 9.  $\beta = 1$   $k_2 = .5$

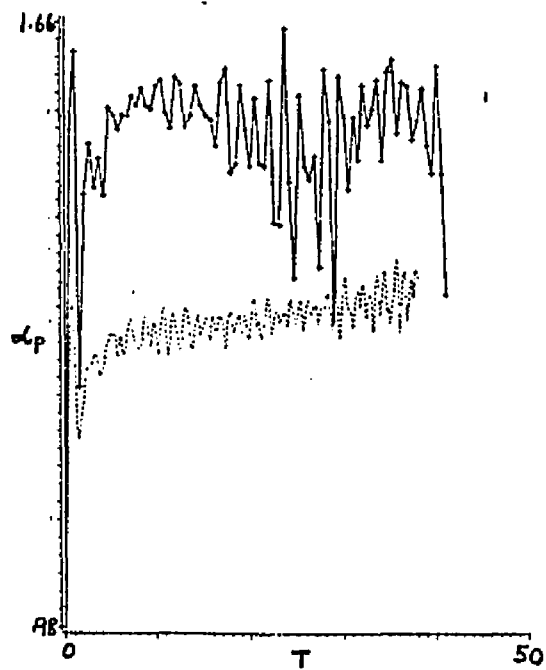
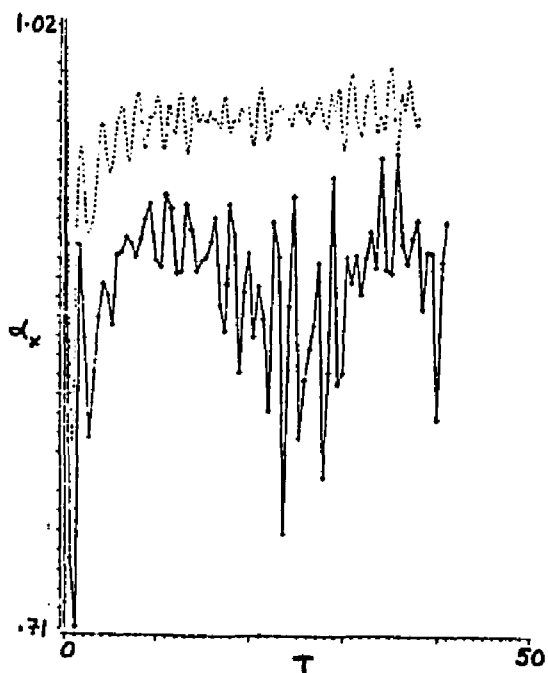
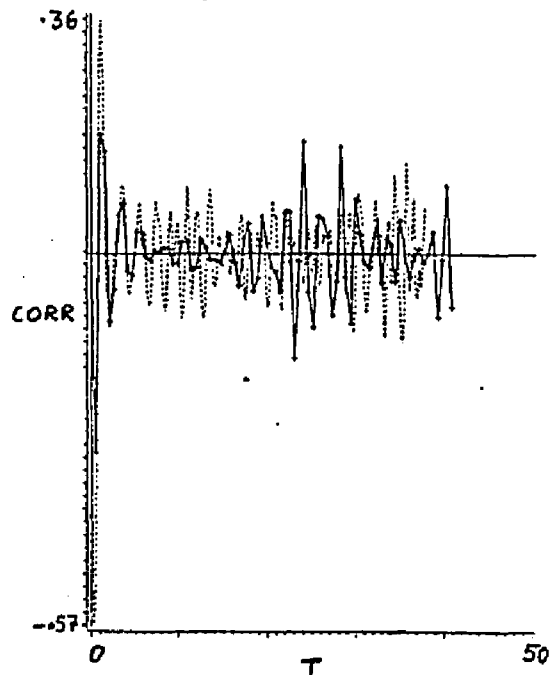
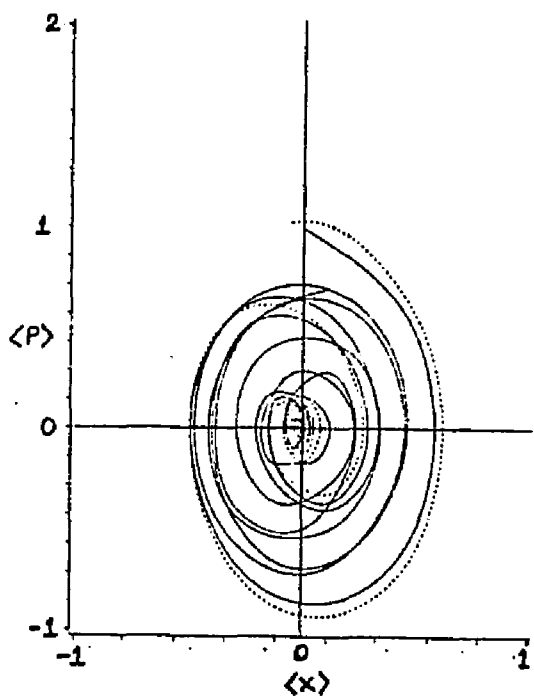


figure 10.  $\beta = .5$   $k_2 = .5$

## Chapter 3

### The Quantum Liouville Equation-A Numerical Approximation

It was seen in the previous chapter that the purely classical development differs significantly from the exact development of the Wigner function. An improvement over the classical may now be obtained by including the quantum term. An approximate computational method is discussed in this chapter to solve the quantum Liouville equation . The solution is expressed as a Markovian process in  $\Delta t$ .

#### 3.1 An approximate expression for the time development

The Liouville equation for the Wigner function is

$$\partial f_{\omega}(t)/\partial t = (L_C + L_Q) f_{\omega}(t) \quad (3.1)$$

A formal solution of equation (3.1) is

$$f_{\omega}(t) = \exp((L_C + L_Q)t) f_{\omega}(0) \quad (3.2)$$

Now with  $\Delta t = t/n$ ,

$$(e^{(L_C + L_Q)\Delta t})^n = (e^{L_C\Delta t} e^{L_Q\Delta t} + O(\Delta t^2))^n$$

This is the operator splitting formula (Trotter product) and it is assumed that  $O(\Delta t^2)$  is well behaved and bounded when applied to states. It can be shown that an

expression correct to  $(\Delta t)^2$  is given by (appendix 3.1)

$$e^{(L_c+L_q)\Delta t} = e^{L_c\Delta t/2} e^{L_q\Delta t} e^{L_c\Delta t/2}$$

However, in a Markovian chain (by this is meant that in an iterative chain, the transition probabilities in the stochastic process will be independent of the previous history of the the system) we have,

$$(e^{L_c\Delta t/2} e^{L_q\Delta t} e^{L_c\Delta t/2})^n = e^{L_c\Delta t/2} (e^{L_q\Delta t} e^{L_c\Delta t}) \dots e^{L_c\Delta t/2}$$

When  $n$  is large the first and the last terms may be ignored. Hence from the expression in the brackets on R.H.S it is seen that the expression to order  $\Delta t$  is effectively accurate to  $(\Delta t)^2$ .

### 3.2 A Numerical Method

A numerical method for studying the time development of  $f_\omega(x,p,t)$  is to approximate the function by a set of points in phase space, the density of points being proportional to the function at that region. The approximation is such that for an arbitrary test function  $g$  we have

$$\int f_{\text{approx}} g \approx \int f g$$

with 
$$f_{\text{approx}} = \frac{2\pi}{N} \sum_{i=1}^N \sigma_i \delta(x-x_i) \delta(p-p_i)$$

where the delta functions represent the point and  $\sigma_i$  is the sign of the function at the point.

Defining

$$\delta(\phi - \phi_i) = 2\pi \delta(x - x_i) \delta(p - p_i)$$

the representation becomes

$$f_\omega(x, p, 0) = \frac{1}{N} \sum \sigma_i \delta(\phi - \phi_i)$$

(In this study the initial function is always chosen as a gaussian and hence all  $\sigma_i$  are positive to begin with.)

At a later time  $\Delta t$ ,

$$\begin{aligned} f_\omega(x, p, \Delta t) &= e^{(L_c + L_q)\Delta t} f_\omega(x, p, 0) \\ &= (N)^{-1} \sum e^{(L_c + L_q)\Delta t} \delta(\phi - \phi_i) \end{aligned} \quad (3.3)$$

To a first approximation in  $\Delta t$  (we have seen that this is good to order  $(\Delta t)^2$  in a Markovian chain )

$$e^{(L_c + L_q)\Delta t} = e^{L_c \Delta t} + (e^{L_q \Delta t} - 1) e^{L_c \Delta t}$$

Substituting in 3.3

$$\begin{aligned} f_\omega(x, p, \Delta t) &= (N)^{-1} [ \sum e^{L_c \Delta t} \delta(\phi - \phi_i) + \\ &\quad \sum (e^{L_q \Delta t} - 1) e^{L_c \Delta t} \delta(\phi - \phi_i) ] \end{aligned} \quad (3.4)$$

Because these operators are linear the motion of each point may be studied separately. Hence each representative point transforms as

$$\delta(\phi - \phi_i) \rightarrow e^{L_c \Delta t} \delta(\phi - \phi_i) + (e^{L_q \Delta t} - 1) e^{L_c \Delta t} \delta(\phi - \phi_i)$$

The first term represents the classical motion and the second the quantum development of the classically shifted point.

### The Classical Development

The motion  $e^{L_c \Delta t} \delta(\phi - \phi_i)$  represents classical

motion and is the solution to the classical Liouville equation.

$$\begin{aligned} (\partial/\partial t) \rho &= L_C \rho \\ &= - \frac{\partial H}{\partial p} \frac{\partial \rho}{\partial x} + \frac{\partial H}{\partial x} \frac{\partial \rho}{\partial p} \end{aligned} \quad (3.5)$$

where

$$\rho = \delta(\phi - \phi_i)$$

The representative point in phase space follows the Hamilton's equation of motion.

$$\dot{x} = (\partial/\partial p)H \quad \text{and} \quad \dot{p} = -(\partial/\partial x)H$$

This defines a trajectory in phase space of the form  $x(t), p(t)$  and the moving point is represented as

$$\rho = \delta(x - x_i(t)) \delta(p - p_i(t))$$

To show that this form satisfies equation(3.5)

L.H.S.

$$\begin{aligned} &= (\partial/\partial t) [\delta(x - x_i(t)) \delta(p - p_i(t))] \\ &= (\dot{x}_i (\partial/\partial x_i) + \dot{p}_i (\partial/\partial p_i)) \delta(x - x_i(t)) \delta(p - p_i(t)) \end{aligned}$$

R.H.S.

$$= ((\partial H/\partial p) (-\partial/\partial x_i) - (\partial H/\partial x) (-\partial/\partial p_i)) \delta(x - x_i(t)) \delta(p - p_i(t))$$

Clearly this is satisfied with

$$\dot{x}_i = (\partial H/\partial p) \quad \dot{p}_i = -(\partial H/\partial x)$$

Hence the solution to the classical equation is also a delta function. The motion is a canonical contact transformation in time. We may denote this point as  $\delta(\phi - \phi_i(\Delta t))$ .

### The Quantum Development

The effect of the quantum development on a point is represented as

$$(e^{L_q \Delta t} - 1) \delta(\phi - \phi_i)$$

The operator  $L_q$  has momentum derivative operators only and hence the expression becomes

$$\begin{aligned} &= 2\pi \delta(x - x_i) (e^{L_q \Delta t} - 1) \delta(p - p_i) \\ &= 2\pi \delta(x - x_i) J(p - p_i) \end{aligned} \quad (3.6)$$

where

$$J(p - p_i) = (e^{L_q \Delta t} - 1) \delta(p - p_i) \quad (3.7)$$

From equation(3.6) it is seen that the effect of the quantum operator on a point is to change it into a function  $J(p - p_i)$  along the momentum axis located at  $x_i$ . Hence the overall picture is as follows: a representative point undergoes a classical motion in time  $\Delta t$ , followed in addition by a quantum development  $J(p - p_i)$  along the momentum axis. The function  $J(p - p_i)$  is such that there is no net change of the normalization of the initial Wigner function, that is

$$\int J(p - p_i) dp = 0 \quad (3.8)$$

To see this, rewrite it as (eqn 3.6)

$$\int e^{L_q \Delta t} \delta(p' - p_i) dp' - \int \delta(p' - p_i) dp' = 0$$

The first term may be written as

$$\begin{aligned} &\int (1 - a \frac{\partial}{\partial p^3} + \text{higher order derivatives}) \delta(p - p_i) dp \\ = &\int_0^{(p-p_i)} (1 - a \frac{\partial}{\partial p^3} + \text{higher order derivatives}) \delta(p - p_i) dp \\ &\quad \text{(integrating by parts)} \end{aligned}$$

which proves the result.

Now with

$$J_{\pm} = |J| \delta_{(\pm, \text{sign}J)}$$

(where  $\text{sign}J$  is the sign of the function  $J$ )  $J$  can be written as

$$J = J_+ - J_-$$

with  $J_+$  signifying the positive part of the function and  $J_-$  the negative part of the function. Hence from 3.8

$$A_i = \int J_+ dp = \int J_- dp$$

Let us multiply and divide  $J_i$  by  $A_i$ . This will make the functions  $J_{i\pm}/A_i$  normalized to unity.

$$J_i = A_i \left( \frac{J_+(p-p_i)}{A_i} - \frac{J_-(p-p_i)}{A_i} \right) \quad (3.9)$$

Summing over all the points (eqn. 3.4)

$$f_{\omega}(x, p, \Delta t) = (N)^{-1} \sum \delta(\phi - \phi_i(\Delta t)) + \\ (2\pi/N) \sum A_i \left( \frac{J_+(p-p_i(\Delta t))}{A_i} - \frac{J_-(p-p_i(\Delta t))}{A_i} \right) \delta(x-x_i(\Delta t)) \quad (3.10)$$

Two computational advantages are obtained by writing the equation in the above form:

### 1. Pair production and Jump probabilities

First, the functions  $(J_i/A_i)$  can be represented in a stochastic manner as follows: by a Monte Carlo process we select a pair of points at  $p_{\pm}$  to represent the

function.  $p_+$  will be a sample point representing  $J_+/A$  and  $p_-$  that representing  $J_-/A$ . i.e. we represent the unit normalized quantum motion by

$$J_i(p-p_i(\Delta t))/A_i \rightarrow \sigma_{+\delta}(p-p_+) + \sigma_{-\delta}(p-p_-) \quad (3.11)$$

where  $\sigma_{\pm} = \pm \sigma_i$ . The probability measure for the selection of a point at  $p_{\pm}$  is given by (also called the jump probability)

$$J_i(p_{\pm}-p_i) / A_i$$

A sampled set representing the quantum function may thus be obtained over a large number of time steps. By decreasing the time steps the equivalent number of points sampled is increased and a better representation for the quantum effects is obtained.

## 2. Creation Probabilities $A_i$

Next consider the multiplicative factor  $A_i$  occurring in Equation 3.10.  $A_i$  now may be interpreted as a creation probability for the point  $i$  to have a quantum motion via a stochastic pair production. For a probabilistic interpretation  $A_i$  must be  $< 1$ . (this can be done by selecting  $\Delta t$  appropriately) A random number generator then selects the points for which the quantum motion is to occur by successively assigning to each of the points  $i$  a probability measure of  $A_i$ .

These selected points then undergo the stochastic pair production as given in 3.11. Hence after each interval of time  $\Delta t$  a new generation of positive and negative points are created which together participate in successive time evolution via the classical-quantum Markovian chain.

## Chapter 4

### Quantum development in the quasi-classical limit. A test of the Stochastic Method

In the previous chapter it was shown that the motion of a point in phase space can, to the first order in  $\Delta t$ , be separated to that of a classical motion, followed by a quantum development represented by the function  $J(p-p_i)$ .

In this chapter a numerical study of the pure quantum development, in the quasi-classical limit is done to test the validity of the probabilistic and stochastic interpretation we have given for the function  $J$  in a numerical procedure.

#### 4.1. The quantum development of a delta function

The quantum motion of a point is given by (eqn3.6)

$$(e^{L_q \Delta t} - 1) \delta(\phi - \phi_i) = 2\pi \delta(x - x_i) J(p - p_i)$$

where

$$J(p - p_i) = e^{L_q \Delta t} \delta(p - p_i) - \delta(p - p_i)$$

In the quasi-classical limit

$$L_q \Delta t = - a \partial^3 / \partial p^3 \quad (4.1)$$

Hence

$$J(p-p_i) = e^{-a\theta p^3} \delta(p-p_i) - \delta(p-p_i) \quad (4.2)$$

Now

$$\begin{aligned} e^{-a\theta p^3} \delta(p) &= e^{-a\theta p^3} \frac{1}{2\pi} \int e^{ipx} dx \\ &= \frac{1}{2\pi} \int e^{iax^3 + ipx} dx \end{aligned}$$

This is the Airy integral. This function decreases exponentially along the +p axis and is oscillatory along the -p axis. However this function is not a suitable choice for computational purposes as the oscillatory amplitude decays asymptotically only as  $(a^{-1/3}p)^{-1/2}$ . What is needed are functions with stronger cut-off rates which will give reasonable values for the creation probabilities  $A_i$  and will also give low probabilities of pair production at large distances from the point.

To achieve this let us now smear out the points by using distributions of width  $\alpha$ -s over it. In addition this procedure is also absolutely necessary because only a finite number of points are used to represent the function and the sum of the smeared points will be a closer representation of the function than a sum of spiked delta functions. Therefore we write

$$\delta(\phi - \phi_i) \rightarrow \delta_\alpha(\phi - \phi_i)$$

where  $\delta_\alpha$  represents a distribution.

By using these distributions, exponentially damped

functions for  $J$  are obtained.

We have studied two such distributions : the lorentzian distribution and the gaussian distribution. The lorentzian decreases as  $1/p^2$  whereas the gaussian decreases exponentially. Therefore the gaussian is found to be a better representation of the delta state. The lorentzian case is treated in detail in Appendix B. Yet another method to study the quantum development was to do a discrete differentiation on the delta state.

(Appendix A)

#### 4.2 The Quantum development of the Gaussian distribution

The quantum development for the Gaussian distribution will be considered now. A normalized Gaussian distribution has the form

$$\delta_{\alpha}(p) = \frac{1}{\sqrt{(2\pi)\alpha}} e^{-p^2/2\alpha^2}$$

with an integral representation

$$\delta_{\alpha}(p) = \frac{1}{\sqrt{(2\pi)\alpha}} \int_{-\infty}^{\infty} e^{i/2py/\alpha - y^2} dy$$

Let

$$\begin{aligned} I(p,a) &= e^{-a\partial^3/\partial p^3} \delta_{\alpha}(p) \\ &= \frac{2 \operatorname{Re}}{\sqrt{2\pi} \alpha} \int_0^{\infty} e^{ia'y^3 - y^2 + ip'y} dy \end{aligned}$$

where  $p' = (\sqrt{2/\alpha}) p$

and  $a' = a(\sqrt{2/\alpha})^3$

### Evaluation of $I(p,a)$

This is evaluated as a series expansion for  $a \ll 1$  and by an asymptotic expansion for large  $p'$  by steepest descent methods, the details of which may be found in appendix 4.

Finally the quantum development is given by

$$J(p,a) = I(p,a) - \delta_\alpha(p)$$

see figure 11-12 for the plots of  $I(p,a)$  and  $J(p,a)$ .

### 4.3 A Numerical Test comparing the exact vs. the stochastic development

The test function chosen is a gaussian of a large width  $\alpha_1$ .

$$f(p) = \frac{1}{\sqrt{(2\pi)\alpha_1}} e^{-p^2/2\alpha_1^2}$$

The exact development is given by

$$e^{Lqt} f(p) = e^{-a' \partial^3/\partial p^3} f(p)$$

and is evaluated as in the previous section. For the stochastic development,  $f(p)$  is represented as a set of smeared delta functions as

$$f_{\alpha_1}(p) = N^{-1} \sum_{i=1}^N \delta_{\alpha_S}(p-p_i)$$

where  $\delta_{\alpha_S}$  is a gaussian delta distribution of smaller width  $\alpha_S$  with  $\alpha_S \ll \alpha_1$ . Now with  $a = a'/n$

$$e^{Lqt} f(p) = (e^{Lqt/n})^n f(p) = (e^{-a\partial^3/\partial p^3})^n f(p)$$

$$\begin{aligned}
&= e^{Lqt/n} \dots [(e^{Lqt/n-1})f(p) + f(p)] \\
&= e^{Lqt/n} \dots f_1(p) \\
&= f_n(p)
\end{aligned}$$

where

$$\begin{aligned}
f_1(p) &= (e^{-a\theta^3/\partial p^3} - 1)f(p) + f(p) \\
&= N^{-1} \sum (e^{-a\theta^3/\partial p^3} - 1) \delta_{\alpha_S}(p-p_i) - \delta_{\alpha_S}(p-p_i)
\end{aligned}$$

$$\begin{aligned}
f_2(p) &= e^{Lqt/n} f_1(p) \\
&= (e^{-a\theta^3/\partial p^3} - 1)f_1(p) + f_1(p)
\end{aligned}$$

etc.

Each step can now be treated as a stochastic evolution .

### Stochastic Development

The quantum motion of each point is given by fig.13

$$\begin{aligned}
(e^{-a\theta^3/\partial p^3} - 1) \delta_{\alpha_S}(p-p_i) &= J(p-p_i, a) \\
&= A \left( \frac{J_+}{A} - \frac{J_-}{A} \right)
\end{aligned}$$

The creation probability A is now the same for all the points. Now, given that a point has been selected, a pair of points are to be created to represent its quantum development in a stochastic manner. This pair is selected as follows: First, a table of values for

$J'_{\pm}(p)$  vs.  $p$  is constructed for  $\alpha$ -s where  $J'_{\pm}$  is

$$J'_{\pm}(p) = \int_{-\infty}^p \frac{J_{\pm} dp}{A} \quad (4.3)$$

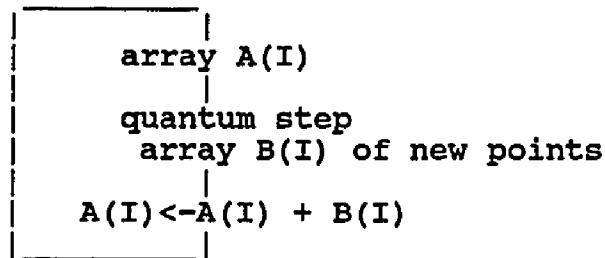
The function  $J'_{+}(p,a)$  vs.  $p$  (see fig.14) can be considered as a mapping of the probability areas  $J_{+}\Delta p/A$  onto a unit line (along the  $y$  axis). The points on this unit line are given an equal a priori probability. A random number generator picks a point on this line and the corresponding value for the momentum gives  $p_{+}$ . A newly created point is now placed at  $\delta(p-(p_i+p_{+}))$  with a sign equal to  $\sigma_i$ . Similarly we select a random point  $p_{-}$  from  $J'_{-}$  to be placed at  $\delta(p-(p_i+p_{-}))$  with sign  $-\sigma_i$ .

#### The Algorithm

By a Monte Carlo process of importance sampling (see section 5.1, initial population) a sampled set of points is chosen to represent the test function. The  $p$  axis is then divided into bins of width  $\Delta p$  and the points are placed in them.

$$f_{\alpha 1} = N^{-1} \sum_b n_b \delta(x-x_b) \sigma_b$$

where  $n_b$  is the number of points in the  $b$ -th bin which lies between  $p_b$  and  $p_b + \Delta p$ . Let the initial list of points be in the array  $A(I)$ . At each time step  $\Delta t$  the newly created points are placed in a separate array of bins  $B(I)$ . Finally add up  $A(I) + B(I)$ . In this summation some negative and positive points cancel. The following loop is executed  $n$  times.



After n time steps a function is reconstructed from the final array as follows: using a complete set of orthonormal Harmonic Oscillator states  $|n\rangle$  the final array of points may be rewritten as

$$\begin{aligned} \sum_b n_b \delta(p-p_b) \sigma_b &= \sum_b n_b \sigma_b \langle p|p_b\rangle \\ &= \sum_{b,n} n_b \sigma_b \langle p|n\rangle \langle n|p_b\rangle \end{aligned}$$

The orthonormal wave functions are given by

$$\langle p|n\rangle = (2^n n! / \pi)^{-1/2} e^{-p^2/2} H_n(p)$$

While using a finite number of points and grids it is necessary to truncate the infinite sum to yield a smooth function. (see section 5.1 reconstruction of function)

### Analysis and Conclusions

An extensive test was done varying all the parameters to see how good the stochastic approximation is to represent the true function. fig.15-22

For the exact solution a gaussian function of width  $\alpha^{-1} = 1$ . was selected and  $a' = .1$  This is represented by the solid line in all the plots. The smearing widths for the delta functions was chosen as  $\alpha^{-s} = .3$  and  $a = .001$

Variation with number ,N

Runs were made for  $N = 1000, 5000, 20000$ . As expected a larger number of points gives a better fit.  
fig. 15

Variation with number of smoothin functions

These show that there is an optimum value for the number of basis functions to be used in a reconstruction procedure. fig. 16

Variation with statistics

To test for statistical variation runs were made with different initial points for  $N = 10000$ .  
See figure 17.

Variation with a

Using  $N=10000$  runs were made with values of  $a = .01, .05, .002$ , and total number of steps of 10, 20, and 50 respectively to reach  $a' = .1$ . It is seen that the general features are reproduced to a good degree within statistical error even for large  $a$ .  
fig. 18.

Variation with  $\alpha$ -s

With  $N = 10000$ , the smearing widths are varied as  $\alpha$ -s = .2, .3, and .4 respectively. Again the agreement is good within statistical deviations. It must be

pointed out that this independence in  $\alpha$ -s occurs only for large N. See next section for tests with N=1000.

fig.19

### Variation with bin-size

The following tests were done with N = 1000.

Although such a small number is bound to produce large statistical variations, in chapter 5 we will be computer limited to use numbers of this order. The statistical correspondence however is not identical to that covered in Chapter 5. We study the effect of variation of bin-size for various values of  $\alpha$ -s.

Set  $\alpha-1 = 1$ ,  $a = .001$ ,  $N = 1000$

1.  $\alpha$ -s = .2 , the comparison is poor. fig. 20
2.  $\alpha$ -s = .3 , we have the general features of the maxima and the minima following the exact curve. fig. 21
3.  $\alpha$ -s = .4 , whereas the smaller bins give better results, the fit becomes progressively bad for higher bin sizes. fig. 22

We conclude that for smaller values of N there is an optimum value of  $\alpha$ -s that best represents the function. This is to be expected because the graininess introduced by a finite number of points will be best smoothed by an optimum value of  $\alpha$ -s. Again we emphasize that for large N, the stochastic curves show a fair independence of  $\alpha$ -s. fig.19

figure 11-14

fig 11  $I(p,a)$  vs.  $p$  for a gaussian distribution. The solid curve is the initial gaussian function for  $\alpha = .3$  The two dotted curves represent the function for values of  $a = .05, .1$

fig.12  $J(p,a)$  vs.  $p$  for values of  $a = .05, .1$

fig.13  $J(p,a)$  vs.  $p$  for  $a = .001$  which is a typical value used in the evaluation of the stochastic time development.

fig.14 The function  $J'$  maps the jump probability measures  $J\Delta p/A$  onto a unit line, the points on which are then selected randomly.

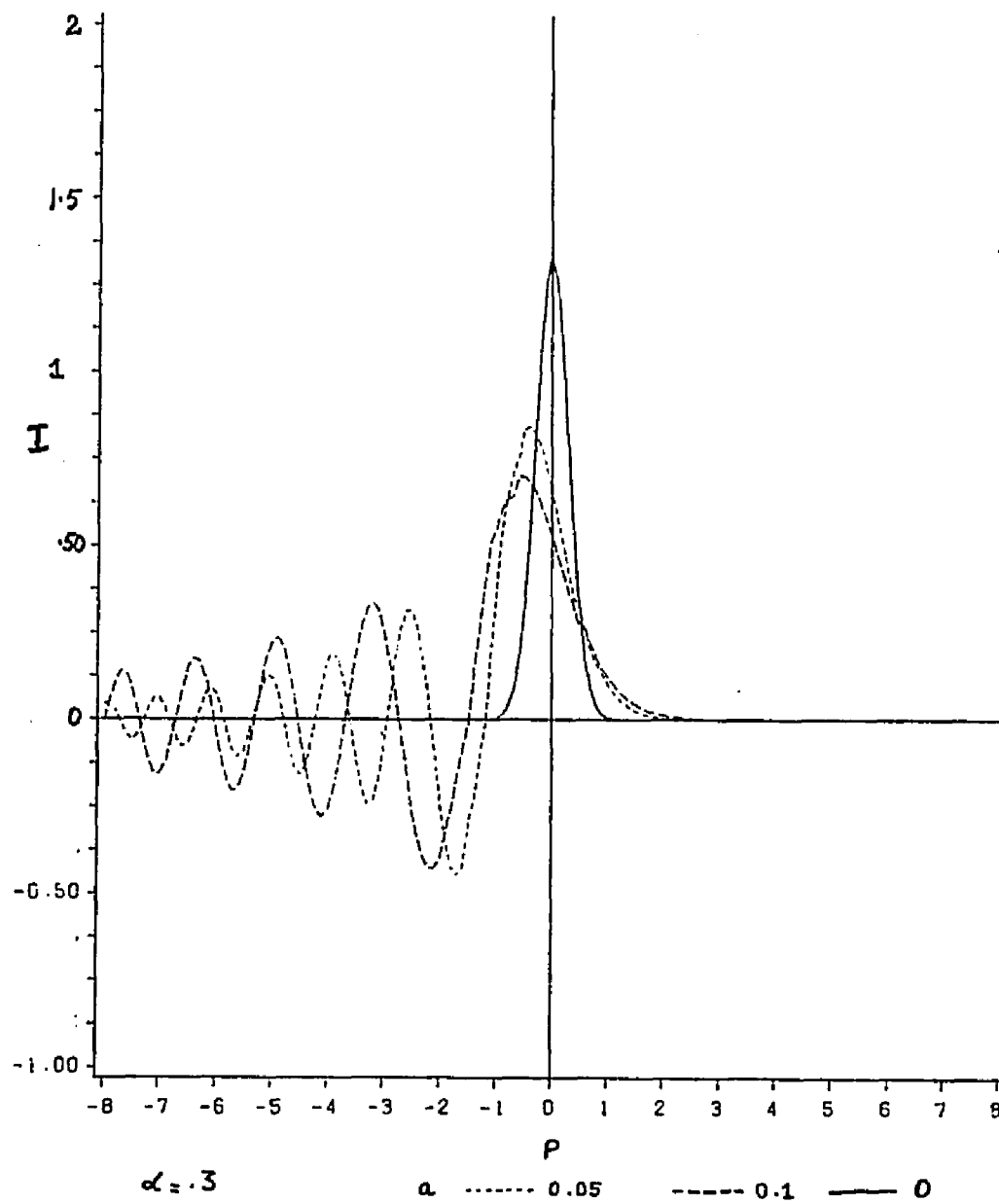


figure 11

## QUANTUM TIME DEVELOPMENT-EXACT

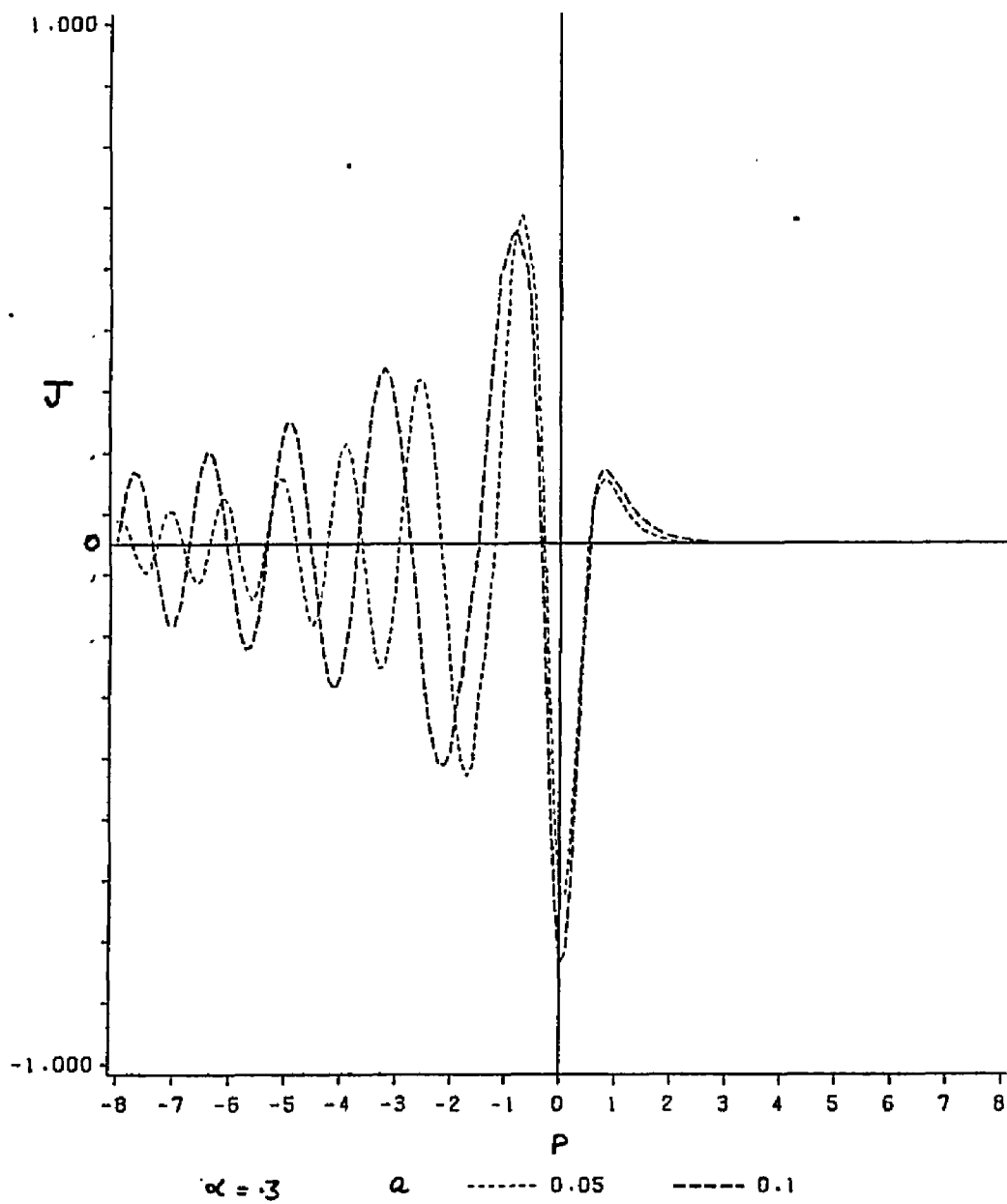


figure 12

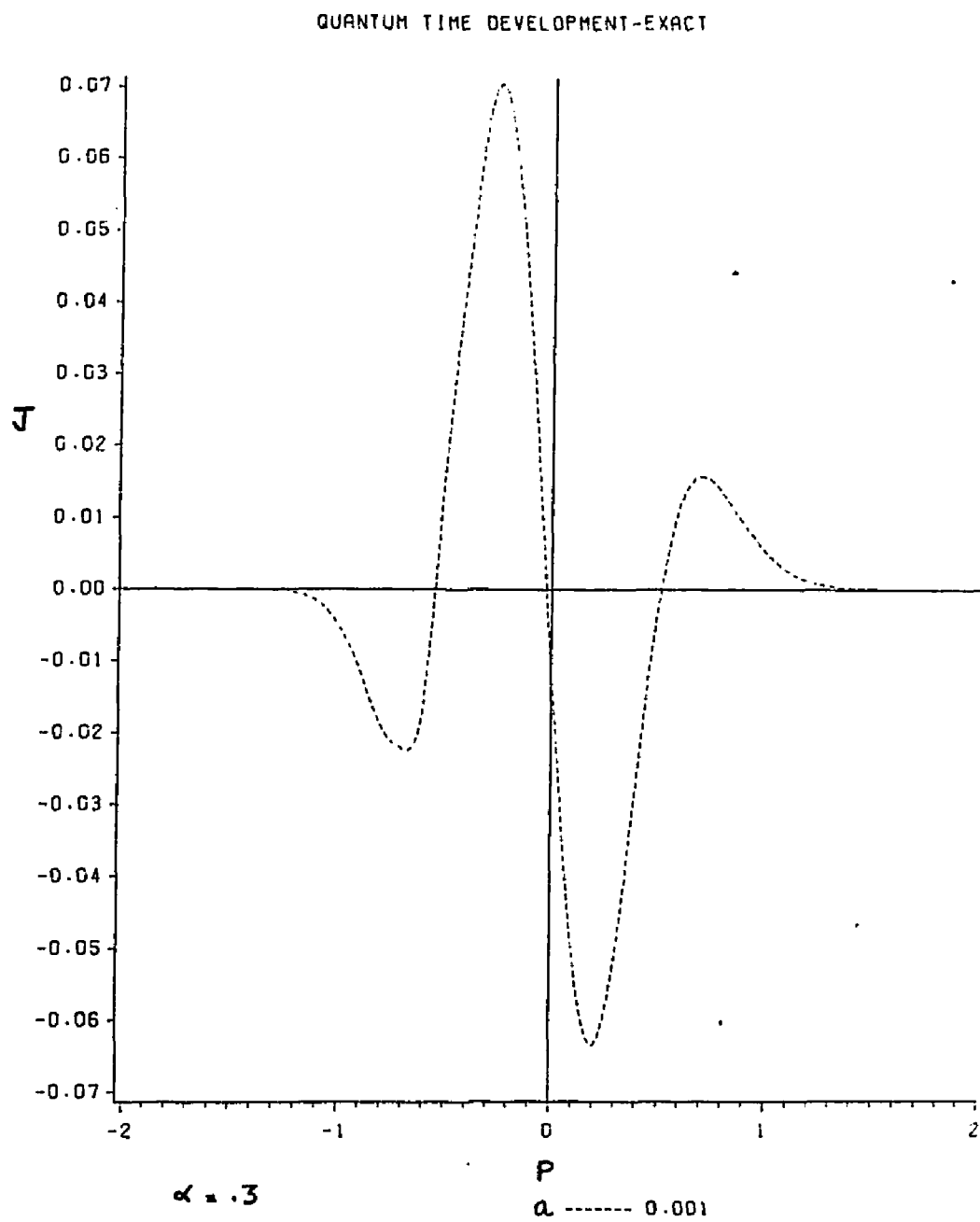


figure 13

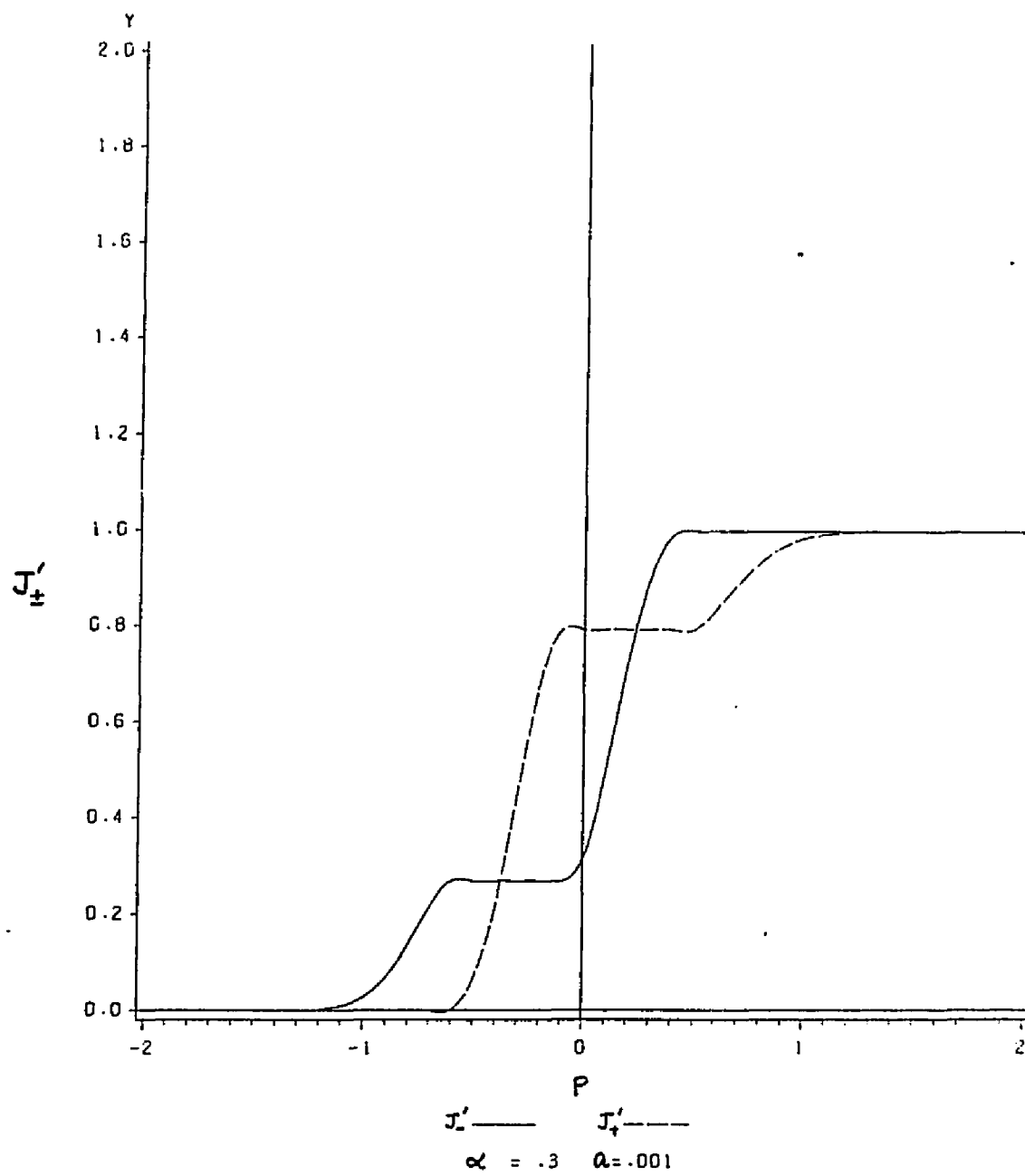


figure 14

figures 15-22

fig 15-19. These pictures compare the stochastic quantum development (the dotted curves) with the exact (solid line).  $a'=.1$  ,  $\alpha-1 = 1$ , bin-size =.05  
 $a=.001$

fig.15 Variation with number

fig.16 Variation with number of smoothing functions

fig.17 Statistical variation

fig.18 Variation with 'a'

fig.19 Variation with  $\alpha-s$

fig. 20-22 Variation with bin-size(annihilation distance) with  $N = 1000$

fig.20  $\alpha-s = .2$

fig.21  $\alpha-s = .3$

fig.22  $\alpha-s = .4$

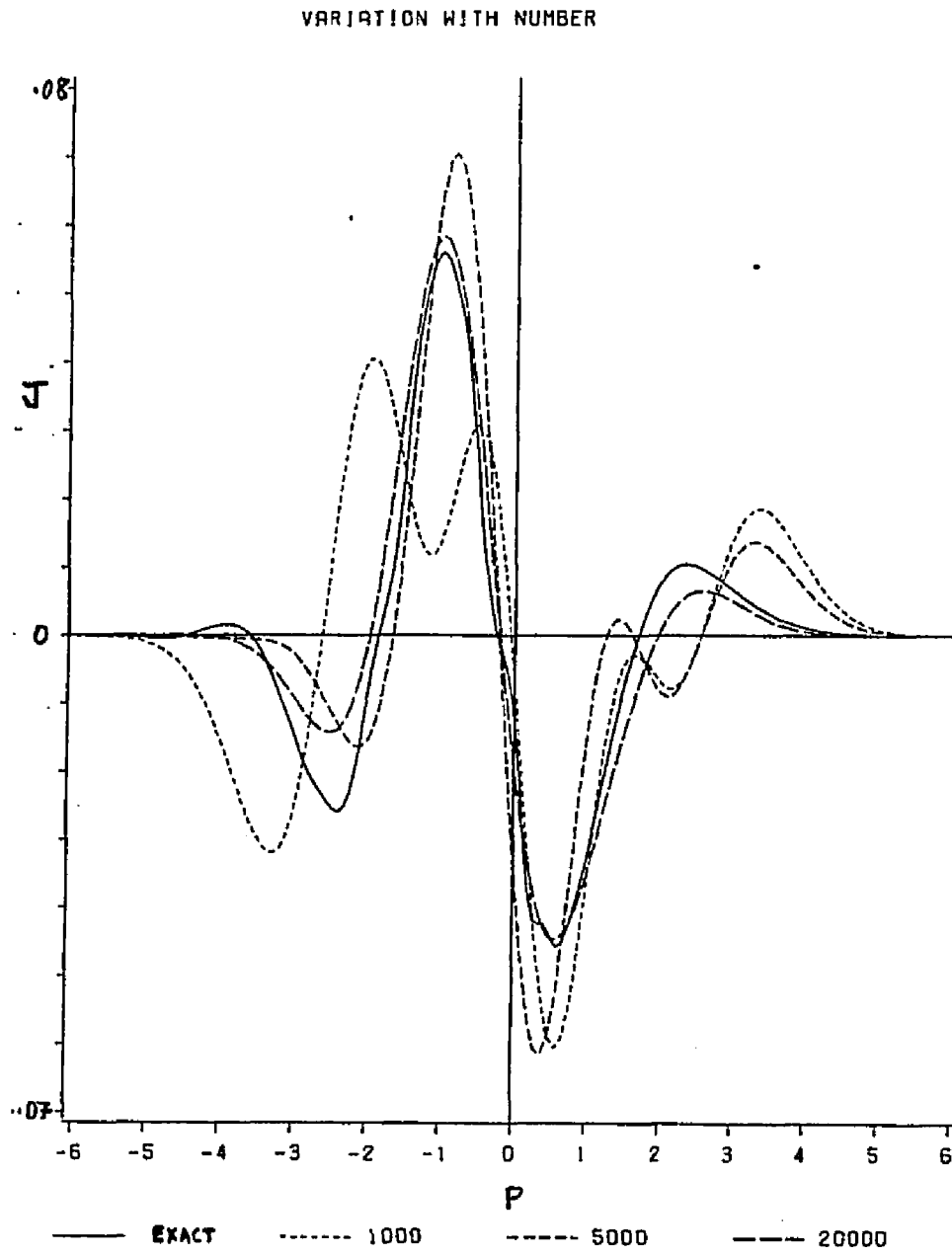


figure 15

## VARIATION WITH NUMBER OF SMOOTHING FUNCTIONS

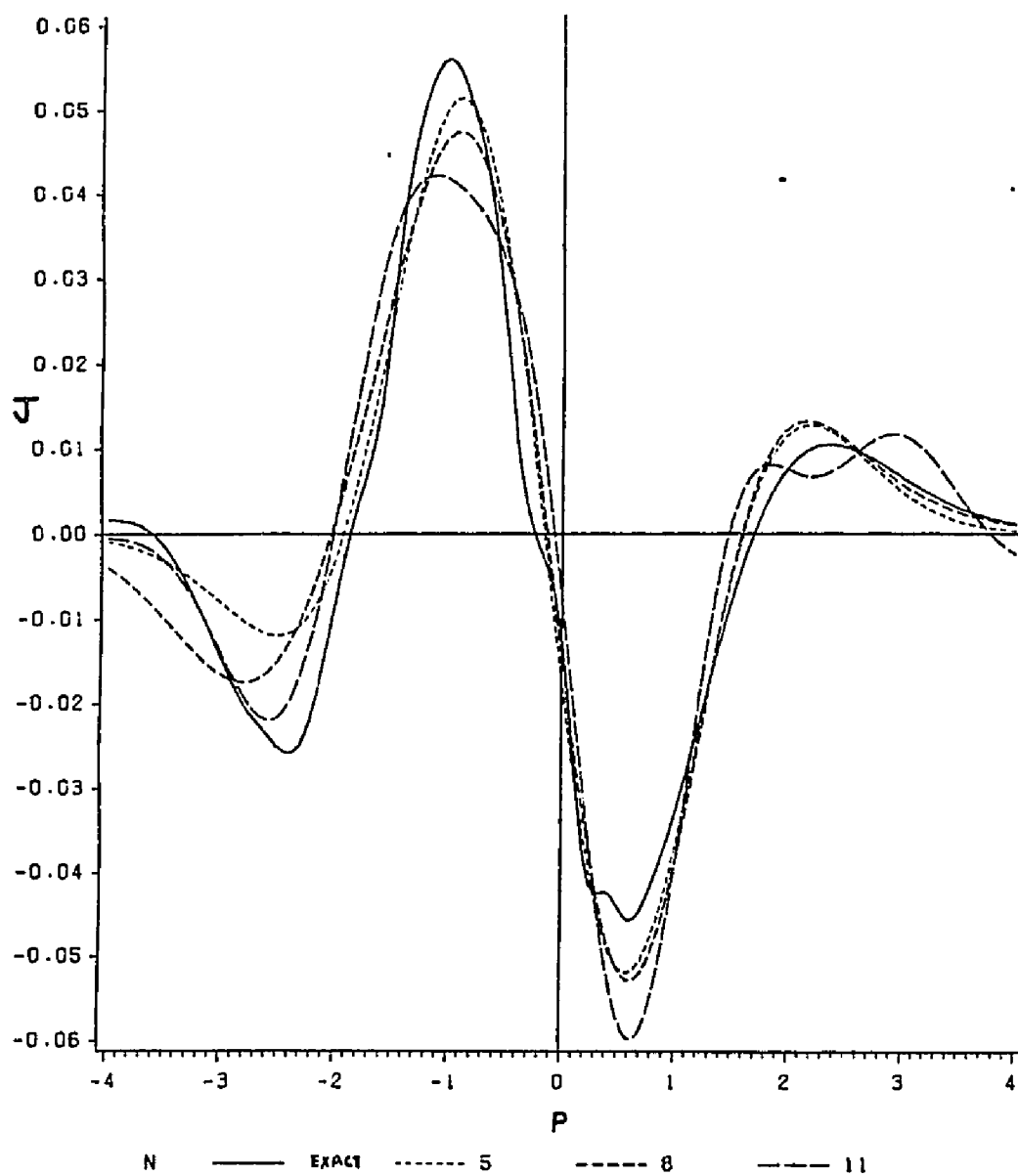


figure 16

STATISTICAL VARIATION

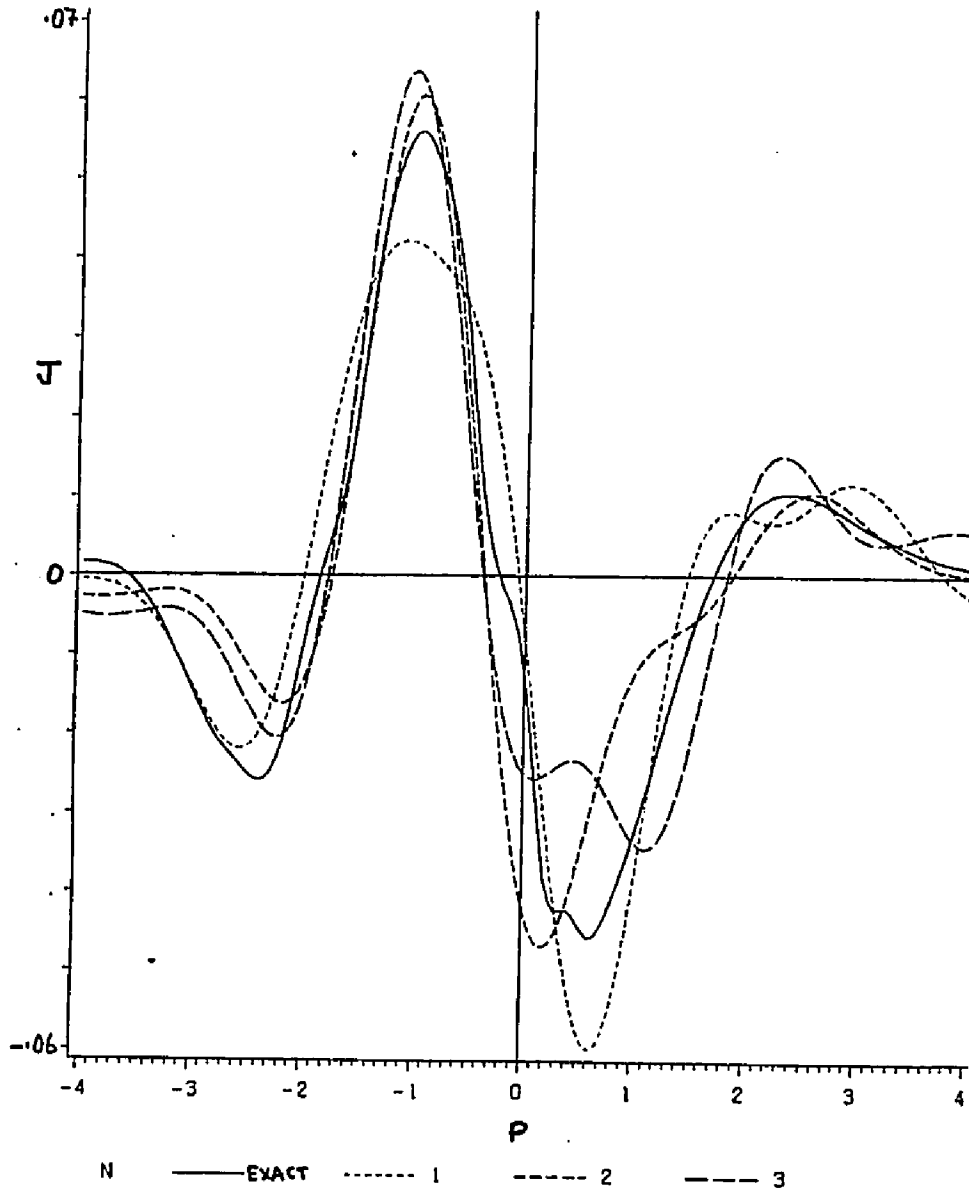


figure 17

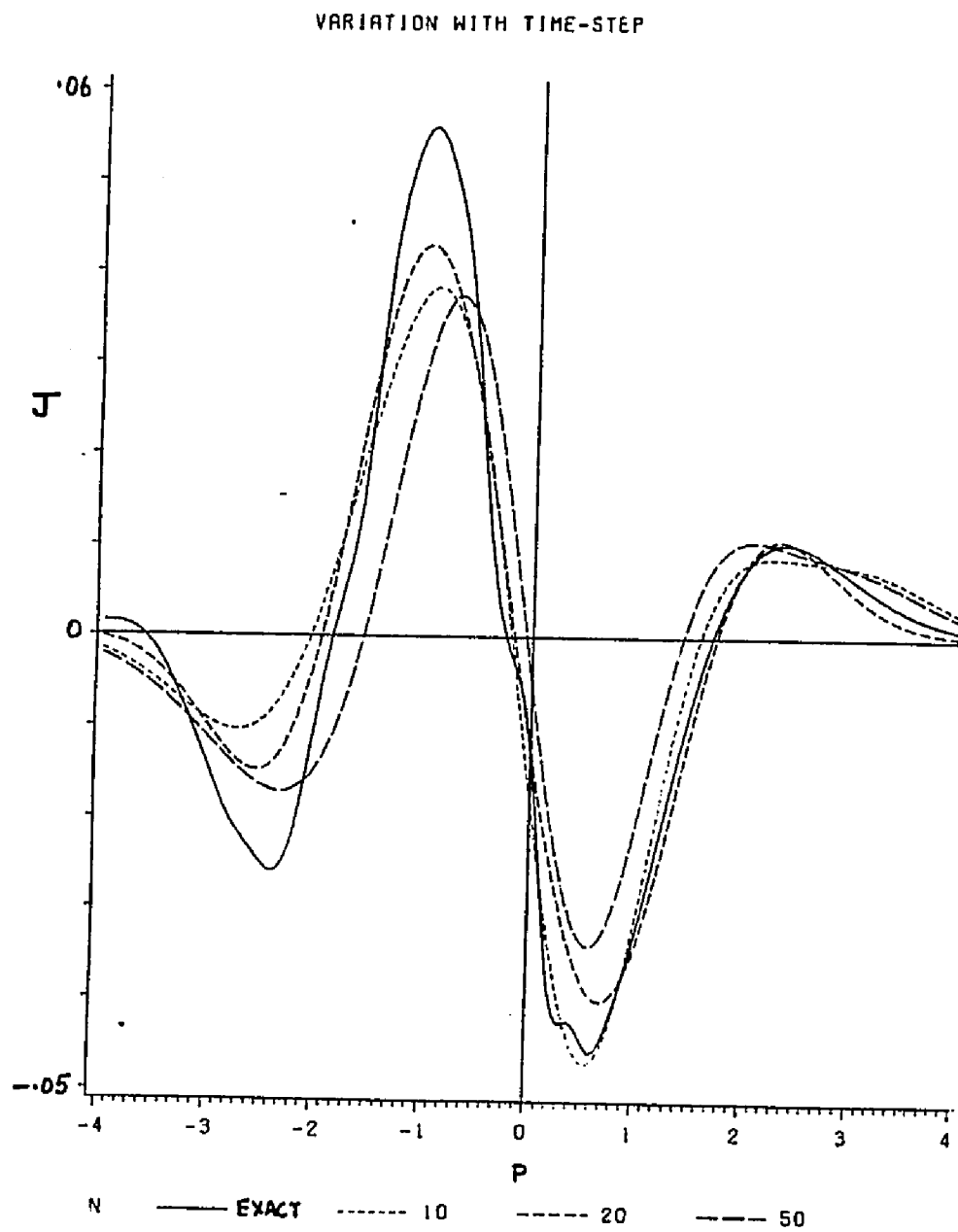


figure 18

VARIATION WITH ALPHA-SMALL

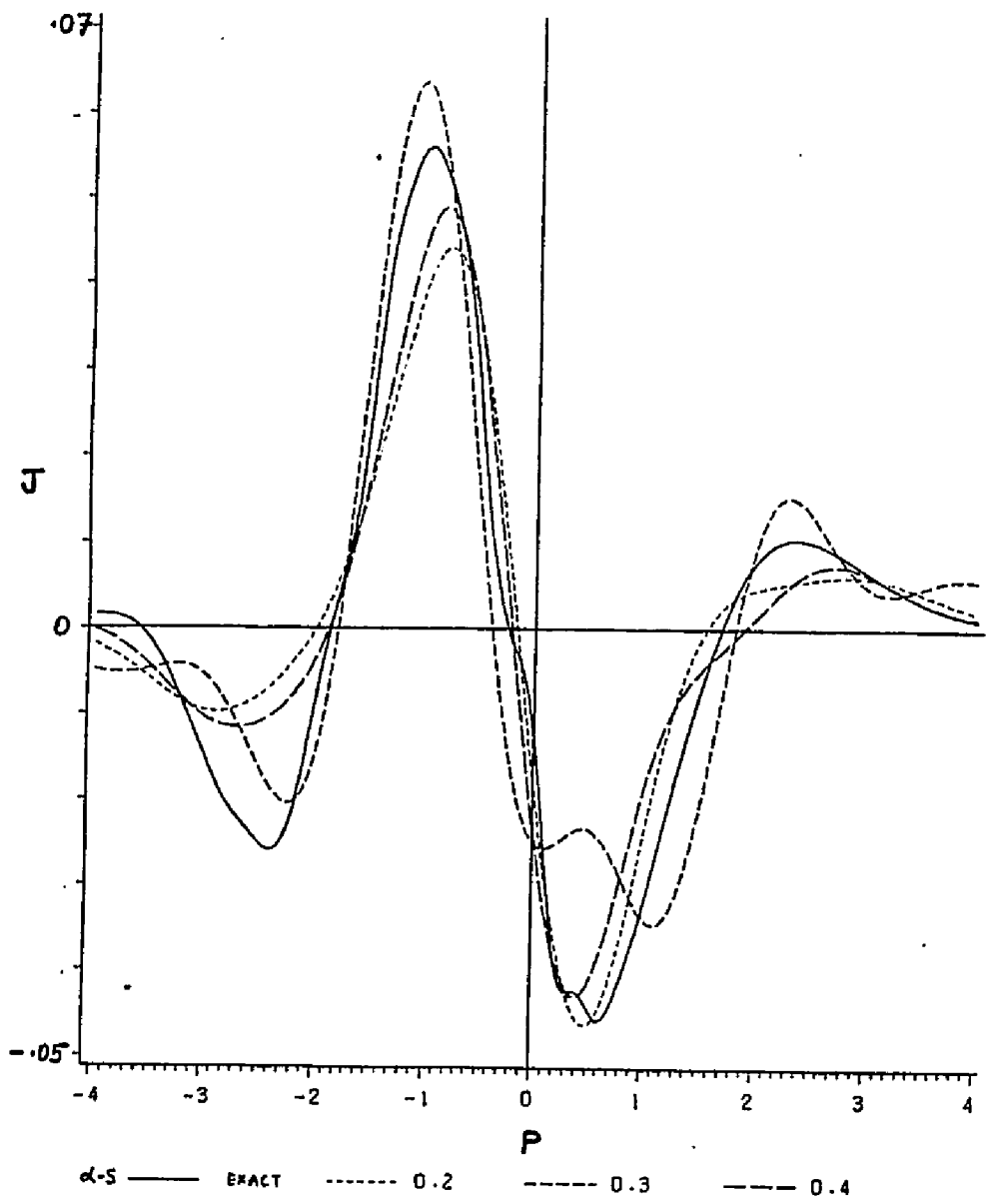


figure 19

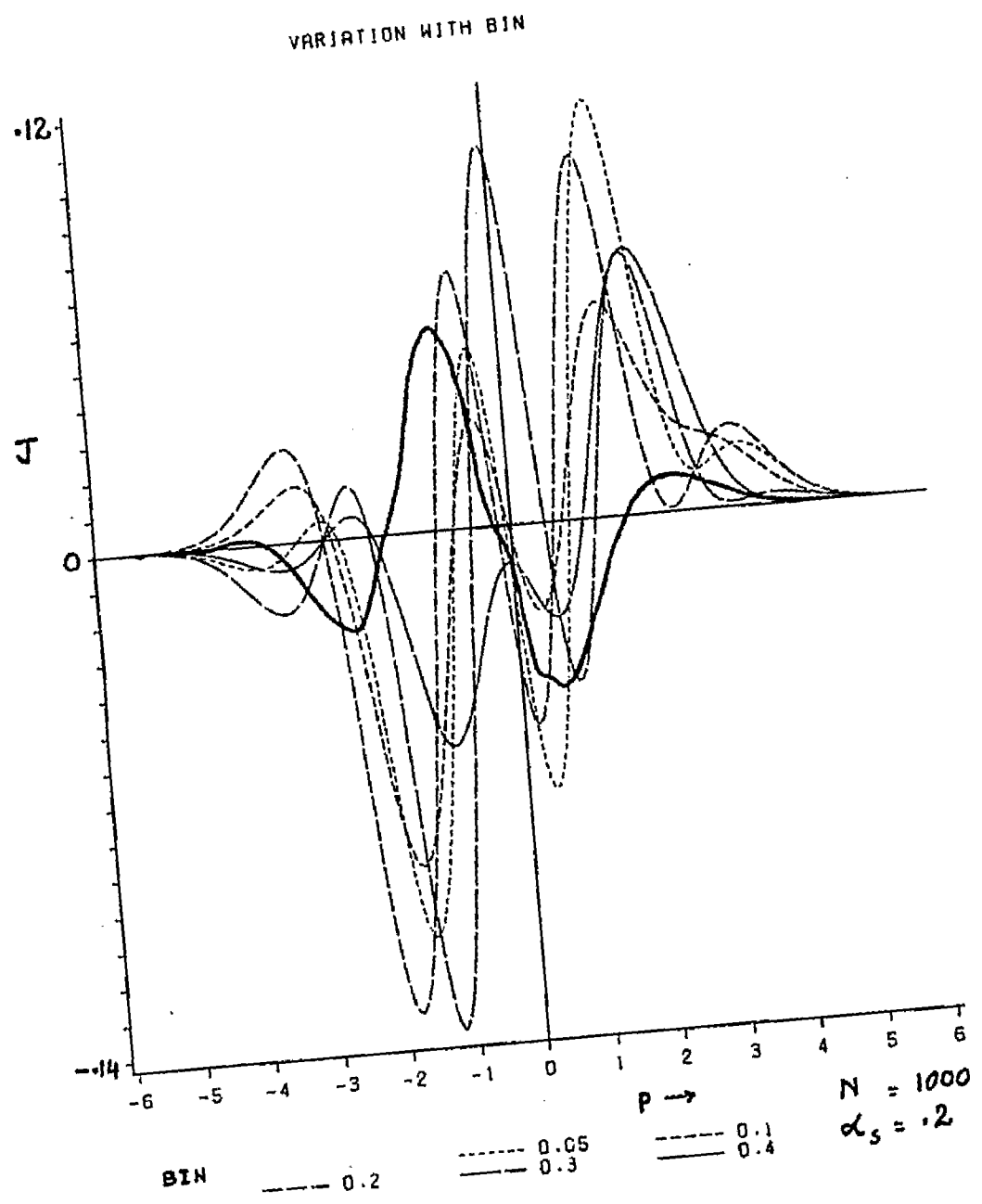


figure 20





## Chapter 5

### The Time Development of the Wigner Function: via the stochastic process

Using the techniques discussed in Chapter 3 and tested out in Chapter 4 we now do a numerical study of the time development of the Wigner function in an anharmonic quartic potential . The system considered is the same as the one that was studied exactly in Chapter 2. The results of the approximate method given here will be compared with the exact and the classical approximation to test for the efficacy of the method.

The Hamiltonian is given by

$$H = \frac{p^2}{2m} + \frac{1}{2} k_1 x^2 + \frac{1}{2} k_2 x^4$$

The equation of motion becomes

$$\begin{aligned} (\partial/\partial t)f_\omega &= -(p/m) \partial_x f_\omega + V' \partial_p f_\omega - (V''''/24) \partial_p^3 f_\omega \\ &= (L_C + L_Q) f_\omega \end{aligned}$$

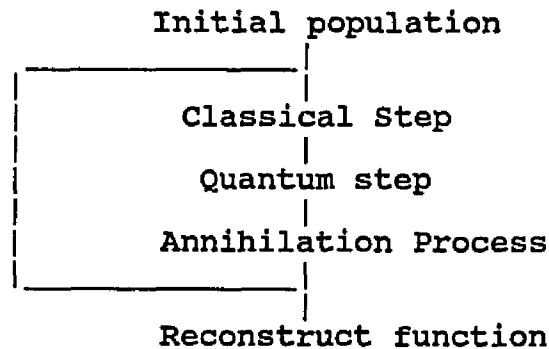
where

$$\begin{aligned} L_C &= -(p/m) \partial_x + V' \partial_p \\ L_Q &= -(V''''/24) \partial_p^3 \end{aligned} \tag{5.1}$$

This is exact for the quartic potential.

### 5.1 The Algorithm

The basic algorithm follows the chart shown below.



We make use of list processing techniques. This is most suitable when several related data cannot be stored in a single array. One then can use pointers (internal addresses) to link them together regardless of its position in the memory storage. (An array is stored in contiguous locations in memory) This is also an efficient process when dealing with a variable number of points when a member of a list may be deleted or inserted without changing the locations of any other members.

Now in the annihilation process, it will be necessary for each point to locate its nearest neighbour. An efficient sorting procedure to locate a nearest neighbouring point will be by sorting only among a set of neighbouring points. Information of these neighbouring points may be easily stored in structures contained in the main list. The advantages accrued from the list processing techniques is most evident for

scattering problems where the effective space considered at any time follows the regions of high interest. Using grids for such purposes in a 3-D calculation will require storage space of the order of  $(L/\Delta x)^3$  where  $L$  is the dimension of the volume considered and  $\Delta x$  the distance between the grid points. In typical 3-D calculations, large grid-sizes have to be used to conform with computer capacity, thereby losing in computational accuracy. In our procedure the storage space will be proportional to the number of representative points, without any loss in accuracy on its coordinates, because these values are stored directly.

The programming language used was PL/I. This was necessary since conventional scientific languages such as Fortran do not feature dynamic allocations.

The algorithm involved in each step is now described in some detail.

### Initial Population

The initial Wigner distribution is given by

$$f_{\omega}(x,p,0) = 2 \exp(-\beta(x-x_0)^2/k^2 - \beta k^2(p-p_0)^2)$$

To choose an appropriate set of points, an arbitrary volume is defined enclosing the function of two variables. A random number generator selects points within this space and only the set of points which fall within the volume of the function is kept. That is, for

a selected random point  $(f_r, x_r, p_r)$  within the volume  
keep only those points that satisfy

$$f_r < f(x_r, p_r)$$

This selection enables us to represent the function as

$$f(x, p) = \frac{2\pi}{N\beta} \sum_i^N \delta(x-x_i) \delta(p-p_i)$$

This is the Monte Carlo method of importance sampling where the probability of selection of a point  $(x, p)$  is proportional to the function at that point.

#### The Classical Step

The classical motion is defined by  $L_C$ . The points follow the Hamilton's equations of motion

$$\frac{dx}{dt} = \frac{\partial H}{\partial p} \quad ; \quad \frac{dp}{dt} = - \frac{\partial H}{\partial x}$$

A second order Runge-Kutta method is used to solve these equations. The points after the classical motion are represented as  $\delta(\phi - \phi_{ic})$

#### The Quantum Step

Using gaussian smeared points, the quantum function  $J(p, a)$  is evaluated.

$$J(p, a) = (e^{-a\theta^3/\theta p^3} - 1) \delta_\alpha(p)$$

A table for  $J'_\pm$  vs.  $p$  is constructed for a series of values of 'a'. For 'a' negative it can be shown (Appendix 5.1) that

$$J(-p, -a) = J(p, a) \quad (5.2)$$

Hence the same table may be used for  $-a$  with an appropriate change in the sign of  $p_{\pm}$ .

For any given point  $(x_i, p_i)$  the portion of the table to be used is determined by  $a = V'''(x_i) \Delta t / 24$ . The newly created points are represented as  $(c$  denoting the classically shifted point)

$$\begin{aligned} & \sigma_i \delta(x - x_{ic}, p - (p_{ic} + \sigma_a p_+)) \\ & \text{and} \\ & -\sigma_i \delta(x - x_{ic}, p - (p_{ic} + \sigma_a p_-)) \end{aligned} \tag{5.3}$$

where  $\sigma_a$  is the sign of 'a' introduced to comply with eqn 5.2 and  $p_{\pm}$  denotes the distances from the  $i$ -th point.

### The Annihilation Process

It is necessary to limit the growing number of points to keep tractability in computing time and memory storage. Now in the reconstruction of the function, the value of the function at any point is determined by the net density of the points at that region. Assuming the function to be fairly slowly varying, it is possible to reduce the accumulation of points by 'annihilating' points of opposite signs provided they are within a certain 'annihilation distance' of each other. These distances must be  $\ll$  than the widths of the functions. By such a procedure pairs of  $\pm$  points will be removed.

Annihilation may be done by two different procedures. One is by a process we call hopping, and the

other by a nearest neighbour annihilation.

### Hopping

Here an immediate annihilation between the parent and it's own created  $\pm$  pair of points are done if they fall within the annihilation zone. Consider the triplet of the initial and its newly created pair of points. Let the distance between the pair of newly created points be

$$d = |p_+ - p_-|$$

and the distance from the parent to the daughter point with the opposite sign be

$$c = |p_-| \delta_{+, \sigma_i} + |p_+| \delta_{-, \sigma_i}$$

Then if

$$c \text{ or } d < \text{annihilation distance} \quad (5.4)$$

then annihilate the two points with opposite signs. This is done as follows: Consider a case where the three points are situated at  $p_i$ ,  $p_i + \Delta p_1$ ,  $p_i + \Delta p_2$ .

Let  $p_i$  be a negative point, and the other two positive, that is the points are represented as

$$-\delta(p - p_i), \delta(p - (p_i + \Delta p_1)), \delta(p - (p_i + \Delta p_2))$$

The average effective position  $\delta(p - \bar{p}_i)$  for these three points can be found as follows. Consider an arbitrary function  $f(p)$  spanning these three points.

Now

$$\int f(p) [-\delta(p - p_i) + \delta(p - (p_i + \Delta p_1)) + \delta(p - (p_i + \Delta p_2))] dp$$

$$= \int f(p) \delta(p - \bar{p}_i) dp$$

where  $\bar{p}_i$  denotes the average position of the 3 points.

$$\text{R.H.S.} = f(\bar{p}_i)$$

$$\text{L.H.S.} = -f(p_i) + f(p_i + \Delta p_1) + f(p_i + \Delta p_2)$$

$$= f(p_i) + (\Delta p_1 + \Delta p_2) f'(p_i)$$

$$= f(p_i + (\Delta p_1 + \Delta p_2))$$

from which we deduce

$$\bar{p}_i = p_i + \Delta p_1 + \Delta p_2$$

Hence the effect of the annihilation of two closest neighbours is to give an appropriate 'hop' of  $\Delta p_1 + \Delta p_2$  to the remaining point. That is to say we replace the three states  $-\delta(p - p_i)$ ,  $\delta(p - (p_i + \Delta p_1))$ ,  $\delta(p - (p_i + \Delta p_2))$  by the single state  $\delta(p - (p_i + \Delta p_1 + \Delta p_2))$ , if a pair of them lie within an annihilation distance.

Most generally, considering the sign of the parent, the new state is written as

$$\pm \delta(p - (p_i \pm (p_+ - p_-))) \delta_{\pm, \sigma_i}$$

### Nearest Neighbour annihilation

After each time step the points are sorted to locate the nearest neighbours. A very efficient method for nearest point search is to store the location (address in main list) of say 4 nearest neighbours. Each

of these 4 have in turn their 4 nearest information. This forms a network. Hence instead of sorting an entire list it is sufficient only to sort among the nearest and their nearest neighbours for points of opposite sign and annihilate and reassign new nearest neighbours.

Hence the main list consists of structures which contain the following information:

1. position (x,p)
2. sign of the point
3. 4 nearest neighbour addresses
4. addresses of which in turn it is a neighbour.

#### Initial assignment of Nearest Neighbours

This initial sorting involves all the points. Two separate lists are formed from the initial list. One is to be sorted in x variables, the other in p variables. Each of these sub-lists also stores the address of the point in the main list.

The 4 nearest neighbours for any point is determined as follows: Select  $\pm 10$  neighbours from the sorted x and p lists where  $\pm$  denotes ascending and descending order in the sorted list. Some of these will have common stored addresses. These represent the nearest points on the plane (x,p). Of these sort and

store the 4 nearest addresses. If this number is less than 4 then increase the upper limit of search from 10 to 20 and so on.

While storing the nearest neighbour addresses it is necessary also to send in the address of the host to the neighbours themselves, that is, each point contains information about its status with respect to every point related to it. This is necessary because during an annihilation when one point is removed from the main list, a member in the 'inverse' neighbour list must also remove it from their nearest neighbour status, otherwise in a list processing method critical errors will occur.

#### Reconstruction of function

The function is reconstructed from the final set of points using a set of Orthonormal Harmonic Oscillator wave functions. (appendix 5.2) The motivation for this choice was made on the basis that the initial state is of a gaussian form, and is thereby intended to give a smoothing of the same nature to the set of points. Truncation of the set is necessary to obtain a smooth reconstructed function. (If the infinite set were used, the details of the discrete points will be revealed.) This method has proved remarkably effective in the reconstruction of the contours.

The value for truncation depends on the number of points and also on the scaling factors used for the orthonormal functions.

## 5.2 Computer Runs

The Hamiltonian is of the form

$$H = p^2/2m + \frac{1}{2} k_1 x^2 + \frac{1}{4} k_2 x^4$$

where  $k_1$  and  $m = 1$  for all cases .

Table 2. lists all the parameters used in the approximate case . The selection of these parameters will be discussed now.

### Selection of Widths

A suitable formula for the choice of widths would be

$$\alpha-s = \sigma / 2 \quad (5.5)$$

with  $\sigma$  the width defined by

$$\sigma^2 = 1 / (2 * \beta)$$

This gives larger smearing widths  $\alpha-s$  for higher mixed states. This is necessary while using the same number of representative points for wider distributions.

### Selection of annihilation distance

This was arbitrarily set with a view to reasonable computing time and the total accumulation of points. A value of .3 proved to be most tractable. Also the distribution falls off at the outer regions of phase space . Therefore one can afford to be less accurate in

these regions . Hence larger 'annihilation values' are set in these regions. The following strategy was used.

$ x ,  p  < 5$	set annihilation = .3
$5 <  x ,  p  < 8$	set annihilation = .4
$ x ,  p  > 8$	set annihilation = .5

This proved to be very useful, also because outer regions of  $x$  have higher probabilities of pair production and will cause an accumulation of nonsignificant  $\pm$  points.

#### Selection of $\Delta t$

This was typically chosen so that  $A_i \ll 1$  at the outer edges. A value of  $\pi/600$  was used for all the runs.

#### Computational time

Typically each time step takes about 20 seconds on an IBM machine. That is, about 2.5 hours for a run upto  $4\pi$ .

#### Results

The contour plots are shown in figures 23-36. In each case the top left picture represents the classical motion as determined by Liouville's Theorem, the top right is the exact as studied in Chapter 2 and the bottom is the approximate as studied in this chapter.

Case1

$$\beta = 1 \quad k_2 = 1 \quad \text{fig.23-25}$$

There is clear indication that the quantum term gives an improvement over the purely classical case. However even by a time of  $2\pi/3$  the peak values have diminished and a spreading has occurred. This may be due to quantum effects being large for high anharmonicity. Hence the creation probabilities are high giving a large number of pair production, which in turn implies more annihilation processes, thus introducing more numerical dissipation errors. (due to large annihilation distances.) The run was stopped at time  $\pi$  because of these effects and a large accumulation of points .

Case 2

$$\beta = 1 \quad k_2 = .5 \quad \text{fig.26-28}$$

The quantum effects are smaller in this case due to the smaller anharmonicity . Spreading sets in at time  $\pi$  and the runs were continued upto  $2\pi$ . The overall comparison of the approximate case with the exact is fairly good.

Case3

$$\beta = .5 \quad k_2 = .5 \quad \text{fig.29-32}$$

The phenomenon of quantum focussing also shows up, thus complementing the study of Chapter 2. Runs could be made to much higher times before the characteristic

numerical dissipation of peaks sets in. It is seen that the peaks tend to lag behind the exact solution.

Case 4

$$\beta = .25 \quad k_2 = .5 \quad \text{fig.33-35}$$

Good results were obtained for values of time upto  $3\pi$ . A three dimensional picture of the function at this time is presented in figure 36.

Table 2

The values of the parameters in the approximate scheme

---

Case	Mix( $\beta$ )	$k_2$	$\alpha-S$	N
1.	1	1	.4	1500
2.	1	.5	.3	1000
3.	.5	.5	.6	1500
4.	.25	.5	.7	1500

---

Figures 23-36

The following pictures represent the contours for the time development of the wigner function. In each case top left represents the classical, top right the exact, and the bottom the approximate contours.

The contours are drawn at increasing steps of .5 beginning at .5 at the outermost contour. Dotted curves start appearing at values of 2.5 and over.

fig 23-25  $\beta = 1, k_2 = .5$  , contours from  $\pi/3$  to  $\pi$   
plotted at intervals of  $\pi/3$

fig 26-28  $\beta = 1, k_2 = .5$  , contours from  $2\pi/3$  to  $2\pi$  at  
intervals of  $2\pi/3$ .

fig. 29-32  $\beta=.5, k_2 = .5$ , contours from  $\pi$  to  $4\pi$  at  
intervals of  $\pi$ . This set shows the time lag.

fig. 32-35  $\beta = .25$   $k_2 = .5$  contours from  $\pi$  to  $3\pi$  at  
intervals of  $\pi$

fig 36. A 3-D picture for the exact and the approximate  
for  $\beta = .25$  ,  $k_2 = .5$  at time =  $3\pi$

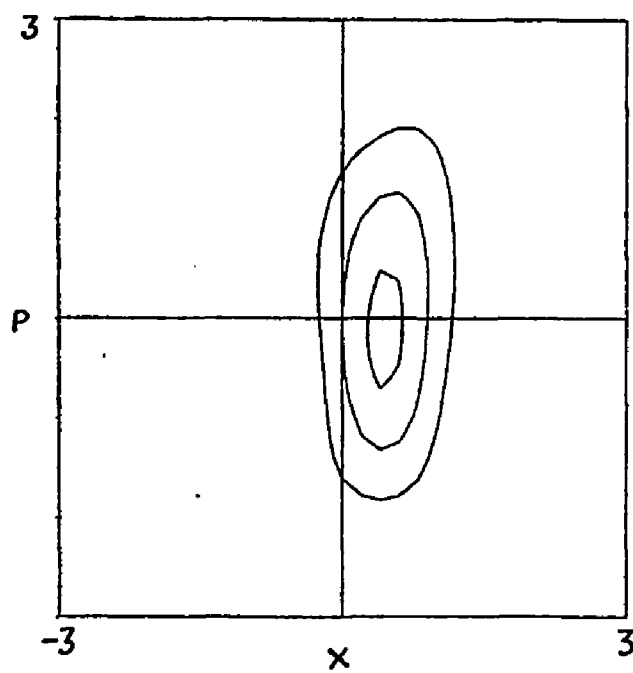
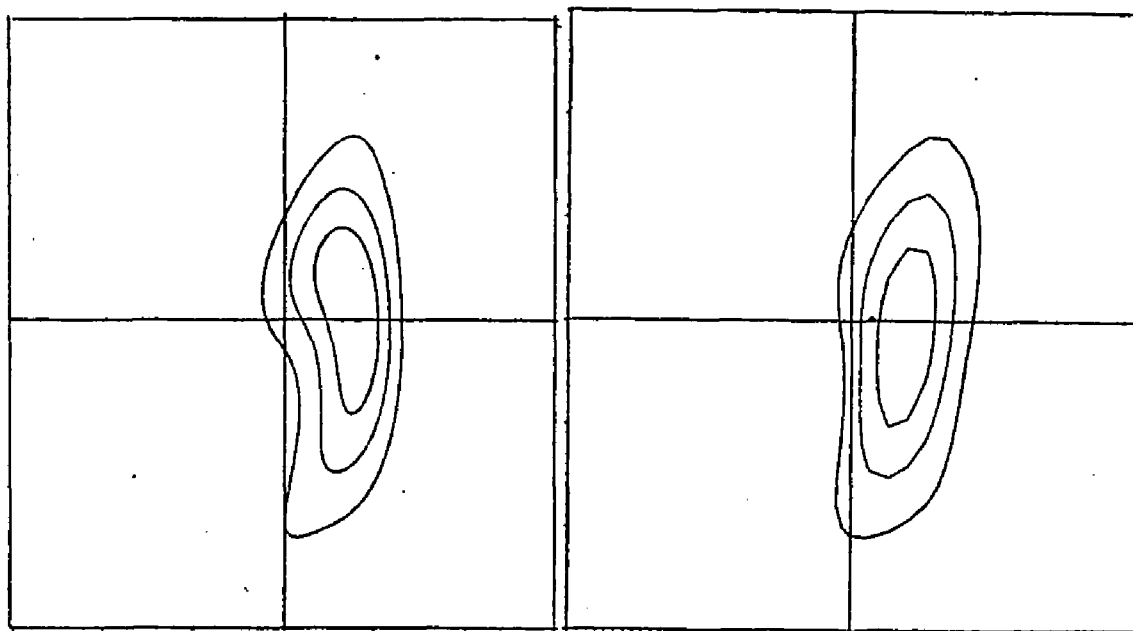


figure 23.  $\beta = 1$   $k_2 = 1$   $\Gamma = \pi/3$

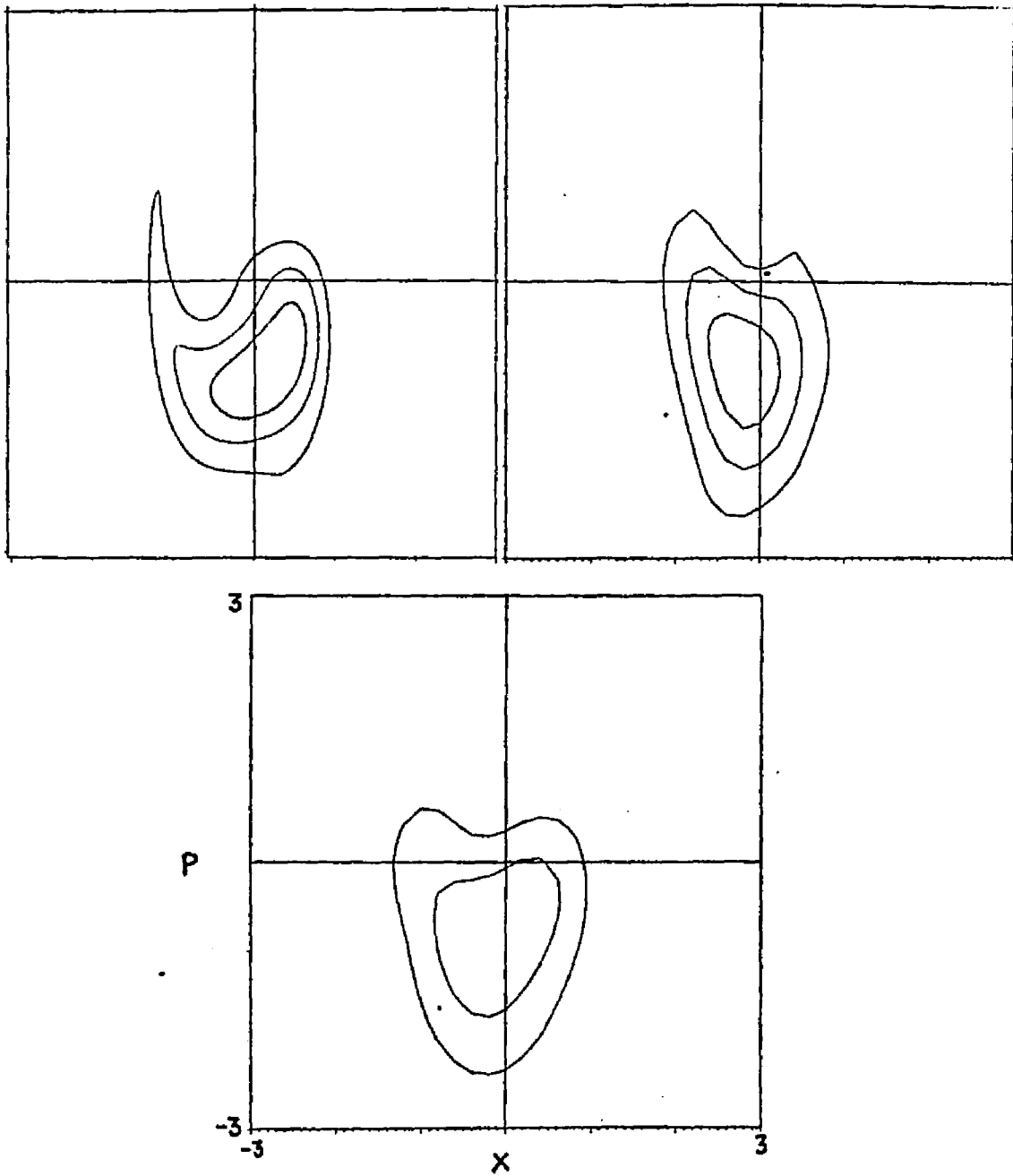


figure 24.  $\beta = 1$   $k_2 = 1$   $T = 2\pi/3$

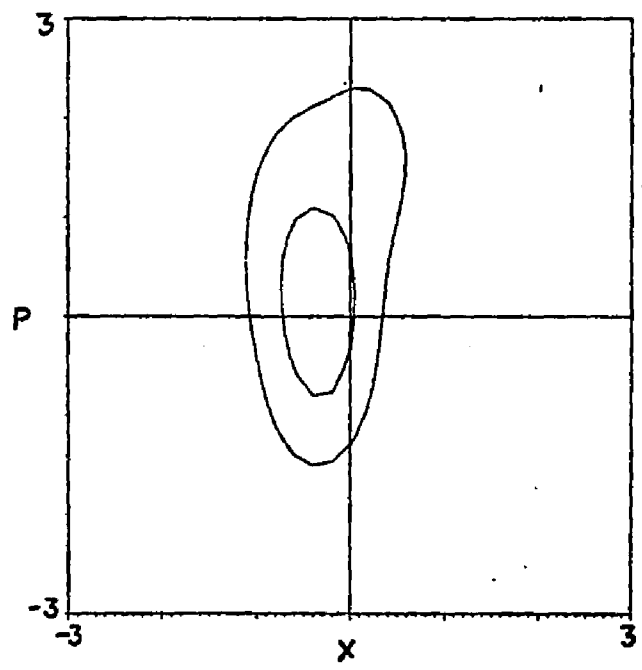
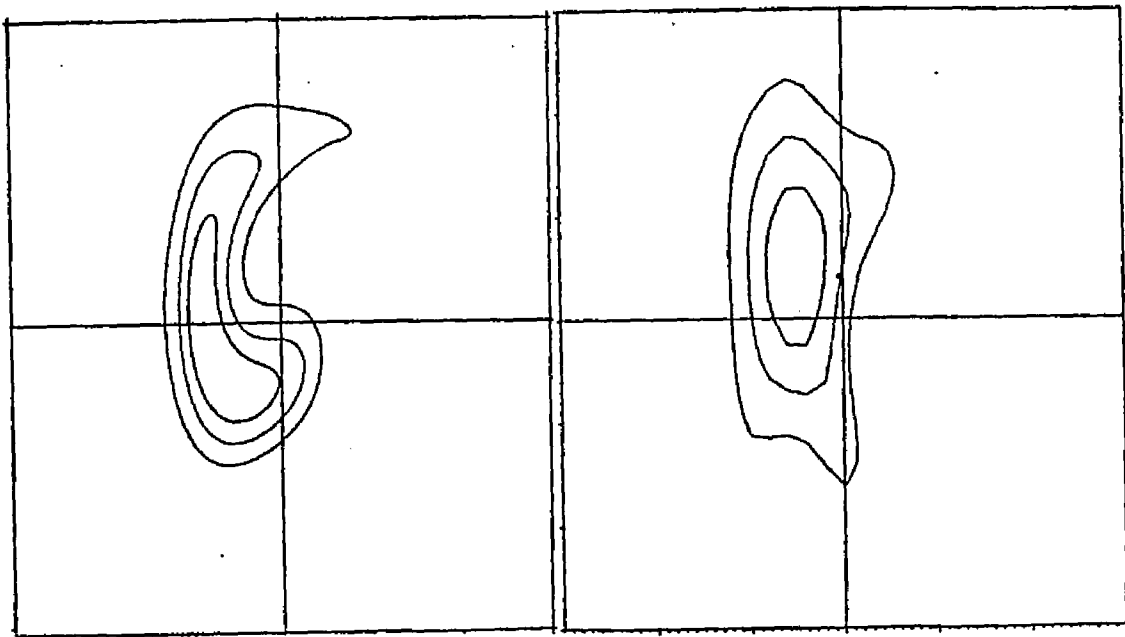


figure 25.  $\beta = 1$   $k_2 = 1$   $T = \pi$

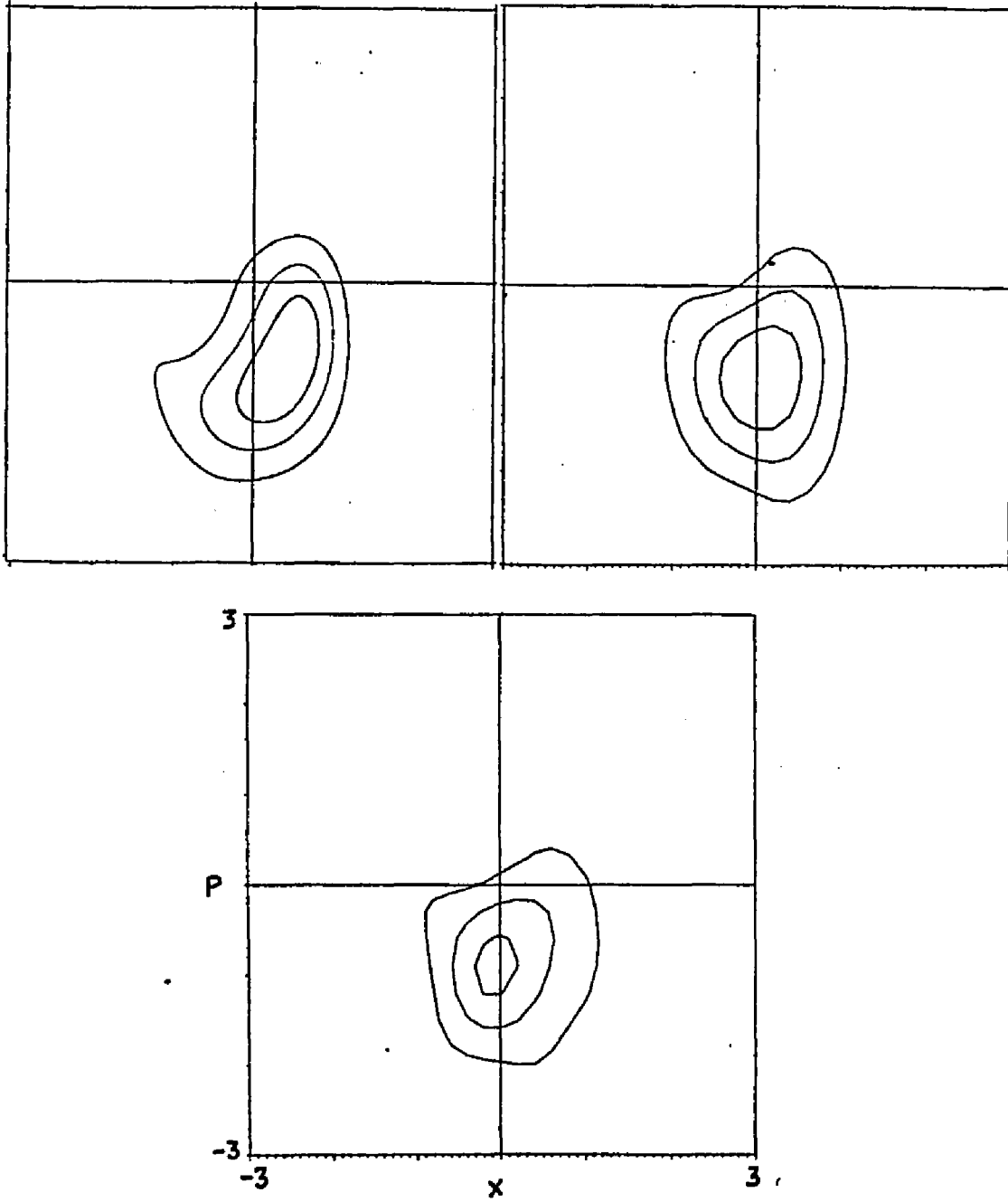


figure 26.  $\beta = 1$   $k_2 = .5$   $T = 2\pi/3$

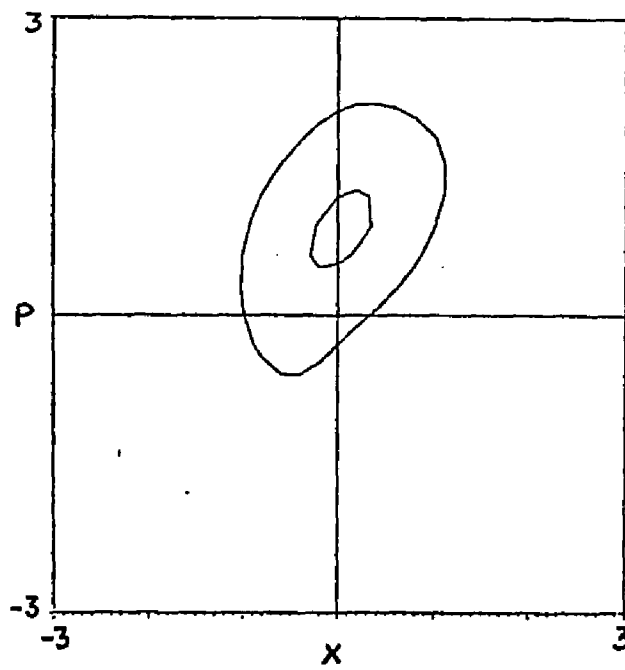
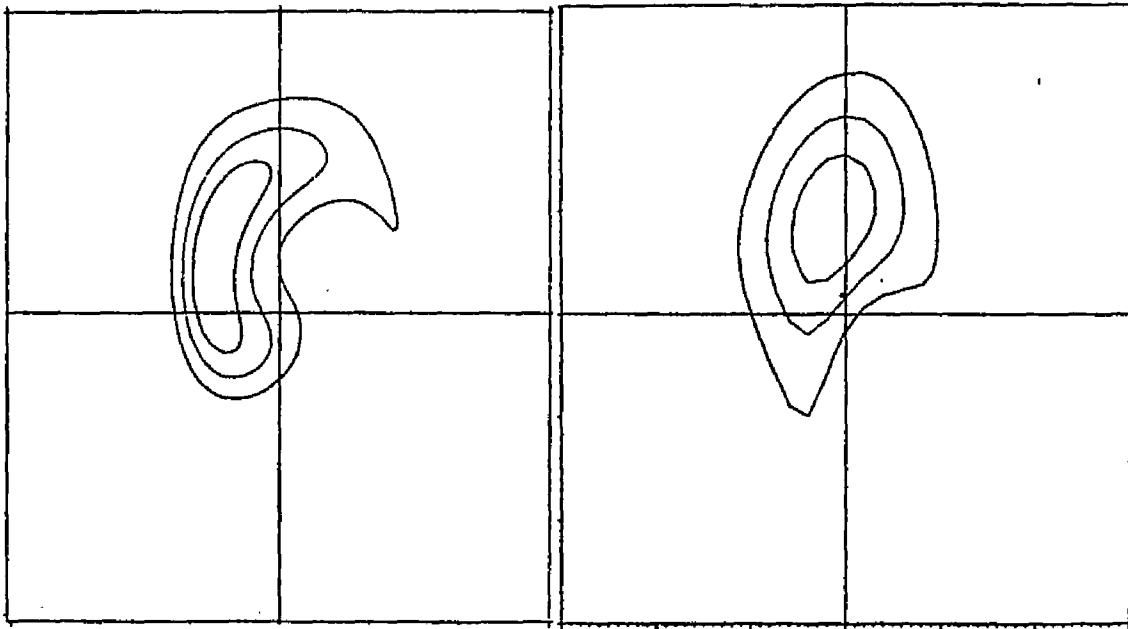


figure 27.  $\beta = 1$   $k_2 = .5$   $T = 4\pi/3$

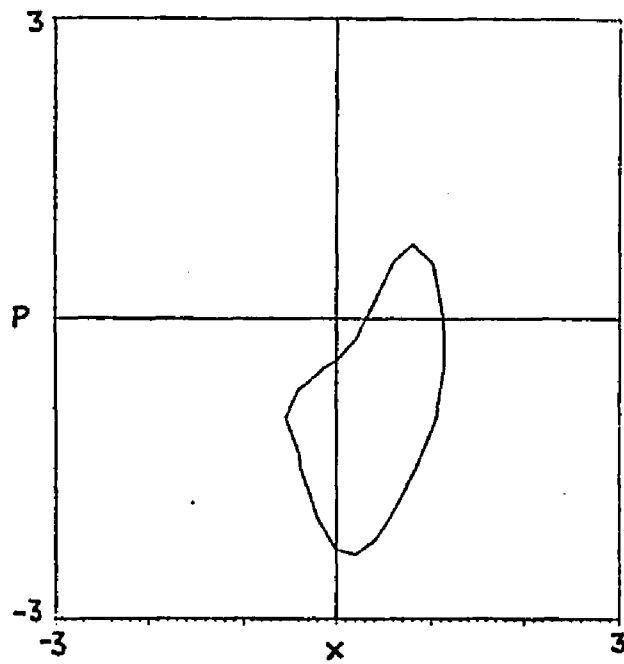
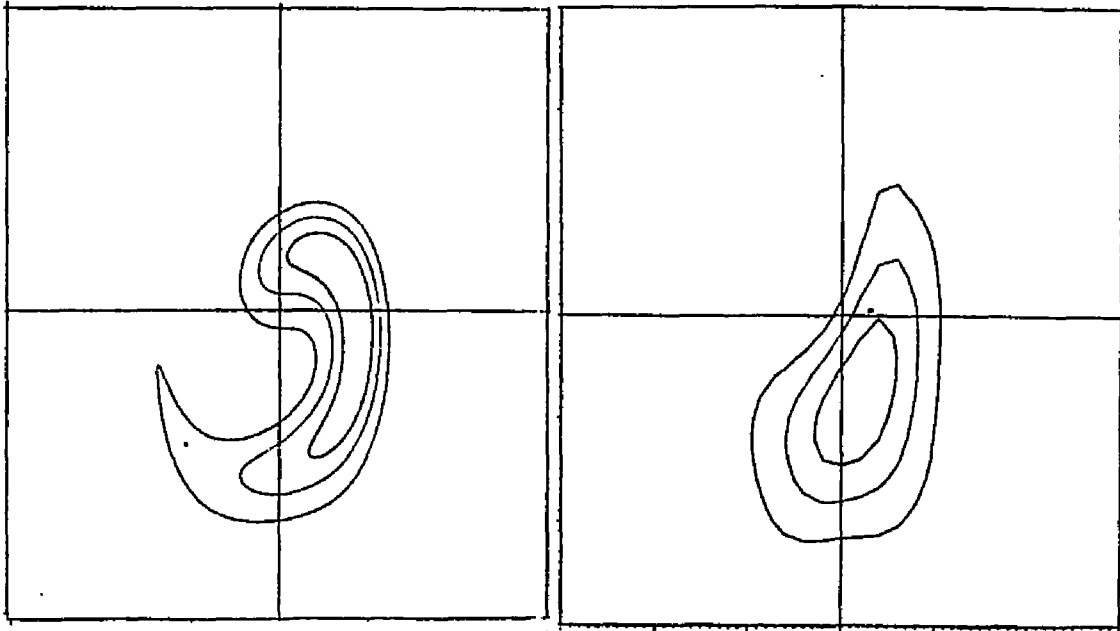


figure 28.  $\beta = 1$   $k_2 = .5$   $T = 2\pi$

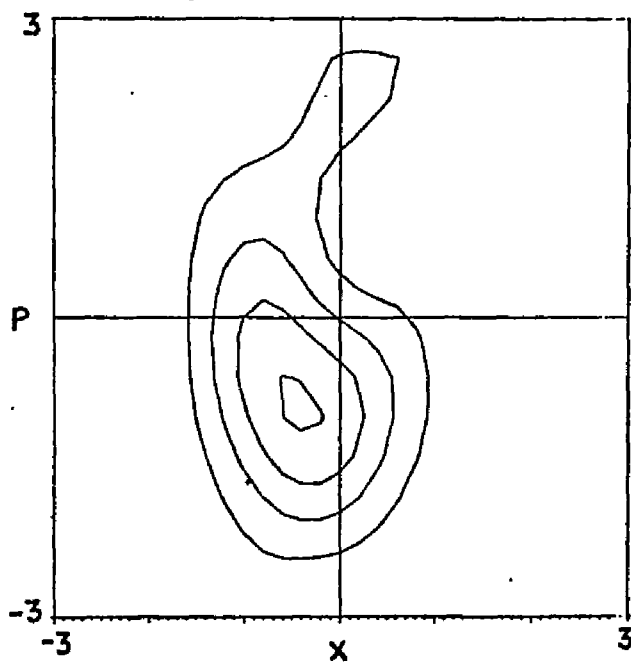
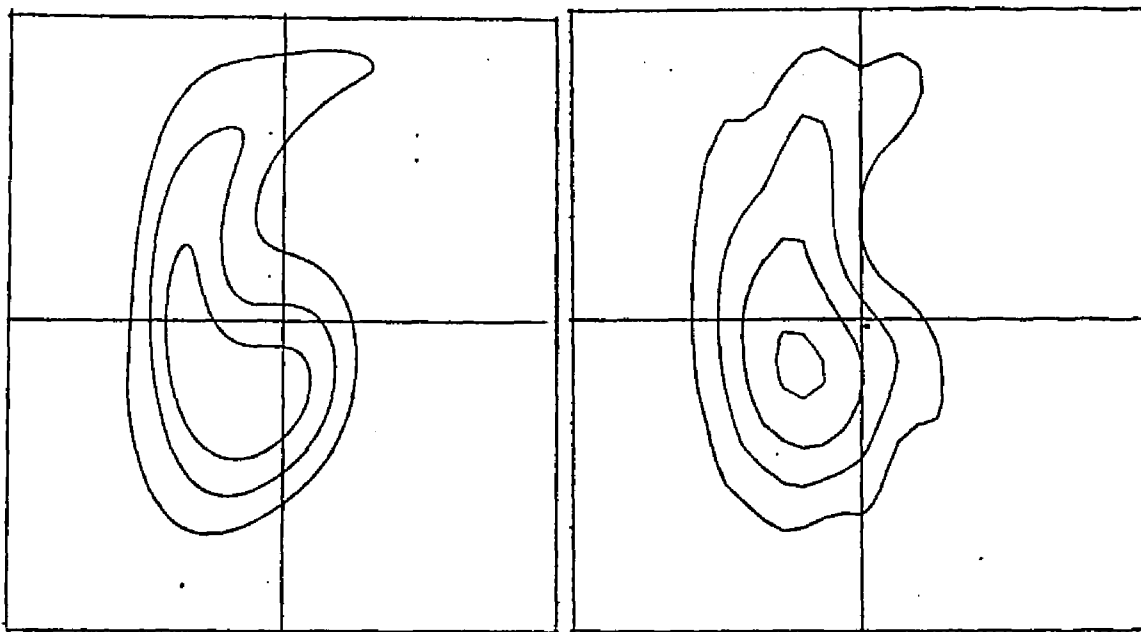


figure 29.  $\beta = .5$   $k_2 = .5$   $T = \pi$

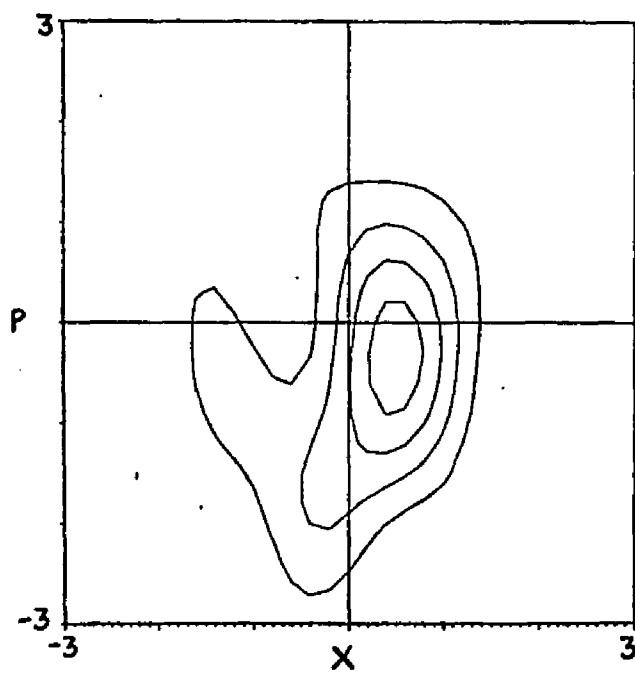
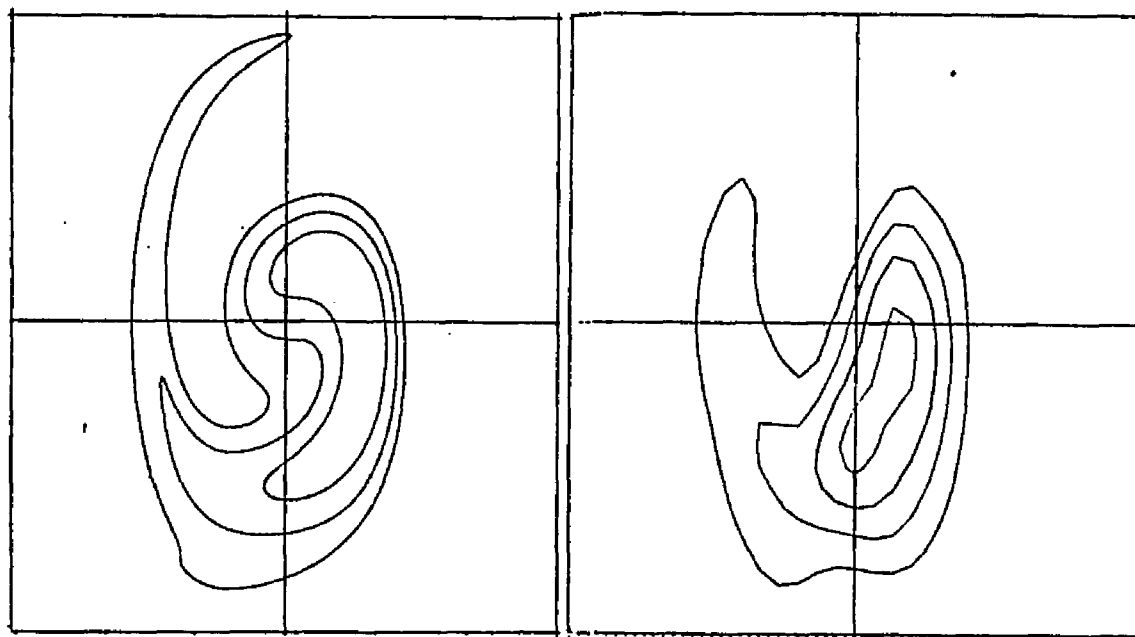


figure 30.  $\beta = .5$   $k_2 = .5$   $T = 2\pi$

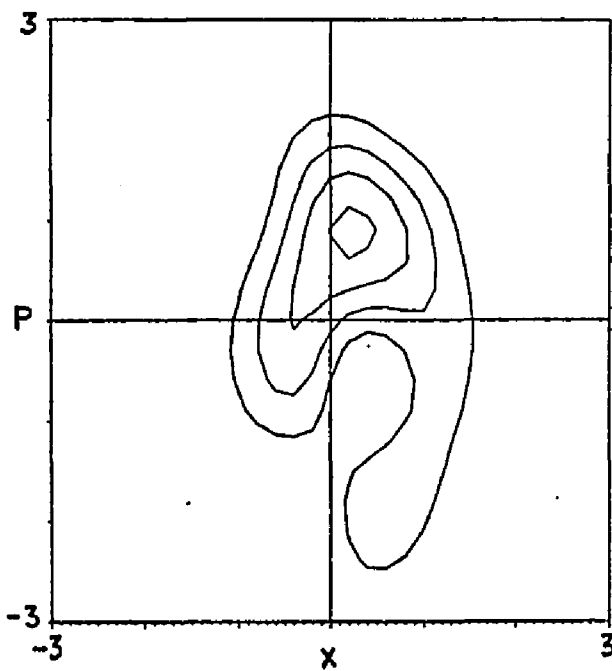
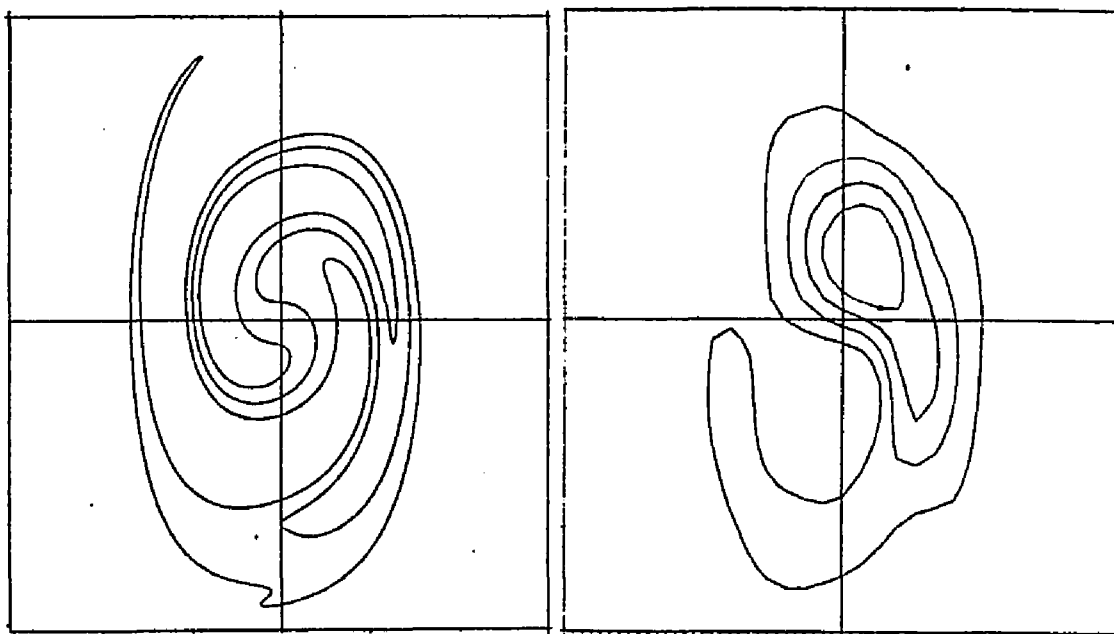


figure 31.  $\beta = .5$   $k_2 = .5$   $T = 3\pi$

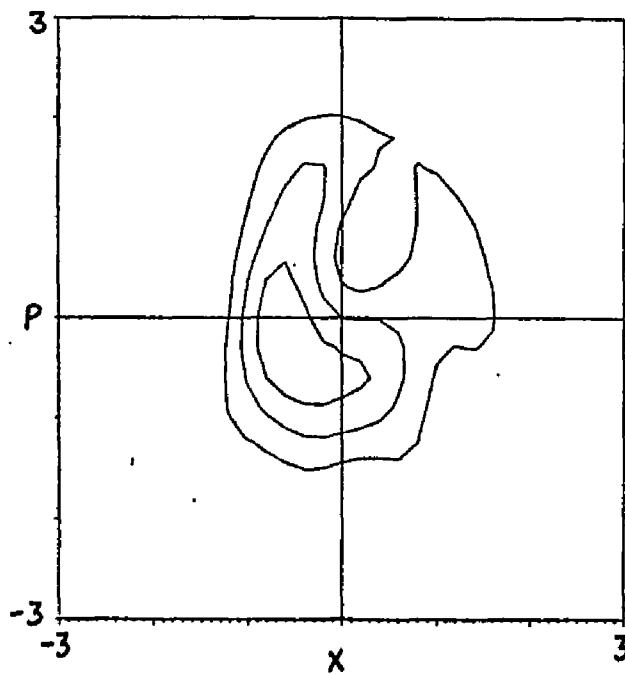
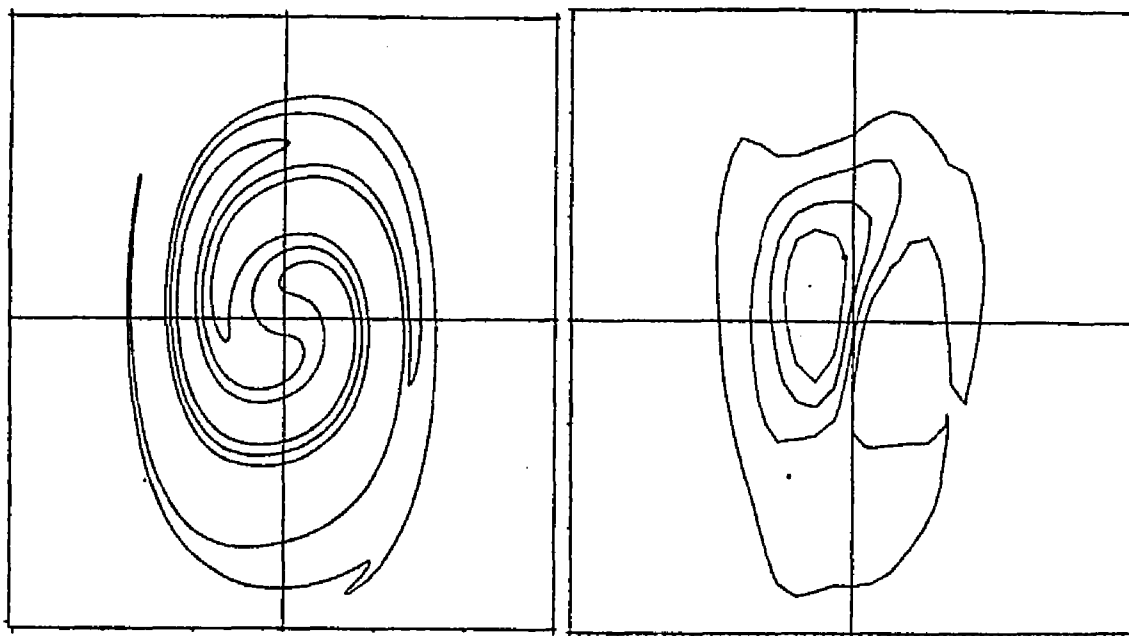


figure 32.  $\beta = .5$   $k_2 = .5$   $T = 4\pi$

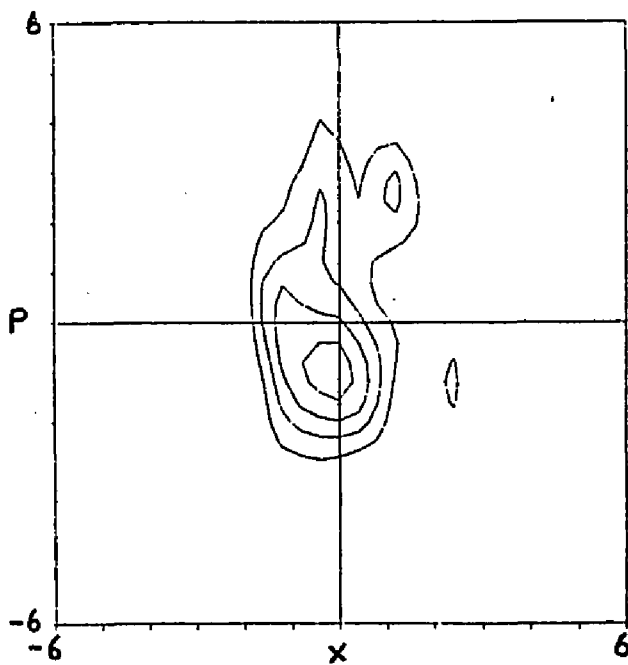
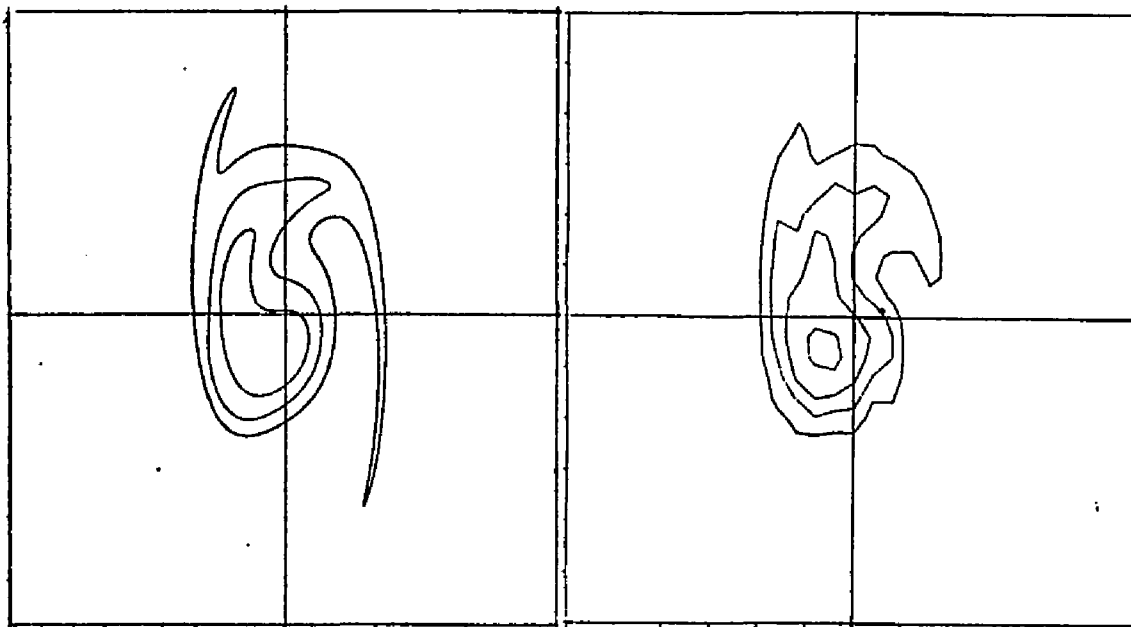


figure 33.  $\beta = .25$   $k_2 = .5$   $T = \pi$

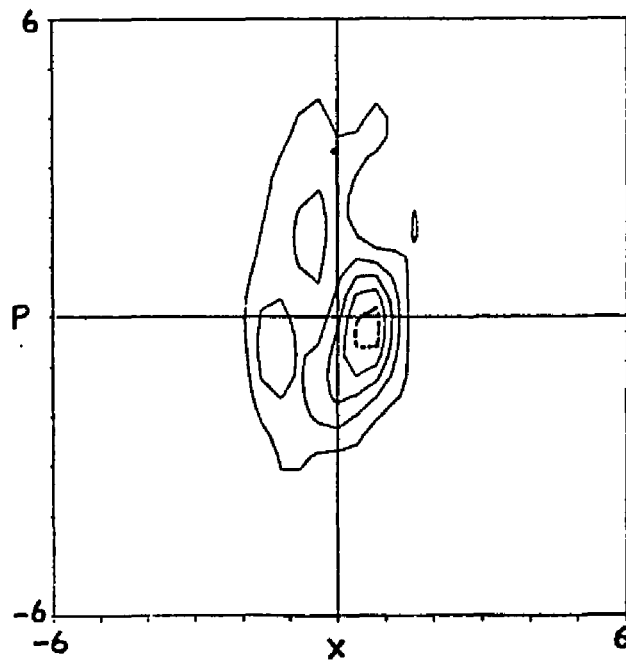
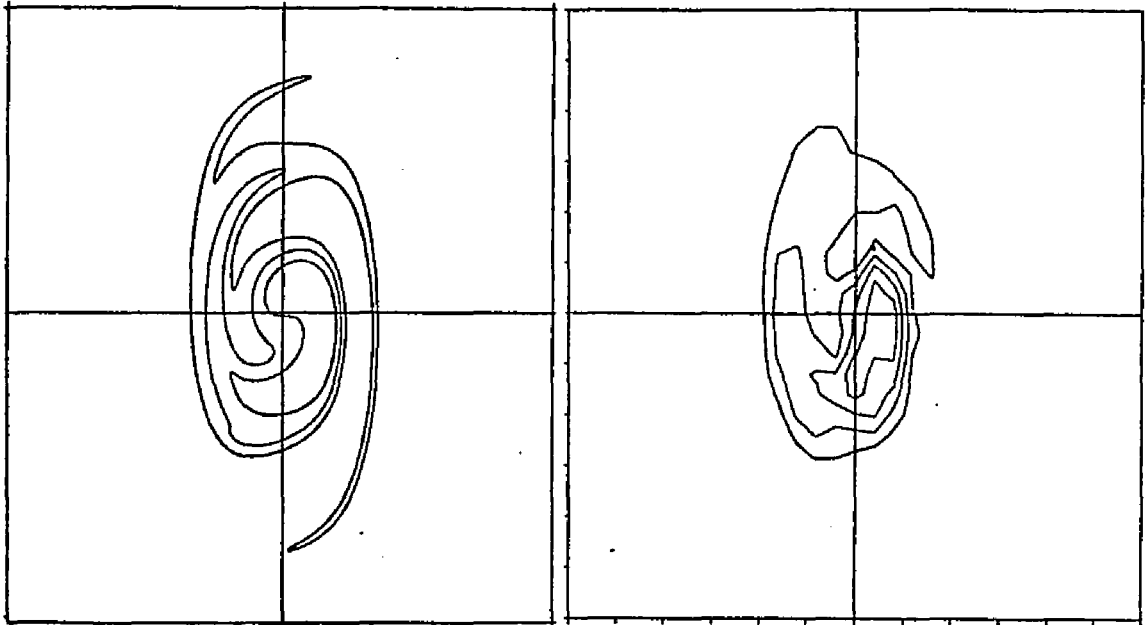


figure 34.  $\beta = .25$   $k_2 = .5$   $T = 2\pi$

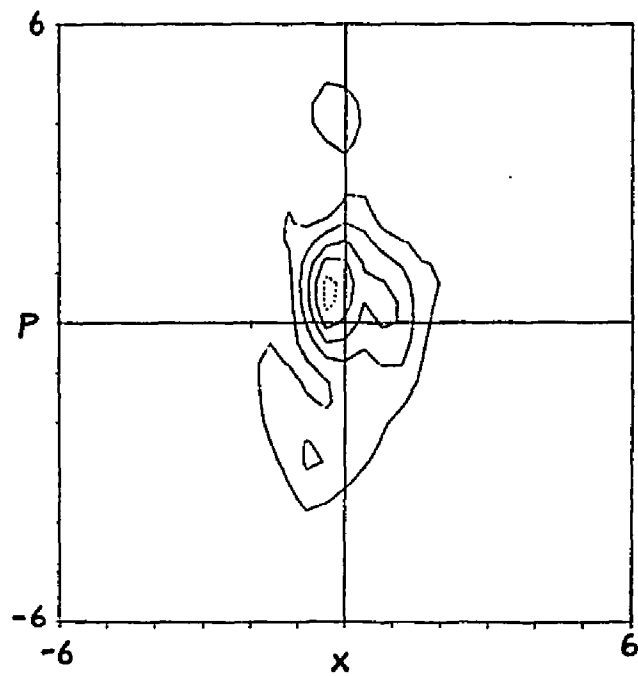
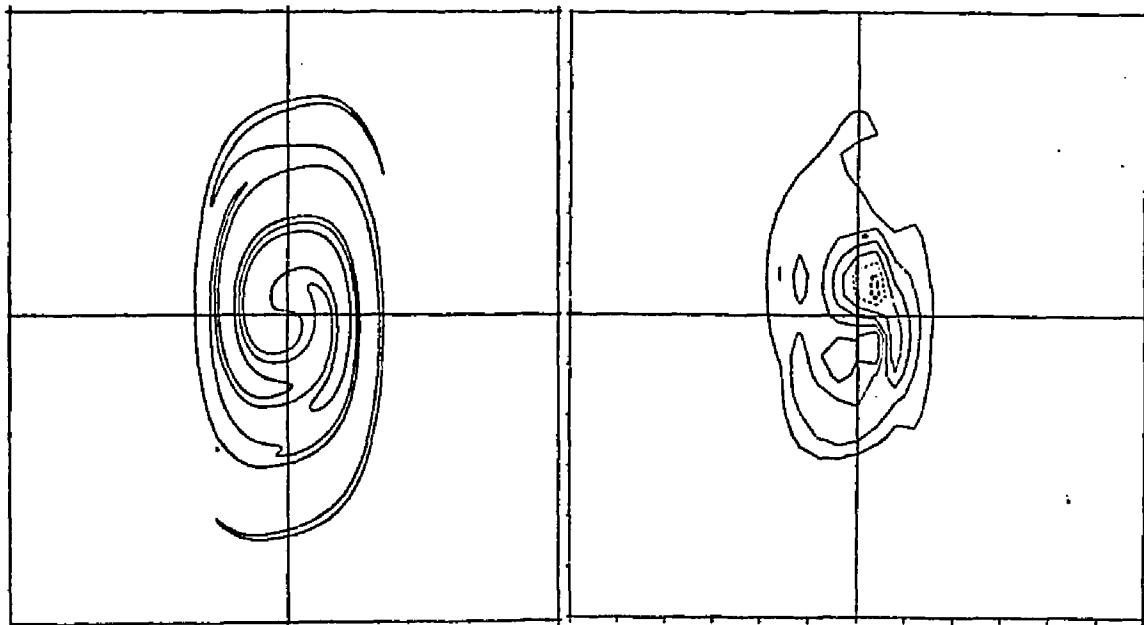


figure 35.  $\beta = .25$   $k_2 = .5$   $T = 3\pi$

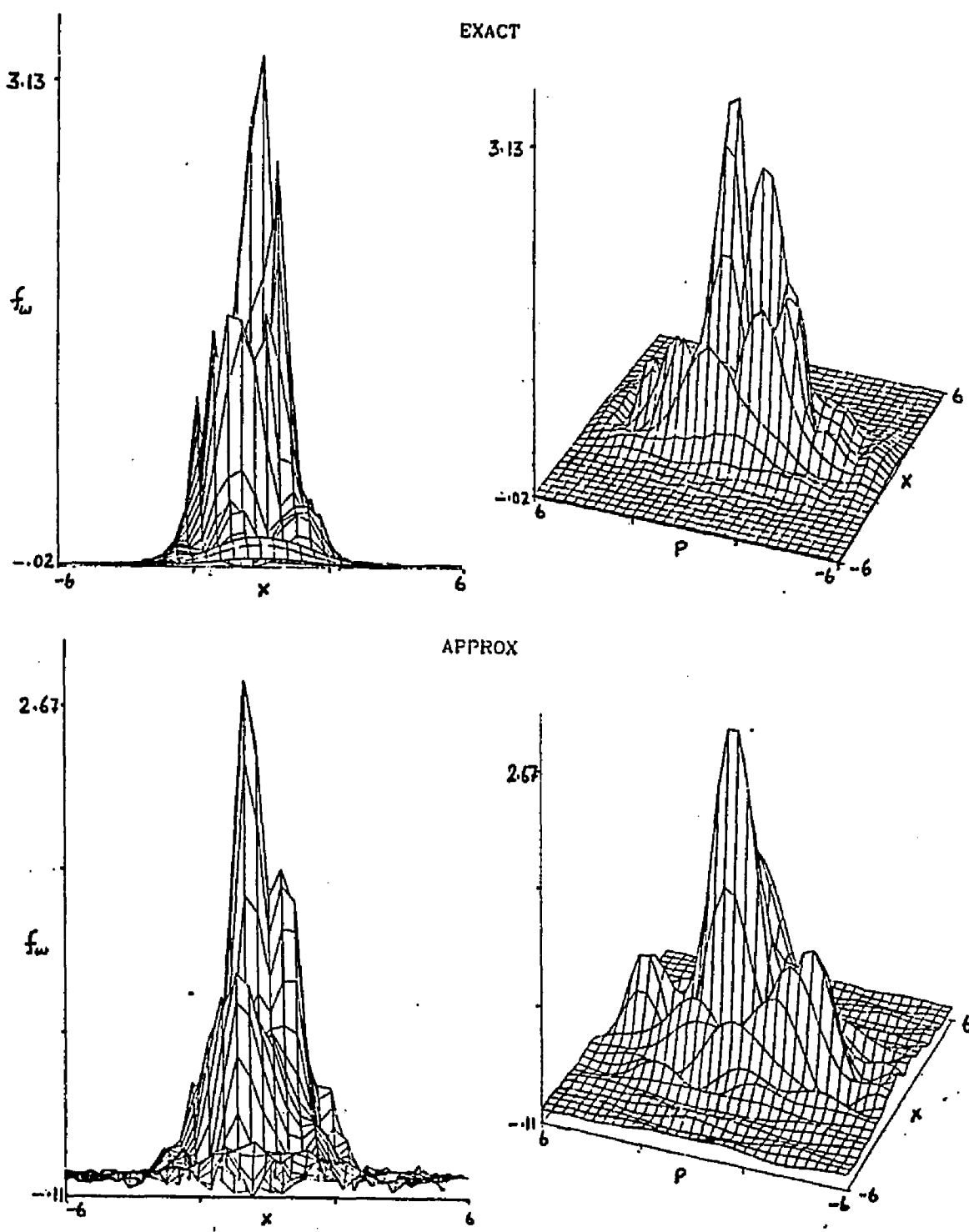


figure 36.  $\beta = .25$   $k_2 = .5$   $T = 3\pi$

### 5.3 Moments of the distribution

The moments for the distribution may be calculated by summing over the contribution from each of the points, for instance

$$\langle x \rangle = \frac{1}{N} \sum x_i \sigma_i$$

$$\langle x^2 \rangle = \frac{1}{N} \sum x_i^2 \quad (5.6)$$

However this procedure has a source of error as seen from the figures 37 . These plots are drawn by calculating the averages of points lying within squares centered at  $\langle x \rangle, \langle p \rangle$  calculated as in 5.6 and increasing its dimension by unity at each step. The average vs. the number of points within this space are plotted. These show that about 10 % of points lying in the outer regions cause large changes in the averages. This is because an error caused by  $\delta n$  at very large distances causes an error in the averages as

$$\epsilon \langle x \rangle \propto \frac{\delta n}{f(x,p)} \frac{x}{N}$$

The sources of these error are mainly due to the large annihilation distances that was given in these outer regions.

See figure 38. for a comparison of the classical, exact, and approximate averages.(all points included)

figures 37-38

fig.37 These pictures show the change in the averages for  $x, p$  when the total number of points included in its evaluation is increased by spanning areas in increasing radii. The pictures are for  $\beta = .5$  and  $k_2 = .5$  and  $N=1500$ . The different lines are for times varying from  $\pi/3$  to  $4\pi$  at intervals of  $\pi/3$ .

It is evident from these pictures that about 10% of the points lying at the outer edges considerably distort the accuracy of the evaluation for  $\langle x \rangle, \langle p \rangle$ .

fig.38 Comparisons of classical, exact and approximate averages. The approximate averages are calculated using all the points. The points are marked at intervals of  $\pi/3$ .

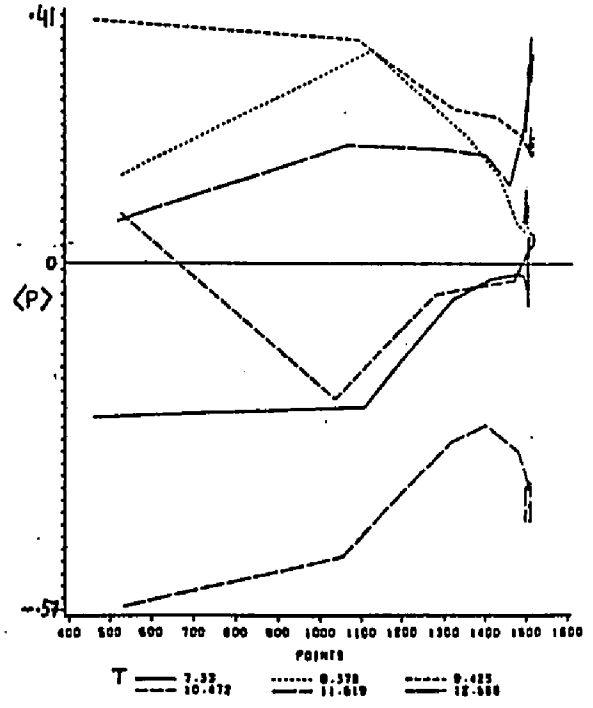
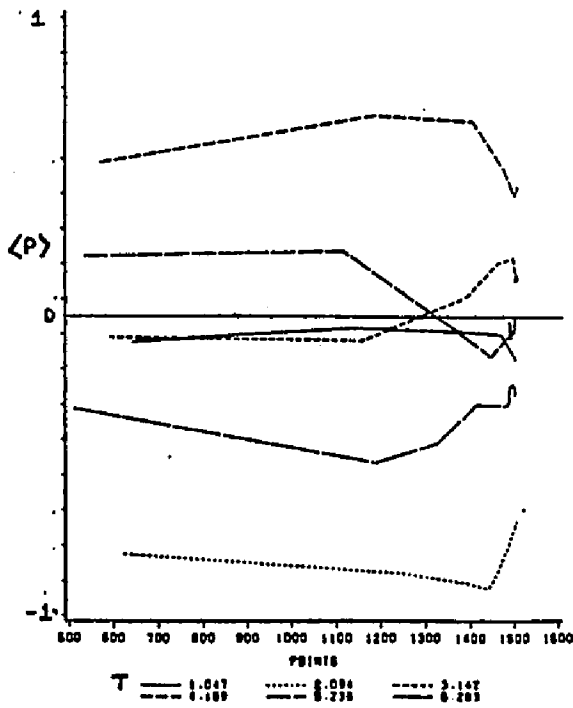
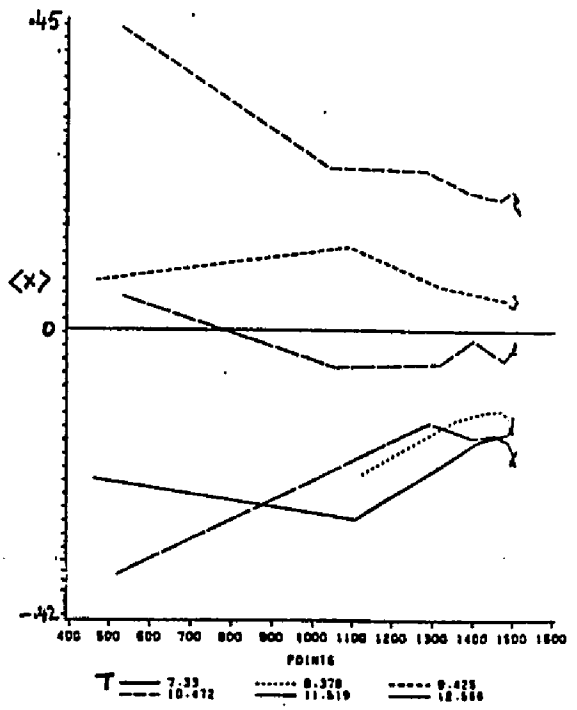
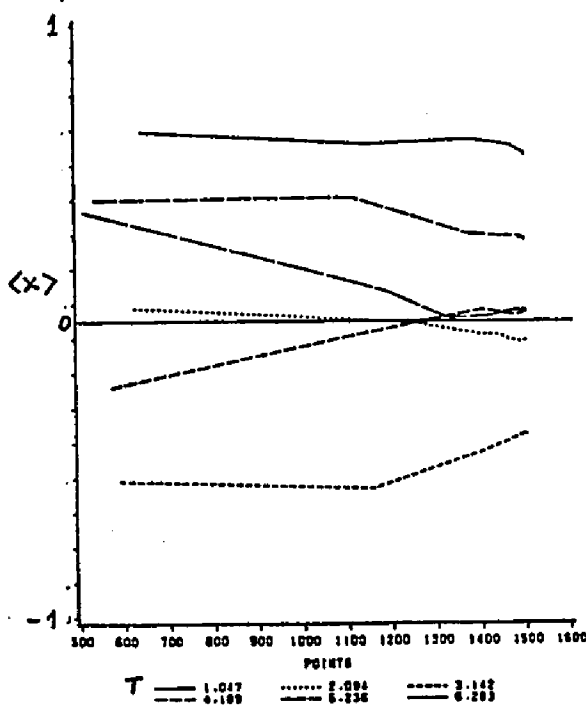


figure 37. Averages vs. number of points for various times in steps of  $\pi/3$  ( $N=1500$ ). Note that about 10% of points in the outlying regions cause large deviations.

$\beta = .5 \quad k_2 = .5$

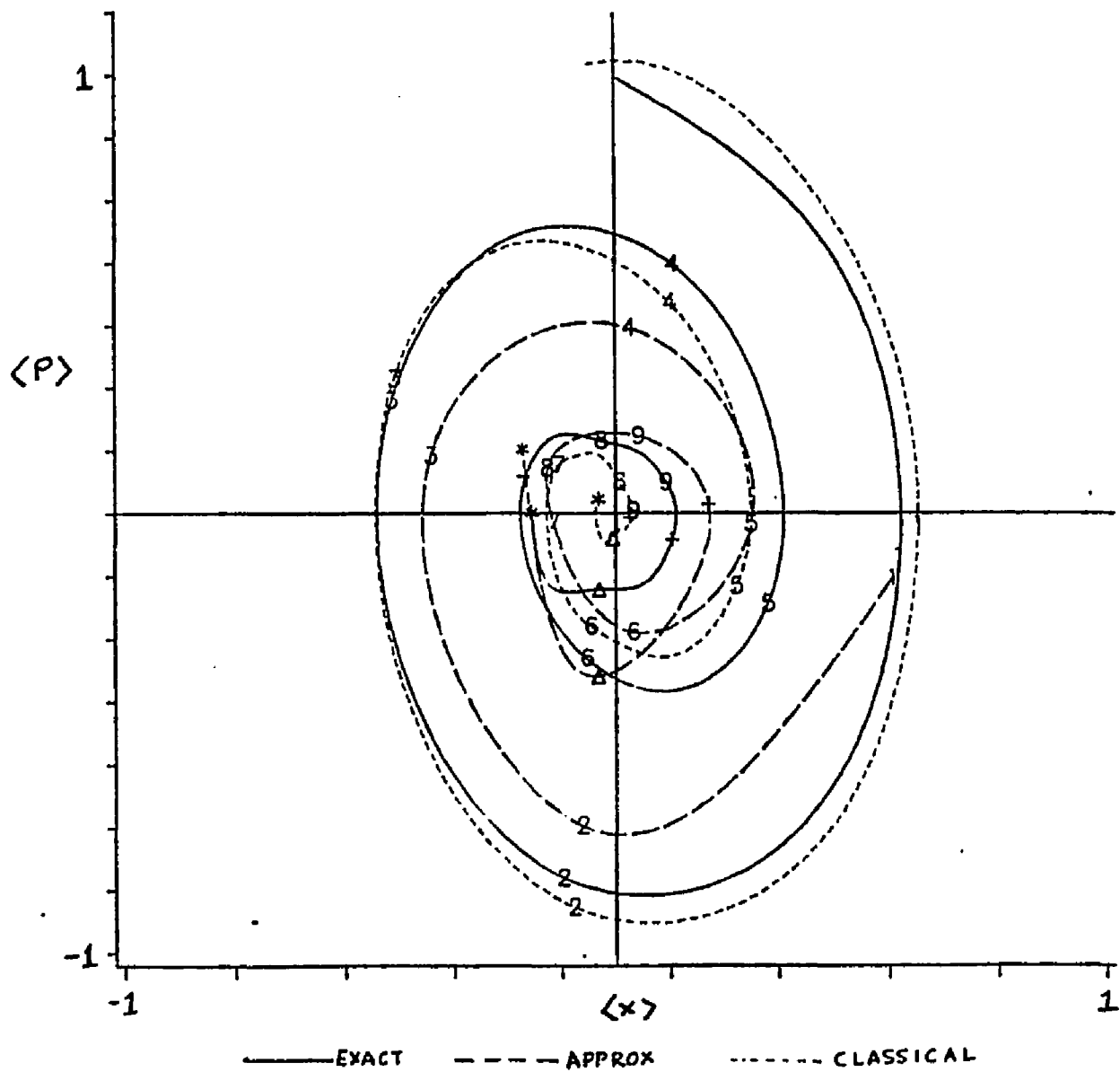


Figure 38. Comparison of classical, exact and approximate averages for  $\beta = .5$ ,  $k_2 = .5$

A Note:

In Chapter 2 it was seen that the classical and quantum averages over long intervals of time differed significantly. Does this contradict Ehrenfest's theorem which states the classical and quantum averages to be the same ? We show in Appendix 5.3 how the quantum Liouville equation does not contradict Ehrenfest's theorem.

5.4 Statistics

There are two sources of statistical errors.

1. In the initial population.
2. In the stochastic time evolution.

The errors for 1 are estimated by taking the averages of 10 different initial population and finding the root mean square deviations. The errors for 2 are estimated by finding the averages of 5 runs after a time of  $\pi/3$  . Only 100 points were used for this purpose because of the large run times involved. The error estimates should be proportional to  $1/\sqrt{N}$ . See Table 3.

Table 3

-----						
Statistical R.M.S. deviations for						
Case	N	time	<x>	<p>	var x	varp
-----						
Initial	1000	0	.02	.01	.03	.03
1.	100	$\pi/3$	.05	.16	.06	.08
2.	100	..	.04	.12	.28	.20
3.	100	..	.06	.04	.02	.04
4.	100	..	.02	.13	.03	.04
4.	200	..	.01	.08	.04	.03
-----						

## 5.5 Conclusions

We see that the approximate numerical technique introduced in this thesis has given very encouraging results in incorporating the quantum effect over the purely classical motion. The results show the method to be most suited to mixed states, as was originally intended.

The sources of errors in this method ,due to a finite number of representative points, large annihilation distances, and the necessity for smearing widths may all well be reduced , but will involve more computer time and memory storage. Such efforts may be undertaken in the future.

## Chapter 6

### 6.1 Summary

Our main objective was to develop a numerical procedure to study the quantum Liouville equation for systems that are quasi-classical . For such systems, the first order quantum correction is sufficient to describe its time evolution.

The procedure incorporates the first order quantum effect as a Markovian stochastic process in a phase space formulation of the quantum Liouville equation, viz, the Wigner formulation.

Using this method, the time evolution of a class of initial state Wigner distributions, representing various mixed states, was studied. The model Hamiltonian used pertained to an anharmonic quartic potential . The results were then compared with the purely classical and exact results. The comparisons show that there is an overall improvement effected by our procedure over the purely classical motion. The method gives improved results for functions that represent highly mixed states.

## 6.2 Future Applications

So far, we have considered only a one dimensional case. The method may be extended to the study of higher dimensions. Whereas in conventional grid techniques the computing needs in a 3-D calculation increases as the cubic power, here we anticipate an increase only by a factor of 3. (This is because each representative point now has 3 components.)

The method is also suited for the numerical study of many-body systems which interact via a local density dependent mean-field such as in TDHF calculations. Such applications include the study of heavy ion collisions where the nuclear densities have slow spatial and momentum variations. Despite the computational errors involved (which increase in time) the method will be suited for such studies because the time of interaction is of the order of  $2\pi$  and hence numerical dissipative effect would not have become a predominant source of error.

It is also hoped that the algorithm will be suited to the study of few body problems. A substantial gain in computing efficiency may be obtained by a reduction from a  $6n$  dimensional grid-space to  $n$  representative points, where  $n$  denotes the number of bodies involved.

As pointed out earlier, the sources of errors in this method, due to a finite number of representative

points and large annihilation distances, may be reduced, but will involve more computer time and memory storage. Such efforts may be undertaken in the future.

## Appendix 1

### An Introduction to quantum Liouville Equation:

#### The density operator formalism of quantum mechanics

This is an alternate formulation of quantum mechanics and is most suited for the study of mixed states. Now a pure state  $\psi(x)$  is a state of maximum information and can be represented by a vector in Hilbert space. The state can be represented as a density operator

$$\rho = |\psi\rangle\langle\psi|$$

A mixed state occurs in situations where one cannot define the state of the system with certainty because of the 'lack of complete information'. Hence only a probability distribution can be assigned for the system to be in one of the many states. Averages are calculated over an ensemble of states. The density operator is given by

$$\rho = \sum P(a) |\psi_a\rangle\langle\psi_a|$$

where  $P(a)$  is the probability that the system is in state  $|\psi_a\rangle$  with the following properties:

- (i)  $P(a) \geq 0$
- (ii)  $\sum P(a) = 1$

(iii) The expectation value of an operator A is

$$\langle A \rangle = \text{tr} [\rho A]$$

The time evolution of the density matrix is derived from Schrodinger equation and is given by the equation

$$i \hbar \partial \rho / \partial t = [H, \rho]$$

This is the von Neumann or the Quantum Liouville equation. The solution is given as

$$\rho(t) = \exp(-iHt/\hbar) \rho(0) \exp(iHt/\hbar)$$

## Appendix 2

### Appendix 2.1

$\langle\langle xp|mn\rangle\rangle$

Special Case      $x = p = 0$

$$\begin{aligned}\langle\langle 00|mn\rangle\rangle &= \int dy \langle -iy|m\rangle \langle n|iy\rangle \\ &= \int dy N_m \exp(-y^2/8) H_m(-y/2) N_n \exp(-y^2/8) \\ &\quad \times H_n(y/2) \\ &= (-1)^m N_m N_n \int dy \exp(-y^2/4) H_m(y/2) H_n(y/2) \\ &= (-1)^n \quad 2 \quad \text{for } m = n \\ &= 0 \quad \text{otherwise}\end{aligned}$$

Symmetries of  $\langle\langle xp|mn\rangle\rangle$

$$\langle\langle xp|mn\rangle\rangle = \int dy e^{ipy} \langle x-iy|m\rangle \langle n|x+iy\rangle$$

$$\begin{aligned}\langle\langle xp|nm\rangle\rangle &= \int dy e^{ipy} \langle x-iy|n\rangle \langle m|x+iy\rangle \\ &= \int dy e^{-ipy} \langle x+iy|n\rangle \langle m|x-iy\rangle \\ &= \langle\langle xp|mn\rangle\rangle^*\end{aligned}$$

$$\begin{aligned}\langle\langle -x -p|mn\rangle\rangle &= \int dy e^{-ipy} \langle -x-iy|m\rangle \langle n|-x+iy\rangle \\ &= \int dy e^{-ipy} (-1)^{m+n} \langle x+iy|m\rangle \langle n|x-iy\rangle \\ &= (-1)^{m+n} \int dy e^{ipy} \langle x-iy|m\rangle \langle n|x+iy\rangle \\ &= (-1)^{m+n} \langle\langle xp|mn\rangle\rangle\end{aligned}$$

$$\langle\langle -xp|mn\rangle\rangle = (-1)^{m+n} \langle\langle xp|mn\rangle\rangle^*$$

Appendix 2.2Density matrix elements for initial distribution

$$\begin{aligned}
f_{\omega}(x,p,0) &= 2\exp[(-\beta(x-x_0)^2/k^2 - \beta k^2(p-p_0)^2)] \\
\langle x-iy | \rho_0 | x+iy \rangle &= \frac{1}{2\pi} \int e^{-ipy} f_{\omega}(x,p,0) dp \\
&= \frac{1}{\pi} e^{-\beta(x-x_0)^2/k^2} \int e^{-ipy - \beta k^2(p-p_0)^2} dp \\
&= \frac{1}{\pi} e^{(-\beta(x-x_0)^2/k^2 - \beta k^2 p_0^2)} \\
&\quad \int e^{-\beta k^2 p^2 + p(-iy + 2p_0 \beta k^2)} dp \\
&= \frac{1}{(\pi \beta k^2)^{\frac{1}{2}}} e^{(-\beta(x-x_0)^2/k^2 - (y^2/4\beta k^2) - iyp_0)}
\end{aligned}$$

Appendix 2.3

To evaluate  $\langle q | \rho_0 | s \rangle$

$$\langle q | \rho_0 | s \rangle = \int dx dy \langle q | x-iy \rangle \langle x-iy | \rho_0 | x+iy \rangle \langle x+iy | s \rangle$$

substitute

$$\begin{aligned}
\langle x-iy | \rho_0 | x+iy \rangle \\
= \left( \frac{1}{\pi \beta k^2} \right)^{\frac{1}{2}} \exp\left( (-\beta(x-x_0)^2/k^2 - (y^2/4\beta k^2) - iyp_0) \right)
\end{aligned}$$

and

$$\langle q | x-iy \rangle = N_q \exp(-(x-iy)^2/2) H_q(x-iy)$$

gives

$$\langle q | \rho_0 | s \rangle = N_1 \exp(-\beta x_0^2/k^2)$$

$$\int dx dy \exp(-\beta_1 x^2 - \beta_2 y^2 + \beta_3 x x_0 - iyp_0) H_q(x-iy) H_s(x+iy)$$

where  $N_1 = N_q N_s / (\pi \beta k^2)^{\frac{1}{2}}$

$$\beta_1 = 1 + \beta/k^2$$

$$\beta_2 = (1 + 1/(\beta k^2)) / 4$$

$$\beta_3 = 2\beta x_0/k^2$$



$$\begin{aligned} & \frac{\partial^q}{z_1} \exp(-z_1^2 \beta_4 + z_1 \beta_6) \\ & \frac{\partial^s}{z_2} \exp(-z_2^2 \beta_4 + z_2 \beta_6^* + z_1 z_2 \beta_5) \Big|_{\substack{z_1=0 \\ z_2=0}} \end{aligned} \quad (1)$$

Now consider

$$\frac{\partial^s}{z_2} \exp(-z_2^2 \beta_4 + z_2 (\beta_6^* + z_1 \beta_5)) \Big|_{z_2=0} \quad (2)$$

Let

$$\begin{aligned} z_2^2 \beta_4 &= \xi_2^2 \\ z_2 (\beta_6^* + z_1 \beta_5) &= 2\xi_2 \xi_2 \theta \end{aligned}$$

Therefore expression (2) becomes

$$\begin{aligned} &= (\beta_4)^{s/2} \frac{\partial^s}{\xi_2} \exp(-\xi_2^2 + 2\xi_2 \xi_2 \theta) \Big|_{\xi_2=0} \\ &= (\beta_4)^{s/2} H_s(\xi_2 \theta) \end{aligned}$$

with

$$\xi_2 \theta = \left( \frac{1}{2\sqrt{\beta_4}} \right) (\beta_6^* + z_1 \beta_5)$$

Substituting in (2)

$$\begin{aligned} &= (\beta_4)^{s/2} \frac{\partial^q}{z_1} \exp(-z_1^2 \beta_4 + z_1 \beta_6) H_s(\xi_2 \theta) \Big|_{z_1=0} \\ &= (\beta_4)^{s/2} \sum_r^q \frac{q!}{r! (q-r)!} \frac{\partial^r}{z_1} H_s(\xi_2 \theta) \frac{\partial^{q-r}}{z_1} \exp(-z_1^2 \beta_4 + z_1 \beta_6) \end{aligned}$$

Now

$$H_s^r = \frac{s!}{(s-r)!} H_{s-r}$$

$$\begin{aligned} & \frac{\partial^r}{z_1} H_s(\xi_2 \theta) \Big|_{z_1=0} \\ &= \left( \frac{\beta_5}{2\beta_4} \right)^s \frac{s!}{(s-r)!} H_{s-r}(\xi_2 \theta) \Big|_{z_1=0} \\ &= \left( \frac{\beta_5}{2\beta_4} \right)^r \frac{s!}{(s-r)!} H_{s-r}(\beta_6^*/2\beta_4) \end{aligned}$$

and

$$\frac{\partial}{\partial z_1} \exp(-z_1^2 \beta_4 + z_1 \beta_6) \Big|_{z_1=0} = (\beta_4)^{(q-r)/2} H_{q-r}(\beta_6/2\beta_4^{\frac{1}{2}})$$

finally

$$\langle q | \rho_0 | s \rangle =$$

$$\frac{1}{k} \left( \frac{q!s!}{2^{q+s} \beta \beta_1 \beta_2} \right)^{\frac{1}{2}} \exp[(-\beta x_0^2/k^2) + (\beta_3^2 x_0^2/4\beta_1) - (p_0^2/4\beta_2)]$$

$$\sum_{r=0}^{\min(q,s)} \frac{1}{r!(q-r)!(s-r)!} (\beta_5/2)^r \beta_4^{(s+q)/2} H_{q-r}(\beta_6/2\beta_4^{\frac{1}{2}})$$

$$H_{s-r}(\beta_6^*/2\beta_4^{\frac{1}{2}})$$

#### Appendix 2.4

The following quantities occur in the expressions for the moments.

$$\begin{aligned} \langle x \rangle_{mn} &= \frac{\beta}{2\pi} \int \langle xp | mn \rangle x dx dp \\ &= \frac{\beta}{2\pi} N_m N_n \int dy e^{ipy} e^{-x^2 - y^2/4} H_m(x - iy) H_n(x + iy) x dx dp \end{aligned}$$

Using

$$\int e^{ipy} dp = 2\pi \delta(y)$$

$$\int e^{-x^2} H_m(x) H_{n+1}(x) dx = 2^m m! \sqrt{\pi} \delta_{m,n+1}$$

and the recurrence formula

$$2x H_n(x) = H_{n+1}(x) + 2n H_{n-1}(x)$$

gives

$$\begin{aligned} \langle x \rangle_{mn} &= \beta N_m N_n \int e^{-x^2} H_m(x) H_n(x) x dx \\ &= (\beta/2) [\sqrt{(2m)} \delta_{m,n+1} + \sqrt{(2m+2)} \delta_{m,n-1}] \end{aligned}$$

$$\langle p \rangle_{mn} = N_m N_n \frac{\beta}{2\pi} \int dy e^{ipy - x^2 - y^2/4} H_m(x - iy) H_n(x + iy) p dx dp$$

Using

$$\int dp e^{ipy} p = -2\pi i \delta'(y)$$

$$\int f(y) \delta'(y) dy = -(d/dy) f(y) \Big|_{y=0}$$

$$\frac{d}{dy} f(x-y) = -\frac{d}{dx} f(x-y)$$

gives

$$\langle p \rangle_{mn} = -\frac{\beta i}{2} N_m N_n \int dx e^{-x^2} [H_m'(x) H_n(x) - H_m(x) H_n'(x)]$$

with

$$H_n'(x) = 2n H_{n-1}(x)$$

and

$$\int e^{-x^2} H_m(x) H_{n+1}(x) dx = 2^m m! \sqrt{\pi} \delta_{m,n+1}$$

$$\langle p \rangle_{mn} = \frac{\beta}{\sqrt{2}} i [-\sqrt{m} \delta_{n,m-1} + \sqrt{(m+1)} \delta_{m,n-1}]$$

$$\langle x^2 \rangle_{mn} = N_m N_n \frac{\beta}{2\pi} \int dy e^{ipy - x^2 - (y^2/4)} H_m(x - iy) H_n(x + iy) x^2 dx dp$$

$$= \beta N_m N_n \int dx e^{-x^2} x H_m(x) x H_n(x)$$

$$= (\beta/2) [(m+1) \delta_{m+1,n+1} + \sqrt{(m+2)(m+1)} \delta_{m+1,n-1} \\ + \sqrt{m(m-1)} \delta_{m-1,n+1} + m \delta_{m-1,n-1}]$$

$$\langle p^2 \rangle_{mn} = N_m N_n \frac{\beta}{2\pi} \int dy e^{ipy - x^2 - (y^2/4)} H_m(x - iy) H_n(x + iy) p^2 dx dp$$

Using

$$\int e^{ipy} p^2 dp = -2\pi \delta''(y)$$

$$\int f(y) \delta''(y) dy = f''(y) \Big|_{y=0}$$

$$(d/dy) H(x-y) = -(d/dx) H(x-y)$$

we have

$$\begin{aligned} \langle p^2 \rangle_{mn} &= -\beta N_m N_n \int e^{-x^2} [-i H_m H_n + (1/4) H_m'' H_n - \\ &\quad i H_m' H_n' + (1/4) H_m H_n''] \\ &= (\beta/2) [\delta_{m,n} - \sqrt{(m-(m-1))} \delta_{m-2,n} + 2m \delta_{m-1,n-1} \\ &\quad - \sqrt{(m+2)(m+1)} \delta_{m,n-2}] \\ \langle xp \rangle_{mn} &= N_m N_n \frac{\beta}{2\pi} \int dy e^{ipy - x^2 - (y^2/4)} H_m(x-iy) H_n(x+iy) xp dx dp \\ &= -\frac{\beta i}{2} \int e^{-x^2} x [H_m' H_n - H_m H_n'] dx \\ &= -\beta i \int e^{-x^2} x [m H_{m-1} H_n - n H_m H_{n-1}] dx \\ &= i\beta/4 [-\sqrt{(m(m-1))} \delta_{m-1,n+1} + \sqrt{(m+1)(m+2)} \delta_{m,n-2}] \end{aligned}$$

Appendix 3

appendix 3.1

perturbative expansion of  $e^{(L_c + L_q)\Delta t}$  to second order in  $\Delta t$

$$e^{(L_c + L_q)\Delta t} = e^{L_c \Delta t} + \int_0^{\Delta t} dt' e^{(\Delta t - t')L_c} L_q e^{L_c t'}$$

(this can be proved by taking time derivatives on both sides)

$$= e^{L_c \Delta t} + \int_0^{\Delta t} dt' e^{(\Delta t - t')L_c} L_q e^{L_c t'} \\ + \int_0^{\Delta t} dt' e^{L_c(\Delta t - t')} L_q \int_0^{t'} dt'' e^{L_c(t' - t'')} L_q e^{L_c t''} + \dots$$

The second term is

$$= e^{L_c \Delta t} \Delta t [e^{-L_c \Delta t / 2} L_q e^{L_c \Delta t / 2}]$$

The third term is

$$= \int_0^{\Delta t} dt' e^{L_c(\Delta t - t')} L_q [t' e^{L_c(t' - t'/2)} L_q e^{L_c t'/2}]$$

$$= e^{L_c \Delta t} \int_0^{\Delta t} dt' t' e^{-L_c t'} L_q e^{L_c t'/2} L_q e^{L_c t'/2}$$

Considering an average value of  $t' = \Delta t / 2$

$$= e^{L_c \Delta t} \Delta t (\Delta t / 2) e^{-L_c \Delta t / 2} L_q e^{L_c \Delta t / 4} L_q e^{L_c \Delta t / 4}$$

$$= (\Delta t)^2 / 2 e^{-L_c \Delta t / 2} L_q^2 e^{L_c \Delta t / 2}$$

Hence we have

$$\begin{aligned}
 e^{(L_C+L_Q)\Delta t} &= e^{L_C\Delta t} + e^{L_C\Delta t/2} [L_Q\Delta t + L_Q^2(\Delta t)^2/2] e^{L_C\Delta t/2} \\
 &= e^{L_C\Delta t} + e^{L_C\Delta t/2} [e^{L_Q\Delta t} - 1] e^{L_C\Delta t/2}
 \end{aligned}$$

### Appendix 3.2

#### Alternate Expansion of $e^{(L_C + L_Q)\Delta t}$

Consider an operator

$$A(\Delta t) = e^{L_C\Delta t} e^{-(L_C + L_Q)\Delta t} e^{L_Q\Delta t}$$

Consider the power series expansion

$$A(\Delta t) = A(0) + \Delta t A'(0) + \Delta t^2/2 A''(0) + \dots$$

$$A(0) = 1$$

$$A' = \frac{dA}{d(\Delta t)}$$

$$= -e^{L_C\Delta t} L_Q e^{-(L_C+L_Q)\Delta t} + e^{L_C\Delta t} e^{-(L_C+L_Q)\Delta t} L_Q e^{L_Q\Delta t}$$

$$A'(0) = -L_Q + L_Q = 0$$

Similarly

$$A''(0) = [L_Q, L_C]$$

Therefore we have

$$e^{L_C\Delta t} e^{-(L_C+L_Q)\Delta t} e^{L_Q\Delta t} = 1 + (\Delta t^2/2) [L_Q, L_C]$$

$$\begin{aligned}
 e^{-(L_C+L_Q)\Delta t} &= e^{-L_C\Delta t} e^{-L_Q\Delta t} + (\Delta t^2/2) e^{-L_C\Delta t} [L_Q, L_C] e^{-L_Q\Delta t} \\
 &+ \dots
 \end{aligned}$$

## Appendix 4

### Appendix 4.1

Evaluation of  $I(p, a) = e^{-a\partial^3/\partial p^3} \delta_\alpha(p)$

#### Small a expansion

$$\begin{aligned} \frac{1}{\sqrt{(\pi 2)^\alpha}} e^{-a\partial^3/\partial p^3} e^{-p^2/2\alpha^2} \\ = \frac{1}{\sqrt{(2\pi)^\alpha}} \sum_n \frac{(-1)^n a^n}{n!} \partial_p^{3n} e^{-p^2/2\alpha^2} \quad (1) \end{aligned}$$

Now Rodrigues formula is

$$H_n(x) = (-1)^n e^{x^2} d_x^n e^{-x^2}$$

from which

$$d_x^{3n} e^{-x^2} = (-1)^{3n} e^{-x^2} H_{3n}(x)$$

which substituted in (1) gives

$$I = (\sqrt{(2\pi)^\alpha})^{-1} \sum_n \frac{a^n}{n! (\sqrt{2\alpha})^{3n}} e^{-p^2/2\alpha^2} H_{3n}(p/\sqrt{2\alpha})$$

$p' \rightarrow \infty$

For large  $p'$  a more suitable form is the integral representation

$$I = \operatorname{Re} \frac{\sqrt{2|p'|}}{\pi \alpha} \int_0^\infty e^{|p'|^{3/2} (ia'x^3 - (x^2/|p'|)^{1/2} \pm ix)} dx$$

(In  $\pm$  the -ive sign is for  $p'$  negative). This is evaluated by the method of steepest descent. Along the path of constant phase, there should be a contribution

from the end point(origin) and a contribution from the saddle point.

Contribution from the origin

We show here that the contribution from the origin is pure imaginary. In the complex  $z$  plane the integral is

$$\int_C e^{|p'|^{3/2}(ia'z^3 - z^2/|p'|^{1/2} \pm iz)} dz \quad (1)$$

For  $|p'| \rightarrow \infty$ , along the steepest path only an infinitesimally small path near the origin contributes. Let the path of constant phase be

$$z = se^{i\phi}$$

Then

$$I = e^{i\phi} \int_0^\epsilon e^{\pm i|p'|^{3/2} se^{i\phi}} e^{i|p'|^{3/2}[ia's^3 e^{3i\phi} - s^2 e^{2i\phi}/|p'|^{1/2}]} ds$$

For small values of  $s$  the second exponential is Taylor expanded, the path of steepest descent being defined by the first exponential.

$$e^{i\phi} = \pm i \quad \text{gives} \quad \phi = \pm \pi/2$$

$$\text{or } z = \pm is$$

i.e the path is along the imaginary axis.

Substituting in (1)

$$I = \pm i \int_0^\infty e^{|p'|^{3/2}[\pm a's^3 \pm s^2/|p'|^{1/2} - s]} ds$$

This integral is pure imaginary and therefore does

not contribute to I.

### Position of the Saddle Point

With

$$f(z) = ia'z^3 - (z^2/|p'|^{\frac{1}{2}}) \pm iz$$

the position of the maxima(s.p.) is given by  $f'(z_0) = 0$

$$z_0 = \frac{-2i}{6a'|p'|^{\frac{1}{2}}} [1 \pm (1+3a'p')^{\frac{1}{2}}]$$

We have 3 cases

- (i)  $1+3a'p' > 0$  : both  $z_0$  lie on the imaginary axis.  
The root closest to the origin is chosen.
- (ii)  $3a'p' = 0$  : both roots collapse to a single point on the imaginary axis.
- (iii)  $1+3a'p' < 0$  : both roots obtain real components.

The root on the real positive half plane is chosen.

$$\underline{(1+3a'|p'|) > 0}$$

For large  $p'$  (in what follows  $p'$  denotes the magnitude)

I =

$$p'^{\frac{1}{2}} e^{p'^{3/2}} f(z_0) \int_c e^{p'^{3/2}} [\frac{1}{2}(z-z_0)^2 f''(z_0) + (z-z_0)^3 f'''(z_0)/6] dz$$

With

$$f''(z_0) = \pm 2p'^{-\frac{1}{2}} (1+3a'p')^{\frac{1}{2}}$$

$$f'''(z_0) = 6ia'$$

$$z - z_0 = se^{i\phi}$$

We choose the -ive sign as this is the first root along the imaginary axis and only  $0 - \epsilon$  contributes along the integral.

Therefore

$$I = e^{i\phi} \int_0^\epsilon e^{-p'(1 \pm 3a'p')^{\frac{1}{2}} s^2} e^{2i\phi + ia'p'^{3/2} s^3} e^{3i\phi} ds$$

Choose the path such that

$$e^{2i\phi} = 1 \quad \text{which gives} \quad \phi = 0$$

$$I = \int_0^\epsilon e^{-p'(1 - 3a'p')^{\frac{1}{2}} s^2 + ia'p'^{3/2} s^3} ds$$

which gives

$$I = \operatorname{Re}(\sqrt{2\pi\alpha})^{-1} e^{p'^{3/2} f(z_0)} \sum \frac{(ia')^n \Gamma[(3n+1)/2]}{n! |1 \pm 3a'p'|^{(3n+1)/4}}$$

$$\underline{1 - 3a'p' < 0}$$

$$I = p'^{\frac{1}{2}} e^{p'^{3/2} f(z_0)} e^{i\phi}$$

$$\int_\epsilon^\epsilon e^{ip'|1 - 3a'p'|^{\frac{1}{2}} s^2} e^{2i\phi + ia'p'^{3/2} s^3} e^{3i\phi} ds$$

Now choose the path such that

$$e^{2i\phi} = i \quad \text{which gives} \quad \phi = \pi/4$$

Therefore

$$\begin{aligned} \int_\epsilon^\epsilon ds &= \int_0^\epsilon ds e^{-p'|1 \pm 3a'p'|^{\frac{1}{2}} s^2} \\ &\quad [e^{ia'p'^{3/2} s^3} e^{3i\pi/4} + e^{-ia'p'^{3/2} s^3} e^{-3i\pi/4}] \\ &= \int_0^\epsilon \sum (ia'p'^{3/2})^n (s^3 e^{3i\pi/4})^n [1 + (-1)^n] e^{-p'|1 \pm 3a'p'|^{\frac{1}{2}} s^2} ds \end{aligned}$$

$$= p'^{-\frac{1}{2}} \sum_{n \text{ even}} \frac{(ia'e^{3i\pi/4})^n \Gamma[(3n+1)/2]}{n! |1 \pm 3a'p'| (3n+1)/4}$$

$$I = \frac{\text{Re}/2}{\pi\alpha} e^{p'^{3/2}f(z_0)+i\pi/4} \sum_{n \text{ even}} \frac{(ia'e^{3i\pi/4})^n \Gamma[(3n+1)/2]}{n! |1 \pm 3a'p'| (3n+1)/4}$$

$$\underline{1-3a'p' \sim 0}$$

The general expression is

$$I' = e^{i\phi} \int_{-\epsilon}^{\epsilon} e^{\pm p'(1 \pm 3a'p')^{\frac{1}{2}} s^2} e^{2i\phi} + ia'p'^{3/2} s^3 e^{3i\phi} ds$$

Choose the path such that

$$e^{3i\phi} = i \quad \text{which gives } \phi = \pi/6$$

$$I' = e^{i\pi/6} \int_{-\epsilon}^{\epsilon} e^{\pm \delta s^2} e^{i\pi/3} - ks^3 ds$$

where

$$\delta = p'(1 \pm 3a'p')^{\frac{1}{2}}$$

$$k = a'p'^{3/2}$$

$$a.(1 \pm 3a'|p'|) > 0$$

Since the maxima lies on the imaginary axis only 0 -  $\epsilon$  contributes (the -ive sign is chosen as this is the nearest root).

$$I' = e^{i\pi/6} \int_0^{\epsilon} \sum_{n=0}^{\infty} \frac{(-\delta s^2 e^{i\pi/3})^n}{n!} e^{-ks^3} ds$$

$$= \frac{e^{i\pi/6}}{3} \sum_{n=0}^{\infty} \frac{(-\delta e^{i\pi/3})^n \Gamma[(2n+1)/3]}{n! 3 k^{(2n+1)/3}}$$

I =

$$\frac{\text{Re}/2}{3\pi\alpha} e^{p'^{3/2}f(z_0)+i\pi/6} \sum_{n=0}^{\infty} \frac{(-(1 \pm 3a'p')^{\frac{1}{2}} e^{i\pi/3})^n \Gamma[(2n+1)/3]}{n! a' (2n+1)/3}$$

b.  $(1+3a'|p'|) < 0$

Choose the +ive sign for the root which lies on the right half plane.

$$I' = e^{i\phi} \int_{-\epsilon}^{\epsilon} e^{\delta s^2} e^{2i\phi} + iks^3 e^{3i\phi} ds$$

Split the integral into two parts

$$= e^{i\phi_1} \int_0^{\epsilon} e^{\delta s^2} e^{2i\phi_1} + iks^3 e^{3i\phi_1} ds + e^{i\phi_2} \int_0^{\epsilon} e^{\delta s^2} e^{2i\phi_2} - ks^3 e^{3i\phi_2} ds$$

For the first integral, the path is that

$$e^{3i\phi_1} = i \quad \text{which gives} \quad \phi_1 = \pi/6$$

and for the second integral

$$e^{3i\phi_2} = -i \quad \text{which gives} \quad \phi_2 = \pi/2$$

$$\begin{aligned} I &= e^{i\pi/6} \int_0^{\epsilon} e^{\delta s^2} e^{i\pi/3} - ks^3 ds + e^{i\pi/2} \int_0^{\epsilon} e^{\delta s^2} e^{i\pi} - ks^3 ds \\ &= \int_0^{\epsilon} \sum \frac{\delta^n}{n!} [e^{i(n+\frac{1}{2})\pi/3} + e^{i(n+\frac{1}{2})\pi}] s^{2n} e^{-ks^3} ds \\ &= \sum \frac{\delta^n}{n!} [e^{i(n+\frac{1}{2})\pi/3} + e^{i(n+\frac{1}{2})\pi}] \frac{\Gamma[(2n+1)/3]}{3k(2n+1)/3} \end{aligned}$$

$$I = \frac{\text{Re}/2}{3\pi\alpha} e^{p'3/2} f(z_0) \sum \frac{(1+3a'|p'|)^{n/2}}{n!} \frac{\Gamma[(2n+1)/3]}{a'(2n+1)/3}$$

$$\times [e^{i(n+\frac{1}{2})\pi/3} + e^{i(n+\frac{1}{2})\pi}]$$

## Appendix 5

### Appendix 5.1

Prove  $J(p, a) = J(-p, -a)$

Now for the Gaussian distribution

$$I(p, a) = \frac{1}{2\pi} \int_{-\infty}^{\infty} e^{iay^3 + ipy - \alpha y^2} dy$$

and

$$\begin{aligned} I(-p, -a) &= \frac{1}{2\pi} \int e^{-iay^3 - ipy - \alpha y^2} dy \\ &= I(p, a) \end{aligned}$$

by a change of variables  $y' = -y$ . Hence

$$\begin{aligned} J(p, a) &= I(p, a) - \delta(p) \\ &= J(-p, -a) \end{aligned}$$

### Appendix 5.2

The function may be reconstructed using a complete set of normalised Harmonic Oscillator Wave functions. This motivation is derived from the initial state being of the Gaussian form.

A delta function may be represented as

$$\begin{aligned} \delta(x-x') &= \langle x | x' \rangle \\ &= \sum_n \langle x | n \rangle \langle n | x' \rangle \end{aligned}$$

where  $|n\rangle$  is a complete set of orthonormal Harmonic Oscillator states. Hence the density at any point is

$$\rho(x,p) = \frac{2\pi}{N\beta} \sum_{n,m} \langle x|n\rangle \langle p|m\rangle \sum_i \langle n|x_i\rangle \langle m|p_i\rangle \quad (1)$$

The summation over  $i$  is converted to a summation over a grid.

$$\sum \langle n|x_i\rangle \langle m|p_i\rangle = \sum w(x_j, x_k) \langle n|x_j\rangle \langle m|x_k\rangle \quad (2)$$

Suitably scaled Harmonic oscillator wave functions must be used for rapid convergence.

$$\langle x|n\rangle = N_n e^{-x^2/2\sigma^2} H_n(x/\sigma) \quad (3)$$

where  $N_n$  is the Normalization factor.

$$N_n = 1 / (\sigma^{\frac{1}{2}} (2^n n! / \pi)^{\frac{1}{2}})$$

From 1,2,3 we get

$$\begin{aligned} \rho(x,p) &= \frac{2\pi}{N\beta} \sum_{n,m} N_n^2 N_m^2 e^{-x^2/2\sigma^2} e^{-p^2/2\sigma^2} H_n(x/\sigma) H_m(p/\sigma) w_{mn} \\ &= \frac{2\pi}{N\beta} \sum_{n,m} N_n^2 N_m^2 e^{-x^2/2\sigma^2} e^{-p^2/2\sigma^2} H_n(x/\sigma) H_m(p/\sigma) w_{mn} \end{aligned}$$

where

$$w_{mn} = \sum_{j,k} w(x_j, x_k) e^{-x_j^2/2\sigma^2} e^{-x_k^2/2\sigma^2} H_n(x_j/\sigma) H_m(x_k/\sigma)$$

We must truncate the  $m,n$  series to obtain a smooth function. Hence a renormalization may be done as follows.

$$R \int \rho_a(x,p) dx dp = 2\pi/\beta$$

where  $R$  is the normalization factor.

Hence

$$\frac{2\pi}{\beta R} = \sum_{n,m} N_n^2 N_m^2 I_n I_m w_{mn}$$

where

$$I_n = \int e^{-x^2/2\sigma^2} H_n(x/\sigma) dx$$

$$= 0 \quad \text{for } n \text{ odd}$$

$$= \frac{\sqrt{\pi} (2n)!}{n!} \left( \frac{1}{2\sigma^2} \right)^n (-1)^n$$

finally

$$\rho(x,p) = R \rho_a(x,p)$$

### Appendix 5.3

It will be shown that even though the long time averages of the classical and quantum motions differ, Ehrenfest's theorem is valid for every instant of time.

#### Ehrenfest's Theorem

This states that the quantum and classical averages are the same for a given distribution.

We now proceed to show that the quantum motion by itself does not change the average position and momenta from the classical average at any instant of time.

To first order in  $\Delta t$  we have

$$\begin{aligned} f_\omega(x,p,t+\Delta t) &= e^{(L_q+L_c)\Delta t} f_\omega(x,p,t) \\ &= e^{L_q\Delta t} e^{L_c\Delta t} f_\omega(x,p,t) \\ &= e^{L_q\Delta t} f_{\omega_c}(x,p,t) \end{aligned}$$

where  $f_{\omega_c}(x,p,t)$  is the distribution after the classical motion. The average after the quantum motion is

$$\begin{aligned}
\langle p \rangle &= \int f_{\omega C}(x, p, t + \Delta t) p \, dx \, dp \\
&= \int [ e^{Lq\Delta t} f_{\omega C}(x, p, t) ] p \, dx \, dp \\
&= \int e^{Lq\Delta t} f_{\omega C}(x, p', t) \delta(p - p') p \, dx \, dp \, dp' \\
&= \int f_{\omega C}(x, p', t) dx \, dp' [ e^{a\partial^3/\partial p^3} \frac{1}{2\pi} \int e^{i(p-p')y} p \, dp \, dy \\
&= \frac{1}{2\pi} \int f_{\omega C}(x, p', t) dx \, dp' e^{-ip'y} \int e^{-iay^3 + ipy} p \, dp \, dy \\
&= \frac{1}{2\pi} \int f_{\omega C}(x, p', t) dx \, dp' e^{-ip'y - iay^3} (-2\pi i) \delta'(y) \, dy \\
&= -i \int f_{\omega C}(x, p', t) dx \, dp' \int e^{-ip'y - iay^3} \delta'(y) \, dy
\end{aligned}$$

By using the following relations

$$\int g(y) \delta'(y) \, dy = -g'(0)$$

$$g(y) = e^{-ip'y - iay^3}$$

$$g'(y) = (-ip' - 3iay^2) e^{-ip'y - iay^3}$$

$$g'(0) = -ip'$$

gives

$$\langle p \rangle = \int f_{\omega C}(x, p', t) p' \, dx \, dp'$$

This shows that the average of  $p$  in time  $\Delta t$  remains unchanged by the quantum motion. A similar proof holds for  $\langle x \rangle$ . This verifies Ehrenfest's theorem.

However

$$d\langle p \rangle / dt = - \langle \nabla V \rangle$$

The R.H.S. is dependent on the distribution. In Chapter 2 it is seen that the quantum distribution is clearly different from the classical over large intervals of time. This difference in the distribution, originating in

quantum effects causes the rate of change in the classical averages to be different for the purely classical and exact developments.

## Appendix A

### Appendix A

#### Stochastic Quantum Development - using a discrete differentiation process

A delta function in phase space may be denoted as  $\langle x, p | x_i, p_i, \sigma \rangle$  where  $x_i, p_i$  are the co-ordinates and  $\sigma$  is the sign of the point.

$$|x, p, \sigma\rangle = \sigma |x, p\rangle$$

The quantum development is given by,

$$(e^{-a\partial_p^3} - 1) \langle x, p | x_i, p_i \rangle = \langle x, p | e^{a\partial_{p_i}^3} - 1 | x_i, p_i \rangle$$

for  $a \rightarrow 0$ ,

$$(e^{a\partial_{p_i}^3} - 1) |x_i, p_i\rangle \approx a\partial_{p_i}^3 |x_i, p_i\rangle$$

Define

$$a\partial_{p_i}^3 |x_i, p_i\rangle = \lim_{\Delta p \rightarrow 0} \frac{|x_i, p_i + \Delta p\rangle - |x_i, p_i - \Delta p\rangle}{2\Delta p}$$

Hence

$$\begin{aligned} & a\partial_p^3 |x, p, \sigma\rangle \\ &= \lim_{\Delta p \rightarrow 0} \frac{a}{(2\Delta p)^3} (|x, p+3\Delta p, \sigma\rangle - |x, p-3\Delta p, \sigma\rangle + 3|x, p-\Delta p, \sigma\rangle \\ & \quad - 3|x, p+\Delta p, \sigma\rangle) \\ &= \frac{a}{8\Delta p^3} \left[ \frac{1}{4} (|x, p+3\Delta p, \sigma\rangle + |x, p-3\Delta p, -\sigma\rangle) \right. \\ & \quad \left. + \frac{3}{4} (|x, p-\Delta p, \sigma\rangle + |x, p+\Delta p, -\sigma\rangle) \right] \end{aligned}$$

The creation probability is  $A = a/(2\Delta p^3)$ . The jump

probabilities are 1/4 for a pair of  $\pm$  points to be created symmetrically at distances  $p \pm 3\Delta p$  and 3/4 for a pair to be created at  $p \pm \Delta p$ .

### Numerical Test

For a test function a gaussian form is considered.

$$f_{\alpha}(p) = (1/\sqrt{2\pi}\alpha) e^{-p^2/2\alpha^2}$$

We follow through the algorithm as given in Chapter 4.

### Results

The figures 39-40 compare the exact curve for  $(e^{-a\theta} p^3 - 1)f(p)$  with the stochastic curves. It is seen that this simple differentiation process gives a remarkable agreement with the exact curve. However the figures 40 show that one has to be very careful in setting the annihilation (bin-size) distances.

figures 39-40

These pictures compare the stochastic development with the exact using a discrete differentiation process for the delta function.

fig 39.  $a' = .1$  ,  $\alpha^{-1} = 1$  ,  $\Delta p = .3$  ,  $N = 5000$   $a = .001$

top left - variation with statistics for 3 different runs.

top right - variation with  $N=1000, 5000, 10000$

bottom left- variation with  $a = .001, .002, .01$

bottom right-variation with  $\Delta p = .2, .3, .4$

fig 40. These pictures study the effect of variation of bin-sizes(or annihilation distance)

top-  $\Delta p = .3$  with bin-size= $.05, .1, .2, .3, .4$

bottom left  $\Delta p = .2$  with bin-size= $.1, .2, .3$

bottom right  $\Delta p = .4$  with bin-size= $.2, .3, .4$

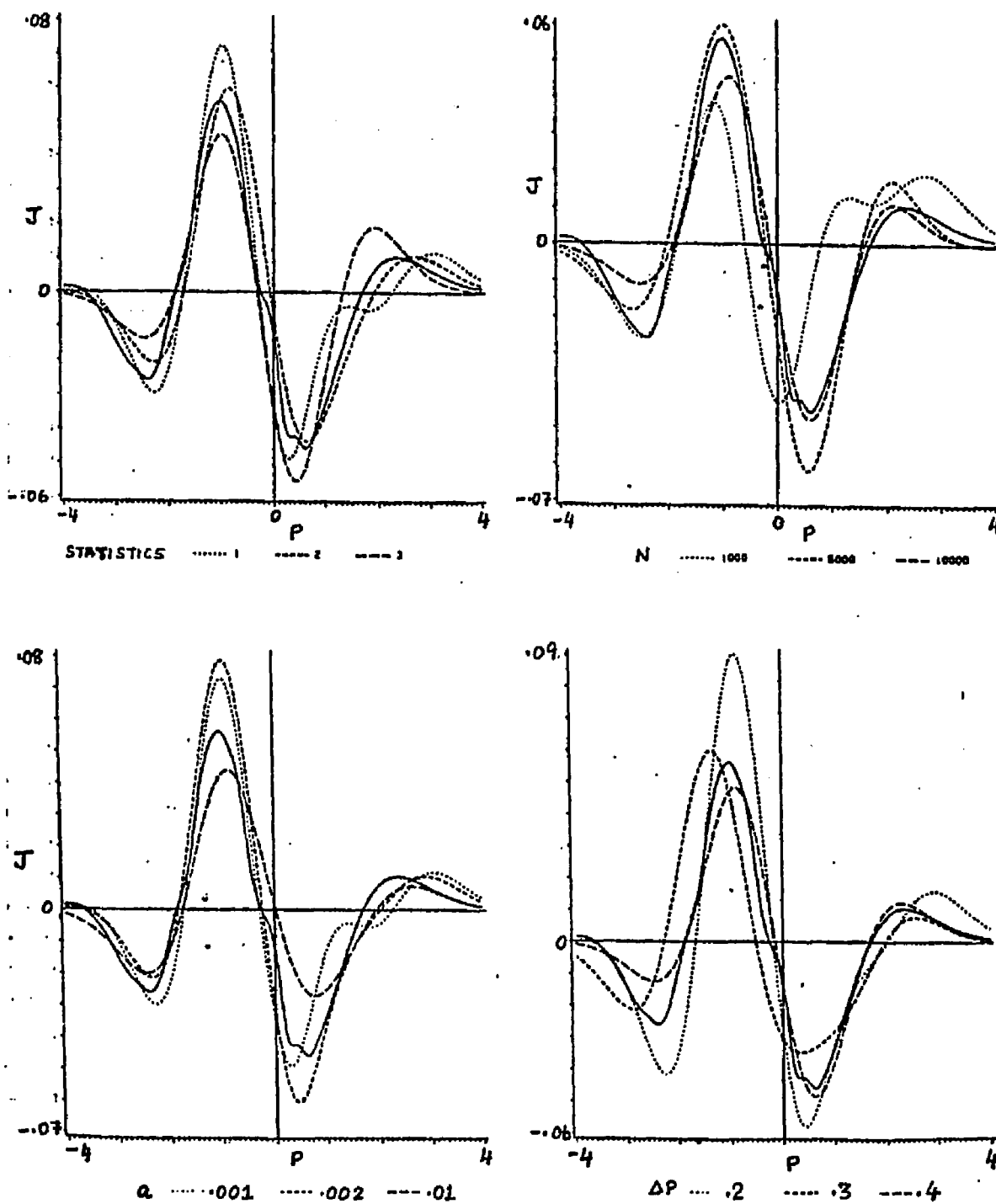


Figure 39. Comparison of exact with stochastic curves  
Discrete differentiation

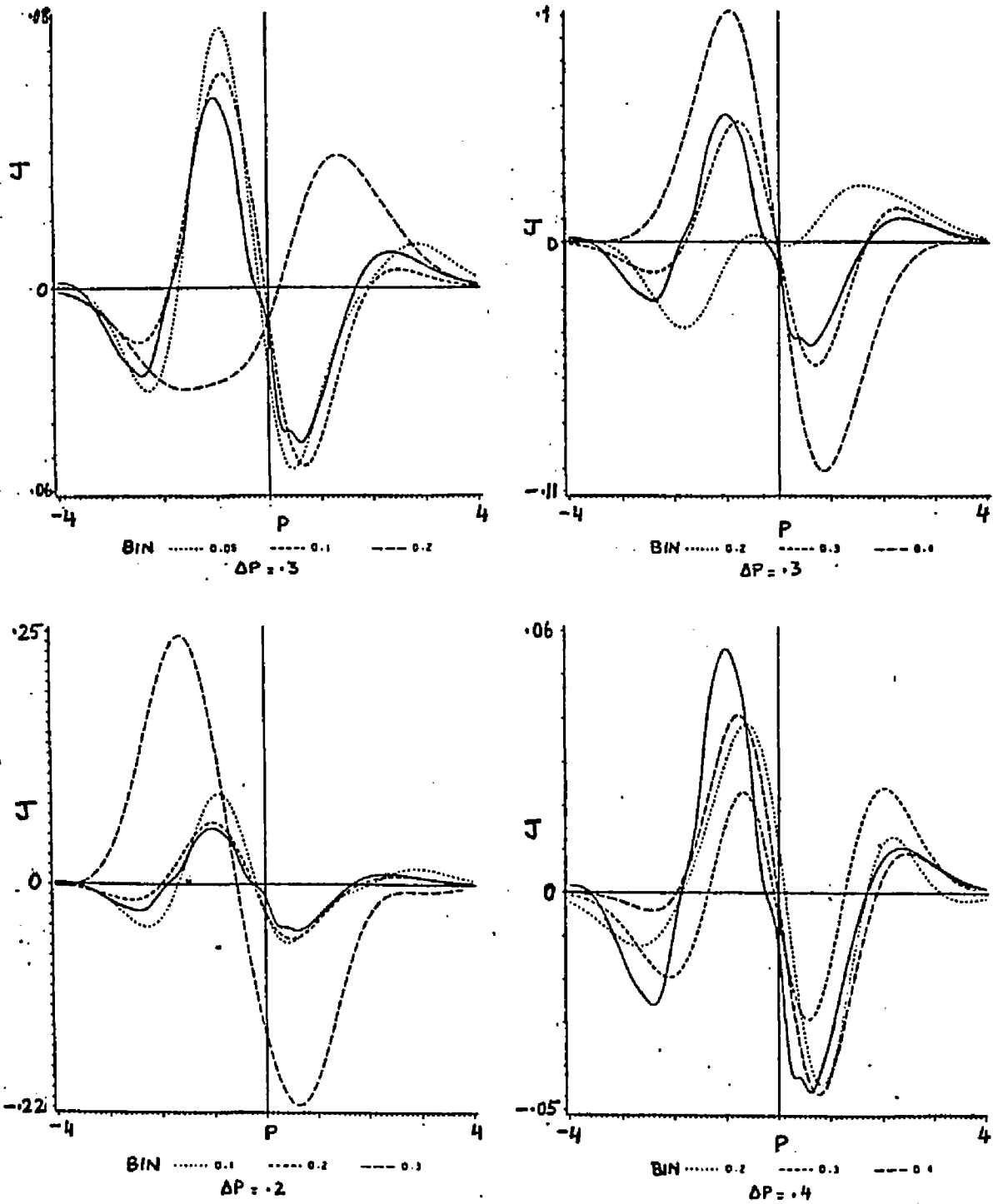


Figure 40. Comparison of exact with stochastic curves  
Discrete differentiation

## Appendix B

### Quantum Development using The Lorentzian Distribution

The Lorentzian distribution is given by

$$\begin{aligned}\delta_{\alpha}(p) &= 2 \operatorname{Re} (i/z) \\ &= 2\alpha/(\alpha^2+p^2)\end{aligned}$$

where

$$z = p + i \alpha$$

with an integral representation

$$\delta_{\alpha}(p) = \frac{1}{2\pi} \int_{-\infty}^{\infty} e^{ipy - \alpha|y|} dy$$

Let

$$\begin{aligned}I(a,p) &= e^{-a\theta^3} \delta_{\alpha}(p) \\ &= \operatorname{Re}(1/\pi) \int_0^{\infty} e^{iay^3 + izy} dy\end{aligned}$$

and the quantum motion is given by

$$J(a,p) = I(a,p) - \delta_{\alpha}(p)$$

The integral is evaluated in Appendix B.1

### Numerical test

The test function is now of the form

$$f_{\alpha}(p) = 2 \operatorname{Re}(i/z) = 2\alpha/(\alpha^2 + p^2)$$

The representative points are smeared by Lorentzians of width  $\alpha'$

$$f_{\alpha'}(p-p_i) = 2\alpha' / (\alpha'^2 + (p-p_i)^2)$$

where  $\alpha' \ll \alpha$

We follow the same algorithm as in Chapter 4

### Results and Conclusions

The stochastic curves show fair consistency for all the variables. However, the negative and outer regions do not match very well with the exact curve.

It is concluded that the Lorentzian function is less suitable than the Gaussian as a smearing function.

figures 41-42

fig 41. The exact quasi-classical development for a lorentzian function.

Top- Functions  $I(p,a)$  and  $J(p,a)$  for values of  $a = .05, .1$

Bottom left- Function  $J(p,a)$  for  $a = .001$

Bottom Right-  $J'_\pm$  for  $a=.001$

Dotted line is for  $J_+$  and solid line for  $J_-$ .

fig 42. Comparisons of stochastic development with the exact.

top left- Variation with statistics for 3 different runs.

top right- Variation with  $N=1000, 5000, 10000$

bottom left- Variation with  $a=.004, .002, .001$

bottom right- Variation with bin-size=.05, .1, .2

# LORENTZIAN DELTA FUNCTION

## QUANTUM TIME DEVELOPMENT-EXACT

ALPHA = .3

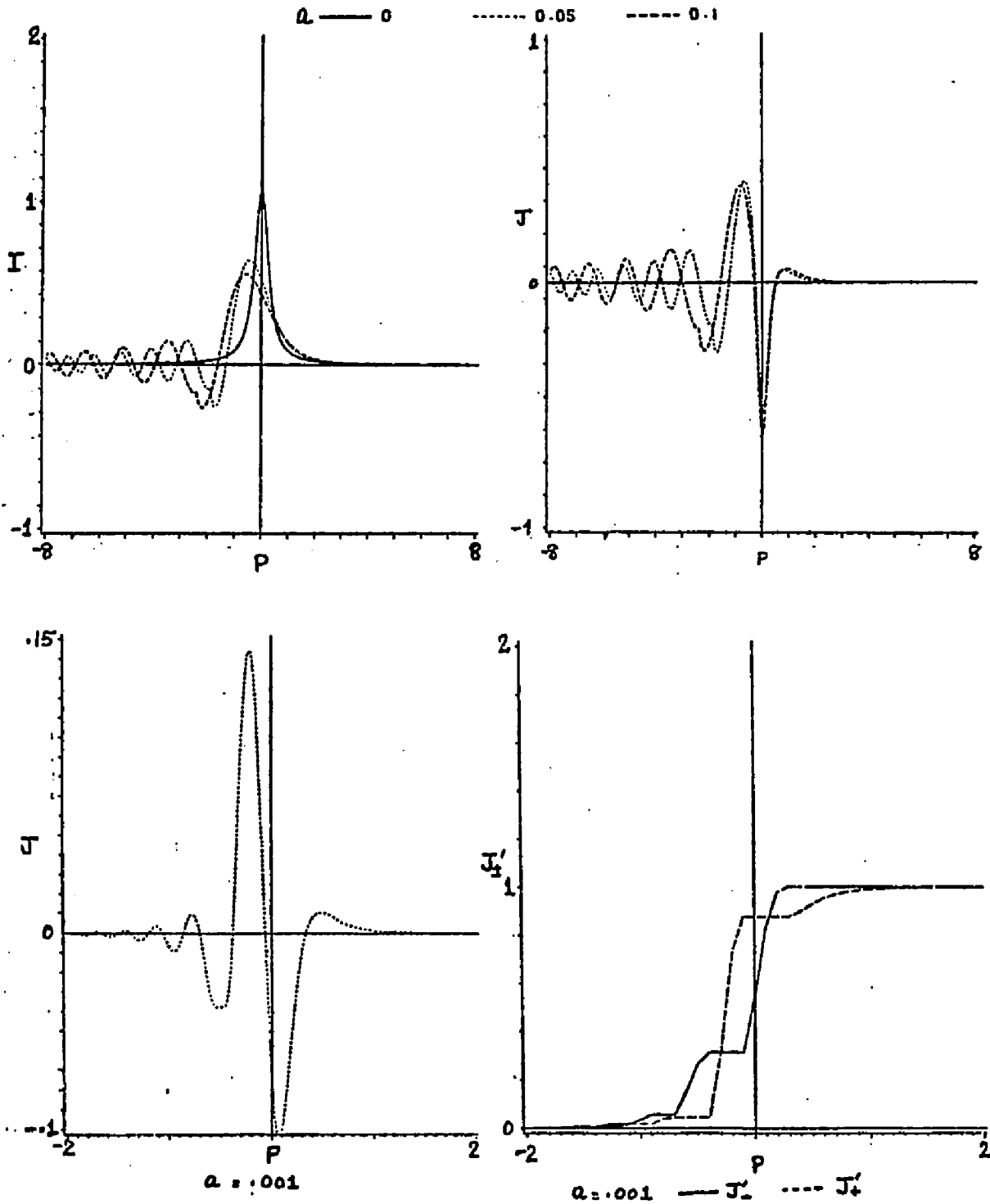


Figure 41. Exact quantum development of a Lorentzian Distribution

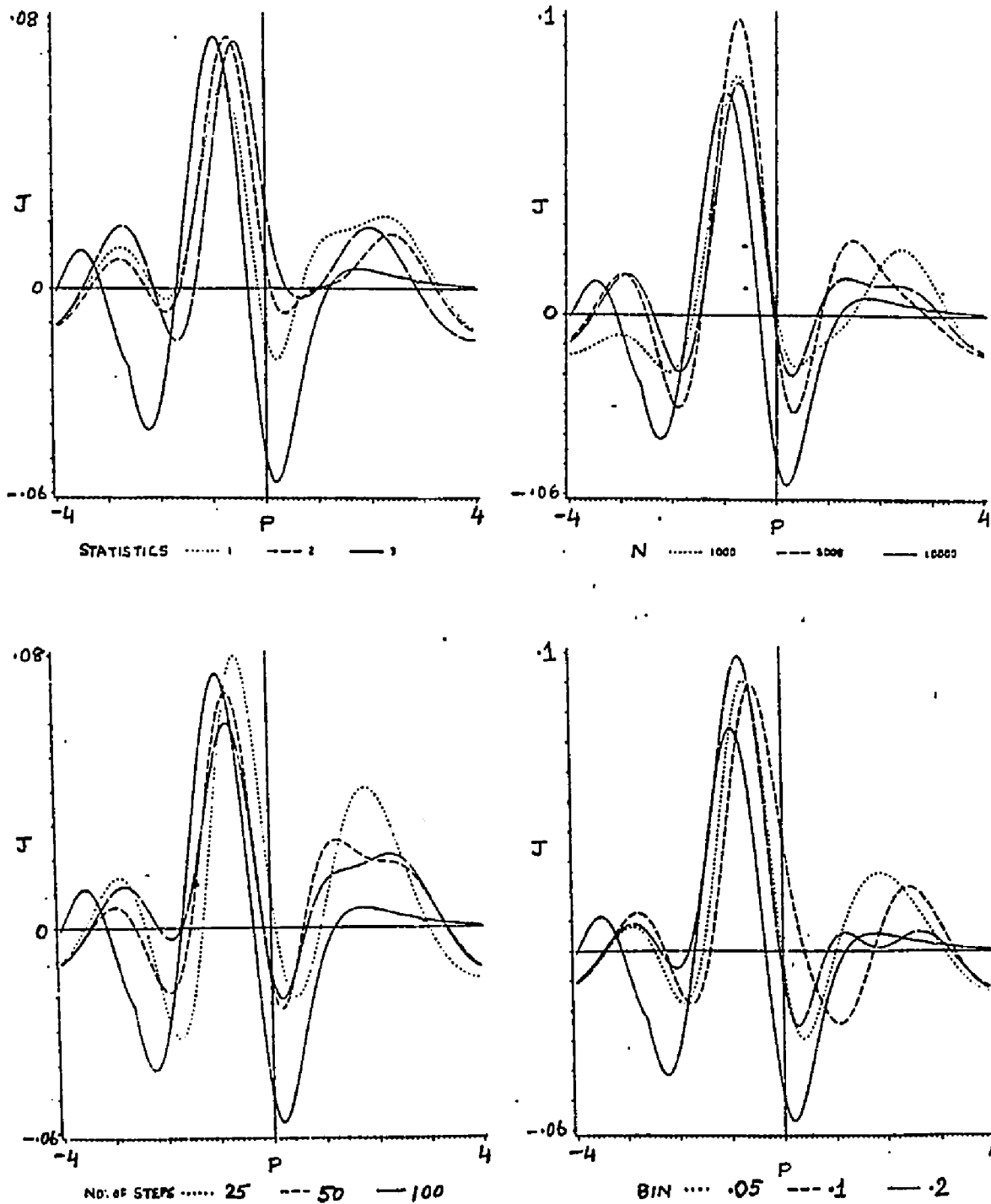


Figure 42. Comparison of exact with stochastic curve for Lorentzian distribution

Appendix B.1Evaluation of the I(p,a)

$$\begin{aligned}
 I(p,a) &= e^{-a\theta} p^3 \delta_\alpha(p) = \operatorname{Re} (1/\pi) \int_0^\infty e^{iay^3+izy} dy \\
 &= \operatorname{Re}(1/\pi) a^{-(1/3)} \int e^{ix^3+i\zeta x} dx
 \end{aligned}$$

$$\text{where } ay^3 = x^3 \quad ; \quad \zeta = a^{-1/3} z \quad ; \quad z = p + i\alpha$$

Small  $|\zeta|$  expansion  $|\zeta| \rightarrow 0$ 

Let

$$I(\zeta) = a^{-1/3} \int e^{ix^3+i\zeta x} dx$$

For small  $\zeta$  expand  $e^{i\zeta x}$  in series.

$$I'(\zeta) = a^{-1/3} \int e^{ix^3} \sum_n \frac{(i\zeta x)^n}{n!} dx$$

which gives

$$I(\zeta, a) = \operatorname{Re} \frac{1}{3\pi a^{1/3}} e^{i\pi/6} \sum (i\zeta e^{i\pi/6})^n \frac{\Gamma[(n+1)/3]}{n!}$$

Large  $|\zeta|$  expansion

For large  $|\zeta|$  asymptotic methods have to be considered. For this a more suitable form of the integral is needed.

$$\text{Let } f(x) = x^3 + \zeta x$$

$$= |\zeta|^{3/2} (t^3 + te^{i\theta})$$

$$\text{with } t = (x/|\zeta|) \quad \text{and } \zeta = |\zeta| e^{i\theta}$$

Then

$$I(\zeta) = \operatorname{Re}|\zeta|^{\frac{1}{2}} / (\pi a^{1/3}) \int_0^{\infty} e^{i|\zeta|^{3/2}(t^3 + te^{i\theta})} dt$$

The integral is evaluated by the method of steepest descent in the complex plane. There is a contribution from the origin and from the saddle point with

$$f(t) = i|\zeta|^{3/2} (t^3 + te^{i\theta})$$

The position of the saddle point ( $t_0$ ) is given by

$$t_0 = \pm \frac{i}{\sqrt{3}} e^{i\theta/2}$$

#### Paths of constant phase

The phase for the integrand in

$$\int_c e^{f(t)} dt \quad \text{is} \quad \phi(t) = \operatorname{Im} f(t)$$

With  $\sqrt{|\zeta|} t = u + iv$

$$\phi(u, v) = u^3 - 3uv^2 + u \cos \theta - v \sin \theta$$

Path of constant phase is given by

$$\phi(u, v) = \text{constant} = c$$

It is easy to show that

$$c(\text{origin}) = 0$$

$$c(t_0) = \frac{2}{3} \sin(3\theta/2)$$

Paths with phase  $c(\text{origin})$  and  $c(\text{s.p.})$  are drawn for various values of  $\theta$ . See fig 43.

figure 43

These figures show paths of constant phase on a complex plane for the function

$$e^{f(t)}$$

with  $f(t) \propto t^3 + t e^{i\theta}$

The constant phases selected are those which pass through the origin(o) and through the saddle-point(+)

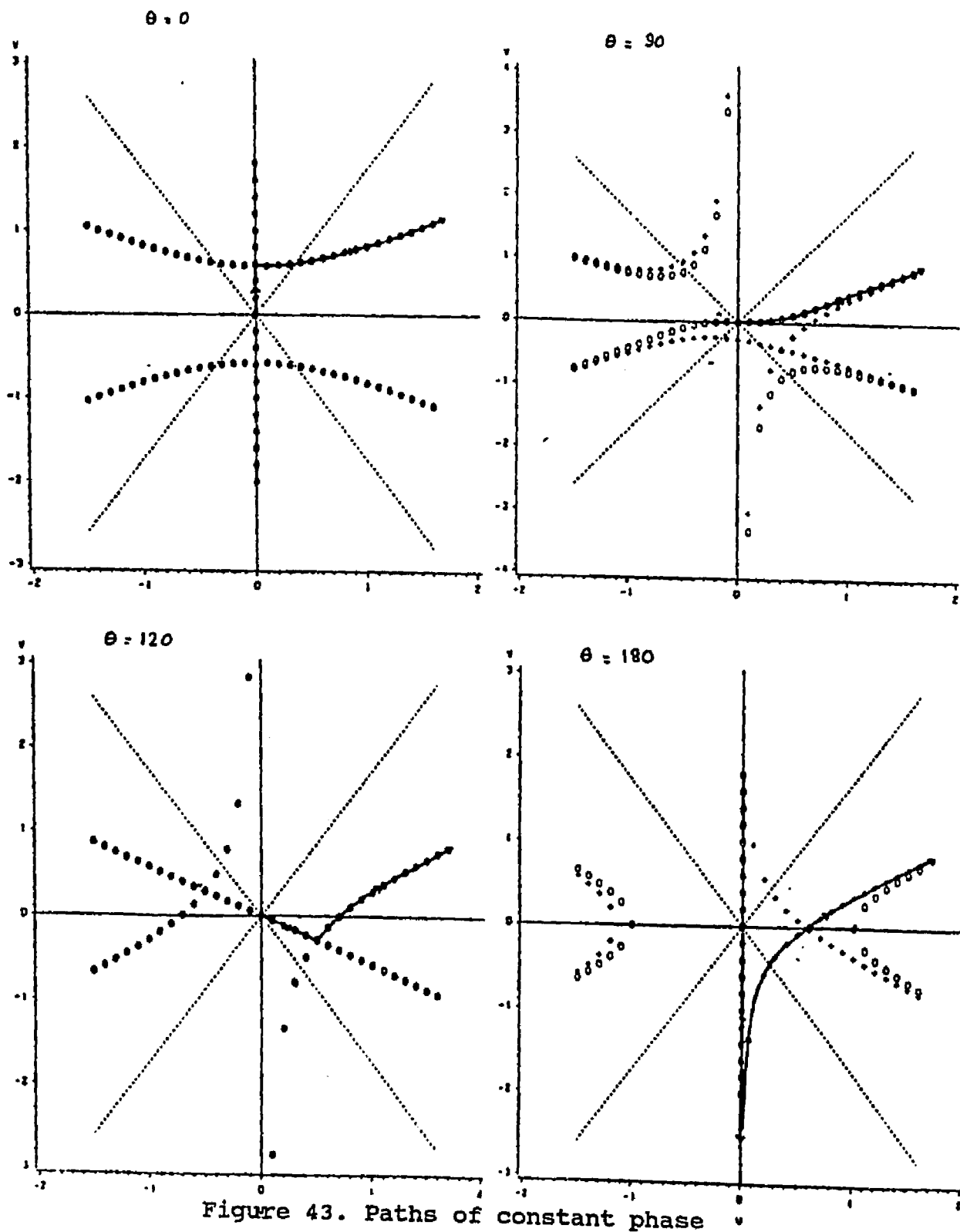


Figure 43. Paths of constant phase

From a study of these paths, the integral may be split into 2 contributions depending on the value of  $\theta$ .

There are 4 cases:

- |                               |   |
|-------------------------------|---|
| (i) $\theta = 0$              | $I = I_{\text{origin}} + \frac{1}{2} I_{\text{s.p.}}$ |
| (ii) $0 < \theta < 120^\circ$ | $I = I_{\text{origin}}$                               |
| (iii) $\theta = 120^\circ$    | $I = I_{\text{origin}} + \frac{1}{2} I_{\text{s.p.}}$ |
| (iv) $\theta > 120^\circ$     | $I = I_{\text{origin}} + I_{\text{s.p.}}$             |

### $I_{\text{origin}}$

Along the path of steepest descent for  $|\zeta| \rightarrow \infty$  only a very small region from origin contributes to the integral. Let

$$I'(\zeta) = \int_C e^{i|\zeta|^{3/2}(t^3 + te^{i\theta})} dt$$

with

$$t = se^{i\phi}$$

$$I' = \int_0^\epsilon e^{i|\zeta|^{3/2} [s^3 e^{3i\phi} + se^{i(\theta+\phi)}]} e^{i\phi} ds$$

Because  $s$  is very small between the limits Taylor expand the cubic term.

$$I' = \int_0^\epsilon \sum \frac{(i|\zeta|^{3/2} s^3 e^{3i\phi})^n}{n!} e^{i|\zeta|^{3/2} se^{i(\theta+\phi)}} e^{i\phi} ds$$

With the steepest path defined by

$$\phi = \pi/2 - \theta$$

$$I' = \sum \frac{(i|\zeta|^{3/2} e^{3i(\pi/2-\theta)})^n}{n!} e^{i(\pi/2-\theta)} \int_0^\epsilon s^{3n} e^{-|\zeta|^{3/2} s} ds$$

Now

$$\int_0^\epsilon s^{3n} e^{-|s|^{3/2}} ds \approx \int_0^\infty s^{3n} e^{-|s|^{3/2}} ds \quad \text{for } |s| \rightarrow \infty$$

which gives

$$I_{\text{origin}} \approx \frac{|s|^{3/2}}{\pi a^{1/3}} \sum \frac{(3n)!}{n! (|s|^{3/2})^{2n+1}} \sin[(3n+1)\theta]$$

$I_{\text{s.p.}}$

The s.p. is at

$$t_0 = -\frac{1}{\sqrt{3}} e^{i\theta/2}$$

Taylor expand near  $t_0$ .

$I =$

$$\begin{aligned} & \int_{t_0 - \epsilon}^{t_0 + \epsilon} e^{|s|^{3/2}} (f(t_0) + \frac{1}{2}(t-t_0)^2 f''(t_0) + \frac{1}{6}(t-t_0)^3 f'''(t_0)) dt \\ &= e^{|s|^{3/2}} f(t_0) \int e^{\sqrt{3}|s|^{3/2}} (t-t_0)^2 e^{i\theta/2} + i|s|^{3/2} (t-t_0)^3 dt \end{aligned} \quad (1)$$

Choose the path such that

$$t-t_0 = s e^{i\phi}$$

Then integral in (1) becomes

$$I' = \int_{-\epsilon}^{\epsilon} e^{\sqrt{3}|s|^{3/2}} s^2 e^{i(\theta/2+2\phi)} + i|s|^{3/2} s^3 e^{3i\phi} e^{i\phi} ds$$

Now for the path of steepest descent  $\phi$  is defined by

$$\theta/2 + 2\phi = \pi$$

$$I' = e^{i(\pi/2-\theta/4)} \int e^{-\sqrt{3}|s|^{3/2}} s^2 + i|s|^{3/2} s^3 e^{3i(\pi/2-\theta/4)} ds$$

The integral in (2) is split into two

(2)

$$\int_0^\epsilon e^{-\sqrt{3}|\zeta|^{3/2}s^2 + i|\zeta|^{3/2}s^3} e^{3i(\pi/2-\theta/4)} ds$$

$$+ \int_0^\epsilon e^{-\sqrt{3}|\zeta|^{3/2}s^3 - i|\zeta|^{3/2}s^3} e^{3i(\pi/2-\theta/4)} ds$$

$$= I_+ + I_-$$

which gives

$$I = \frac{\operatorname{Re} i}{\pi a^{1/3} (3\zeta)^{1/4}} e^{(2/3/3)\zeta^{3/2}} \sum_{\text{even}} \frac{\Gamma(3n+1)/2}{(3\zeta)^{3n/4} n!}$$

For  $\theta = 0$ ,

$$t_0 = i/\sqrt{3}$$

$$I = \int e^{|\zeta|^{3/2}f(t_0) - 3|\zeta|^{3/2}(t-t_0)^2 + i|\zeta|^{3/2}(t-t_0)^3} dt$$

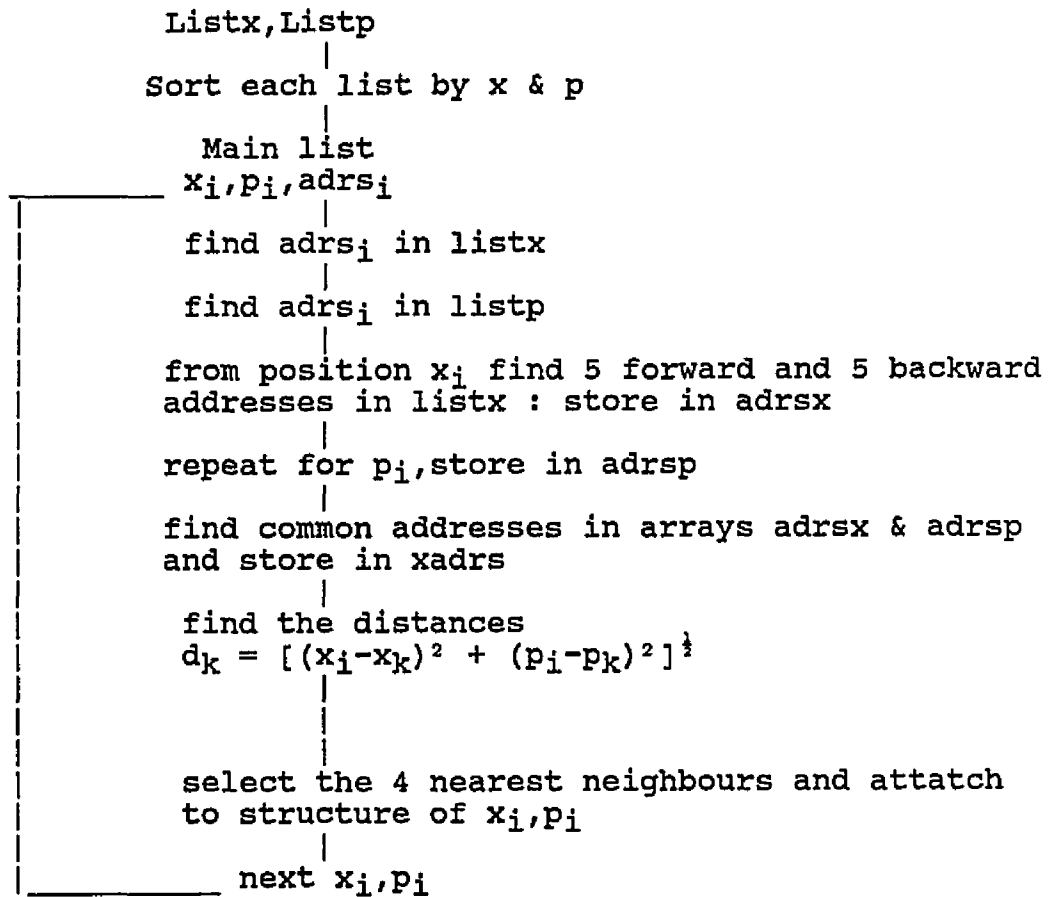
Now only  $\int_0^\infty$  contributes to the integral on the right half plane.

$$I = \frac{\operatorname{Re}}{2\pi a^{1/3} (3|\zeta|)^{1/4}} e^{-(2/3/3)|\zeta|^{3/2}} \sum \left( \frac{i}{(3|\zeta|)^{3/4}} \right)^n \frac{\Gamma[(3n+1)/2]}{n!}$$

## FLOW CHARTS

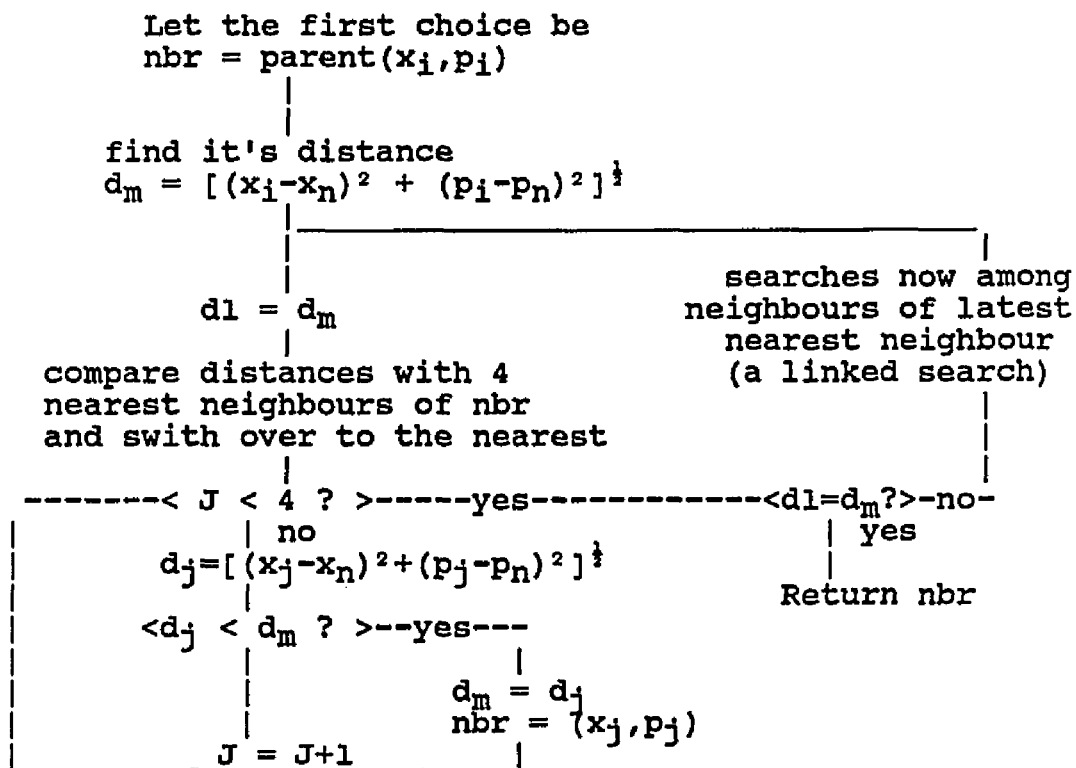
### Initial Assignment of Neighbour:

Create 2 lists containing x & p variables with the corresponding addresses in the main list



A shortest path to locate nearest neighbours

The points  $(x_n, p_n)$  that do not undergo hopping are attached to the main list. The nearest neighbour is found by a shortest path as follows:





### Bibliography

1. E.Wigner, Phys.Rev.40,749, (1932)
2. T.Takabayasi, Progress of Theoretical Physics 11  
341(1954)
3. K.Imre,E.Ozizmir, M.Rosenbaum, P.F.Zwiefel,  
J.math.Phys.8,1097(1967)
4. N.L.Balazs,&G.G.Zipfel,Jr,Annals of Physics 77, 139  
(1973)
5. E.A.Remler, Annals of Physics 95 455(1975)
6. H.J.Korsch, J.Phys.A:Math Gen12 811, (1979)
7. P.Carruthers and F.Zachariasen,Reviews of Modern  
Physics 55 245 (1983)
8. P.Bonche, S.Koonin,J.W.Negele,Phys.Rev.C 3,1226  
(1976)
9. C.Y.Wong Phys.Rev.C 25 1460 (1982)
10. Hai Wong Lee & Marlan O.Scully , J.Chem.Phys  
77,4604,(1982),Foundations of Physics 13 61,(1983)
11. M.Ploszajczak & M.J. Rhoades-Brown , Phys.Rev.Lett.  
55 147,(1985)
12. F.J. Narcowich ,Physica 134a ,193 (1985)
13. G.J.Milburn, Phys.Rev.A 33 674,(1986)
14. B.Leaf , J.Math.Phys 9 65,(1968)
15. E.J.Heller , J.Chem.Phys. 65 1289,(1976) J.Chem.Phys  
67 ,3339,(1977)

16. J.G. Kruger & A.Poffyn , Physica 85a 84 (1976)
17. M.V.Berry, Phil.Trans.R.Soc. London 287 ,30,(1977)
18. N.L.Balazs, Physica 102a ,236 (1980)
19. R.F. O'Connell & E.P.Wigner, Phys. Letters 83a  
145,(1981), Phys Letters 85a 121 (1981)
20. J.P.Dahl,Physica Scripta 25 ,499 (1982)
21. U.Fano ,Reviews of Modern Physics 29 ,74 (1957)
22. W.A.Lyle,Thesis,College of William & Mary,  
unpublished (1983)

## VITA

Sarah John

Born in Trivandrum, Kerala, India on February 18, 1953. Obtained a B.Sc. degree in Physics from University College, Trivandrum in 1971, and an M.Sc. degree in Physics from the same institution in 1973.

Entered College of William and Mary as a graduate student, with a teaching assistantship in Sept. 1981 and completed all requirements for a Masters Degree in Physics in Sept. 1982.